63-2-4

TRG

296 839

TECHNICAL RESEARCH GROUP
2 AERIAL WAY • SYOSSET, NEW YORK

RADC-TDR-62-577 November 1962

"Microwave Amplification by Resonance Saturation"

Final Report
Contract AF30(602)-2033

November 1962

Prepared by:

TRG, Incorporated
2 Aerial Way
Syosset, New York

Prepared for:

Rome Air Development Center
Air Force Systems Command
United States Air Force
Griffiss Air Force Base
New York

PATENT NOTICE:

When Government drawings, specifications, or other data are used for any purpose other than in connection with a definitely related Government procurement operation, the United States Government thereby incurs no responsibility nor any obligation whatsoever and the fact that the Government may have formulated, furnished, or in any way supplied the said drawings, specifications or other data is not to be regarded by implication or otherwise as in any manner licensing the holder or any other person or corporation, or conveying any rights or permission to manufacture, use, or sell any patented invention that may in any way be related thereto.

ASTIA NOTICE:

Qualified requestors may obtain copies of this report from [illegible], Arlington Hall Station, Arlington 12, Virginia. ASTIA Service for the Department of Defense contractors are available through the "Field of Interest Register" on a "need-to-know" certified by the cognizant military agency of their project or contractor.

OTS NOTICE:

This report has been released to the Office of Technical Services, United States Department of Commerce, Washington 25, D.C., for sale to the general public.

RADC-TDR-62-577 November 1962

"Microwave Amplification by Resonance Saturation"

by Benjamin Senitzky
Gordon Gould

TRG, Incorporated
2 Aerial Way
Syosset, New York

Final Report
Contract AF30(602)-2033
Project: 128

Prepared for:

Rome Air Development Center
Air Force Systems Command
United States Air Force
Griffiss Air Force Base
New York

FOREWORD

This report describes the work performed by Department 2 of Technical Research Group, Inc. for Rome Air Development Center on Contract AF 30(602)2033. This contract calls for the research directed towards the design of ultra-sensitive low noise amplifiers in the mm-wave region of the electromagnetic spectrum.

We would like to acknowledge the assistance of A. Simmons, S. Cutler, O. Giddings, M. Piltch, and R. Olsen during the course of this program.

Abstract

A new amplification principle is introduced based on non-linear response of a saturated resonance absorption. The amplification and bandwidth of a travelling wave device based on this principle is derived. Experimental results on amplification obtained with iron-doped rutile as the active medium at 81.3 kMc are found to be in agreement with theory.

TABLE OF CONTENTS

LIST OF FIGURES AND TABLES

(Con't)

LIST OF FIGURES AND TABLES (CONT'D.)

1. Introduction

This report describes a theoretical and experimental study program of low noise mm wave amplifier principles and devices. During the preliminary phase of this program a theoretical study was made of amplifiers based on the Maser principle. This study is presented in Appendix I. During the course of the Maser study a new amplification principle was discovered. The major part of the program was then devoted to a theoretical and experimental study of the new principle which is described in detail in Section 2. This principle can be stated briefly as follows: If a strong local oscillator and a weak (incoming) information signal are transmitted through a medium which absorbs constant absolute power, the gain of the information signal can, under certain conditions, equal the attenuation of the local oscillator signal. Because constant power is lost in the medium we will call an amplifier based on this principle a Constant Loss Amplifier (CLA).

Particularly suitable CLA media for mm wave applications are those which exhibit power saturation of a microwave resonance absorption. If the local oscillator saturates the resonance and the frequency of the weak information signal falls within the resonance line width, the information signal can, under certain conditions, be amplified.

The amplification characteristics of two types of resonant media were analyzed: crystalline solids with electron paramagnetic spectra and molecular gases with rotational spectra. The results of

this analysis, presented in Section 2, are that at low local oscillator power levels where the media exhibit linear resonance absorption, both the local oscillator and information signal suffer the same fractional power loss per unit length, α_ℓ. As the local oscillator power is increased so that the resonance absorption becomes saturated, the information signal gain per unit length, α_G, can reach a maximum value of $\alpha_\ell/8$. These results were then computed for specific materials. At 81.3 kMc, the maximum gain, α_ℓ, for the electron paramagnetic resonance of iron (Fe^{+++}) doped rutile (TiO_2) at 4.2°K was estimated as 0.05 cm^{-1} in approximate agreement, with experiments to be described in this report. At 86.0 kMc, the maximum gain for the rotational resonance of hydrogen cyanide (HCN^{15}) gas at room temperature was computed as 0.0012 cm^{-1} in good agreement with experiments described elsewhere.(1)

The bandwidth of the CLA in a travelling wave structure was found to be a function of the relaxation times associated with the resonance transitions. If the frequency deviation of the information signal from the local oscillator signal is of the same order of magnitude as the reciprocal of the relaxation time, the Fourier components of the oscillating dipole moment induced by the microwave field must be calculated using quantum mechanical perturbation theory. The effect of the medium on the radiation can then be represented in terms of a

---

(1) RADC-TDR-62-438. Copies of this Technical Note are available from ASTIA Document Service Center, Dayton 2, Ohio. A net gain of 1.5 db was observed in a travelling wave structure at a pressure of 30 microns with a bandwidth of about 4 Mc and a local oscillator power of 5 mw.

complex susceptibility. A significant result of this analysis presented in Section 2 is that the bandwidth for the experimental conditions encountered in the solid medium is somewhat greater than $(\pi T_1)^{-1}$ where T_1 is the spin lattice relaxation time. For this experiment, T_1 was estimated to be about 10^{-5} sec so the bandwidth is of the order of 3×10^4 sec. The bandwidth for the gas is somewhat greater than $(\pi T)^{-1}$ where T is the collisional relaxation time which is inversely proportional to pressure. This bandwidth can be made greater than 20 Mc.

The amplification characteristics of the CLA using the electron paramagnetic resonance of iron doped rutile at 81.3 KMc were experimentally investigated in a tunable travelling wave structure. The whole amplifier assembly, consisting of a minute rutile filled guide, transition sections to air filled guide and tuning superconducting electromagnet, weighed less than one ounce (Section 3). A relative signal gain was observed (Sect. 4) in agreement with theory, although the gain was not sufficient to overcome the wall and material losses.(2)

The practical advantages of the CLA over existing amplifiers in the mm wave region may be listed here

- single frequency band operation - simpler structure (gases and solids)
- no higher frequency pump requirement (gases and solids)
- room temperature operation (gases)

---

(2) This condition was not encountered with the gaseous medium described in reference (1) because the wall losses were sufficiently small.

- tunability (gases and solids)
- operation readily extended to frequencies above 100 kMc (gases).

The noise characteristics of this device have not been measured but it appears from theoretical considerations that the main source of noise (due to the local oscillator output spectrum) can be eliminated by a) filtering, using a high Q cavity b) balancing - by techniques used for balanced mixers.

Because of the high wall and material losses and narrow bandwidth encountered in the solid CLA medium, the use of gaseous media is recommended.

2. CLA Theory

In order to explain the amplification principle we will first consider an idealized medium with well-defined mathematical properties and then consider the realizable media such as iron doped rutile and hydrogen cyanide which could be used in practice. We will show how in the limiting case the properties of these media approach that of the idealized medium. The analysis and experimental test are easier to perform where the incoming information signal is in the form of two equally spaced sidebands around the local oscillator frequency (corresponding to either amplitude or frequency modulation of the local oscillator). Therefore this will be the case primarily considered below. The case where the incoming information signal is in the form of a single sideband can be considered as a superposition of two amplitude and two frequency modulation sidebands, and will also be discussed.

Consider two information carrying signal sidebands coming into the amplifier with frequency $\nu + \Delta\nu$ and $\nu - \Delta\nu$ and power P_s as shown in Fig. 1. Let a local oscillator supply the power P_c which is much larger than P_s. If the phase of these three components is adjusted for amplitude modulation, the sum of these components will give rise to the instantaneous power as a function of time curve shown in Fig. 1.b. We now consider this power incident on an idealized medium which has the following definite non-linear property: It can absorb only a constant absolute amount of power averaged over a time interval long compared to the local oscillator period but short compared to the modulation period. Another way of stating this is to say that the response or

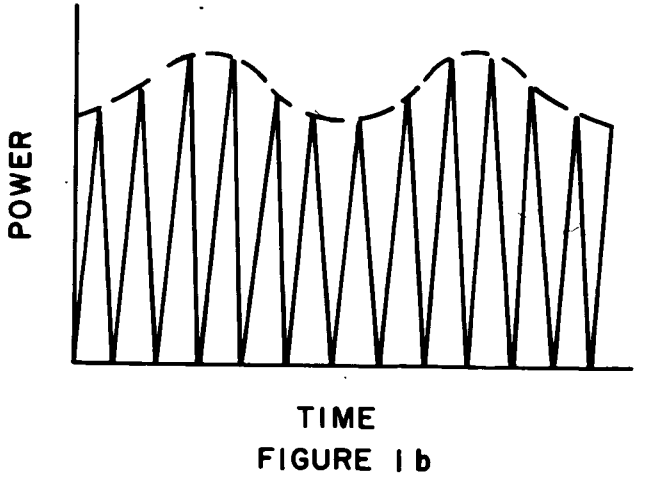

FIGURE 1b

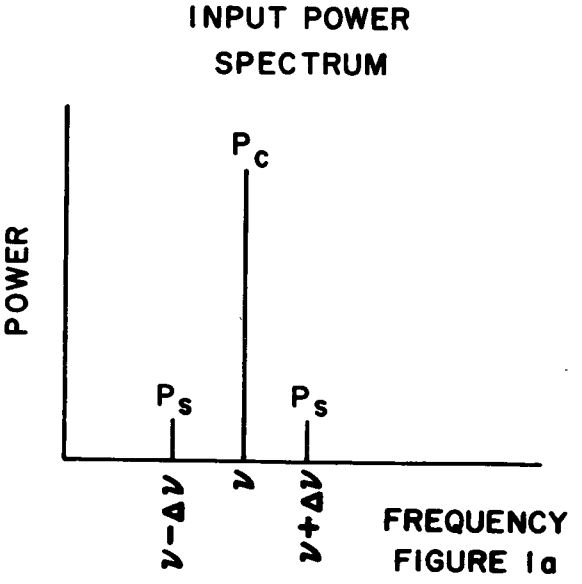

FIGURE 1a

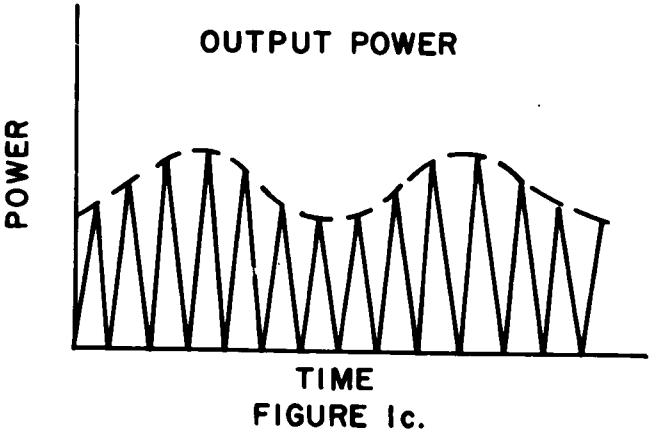

FIGURE 1c.

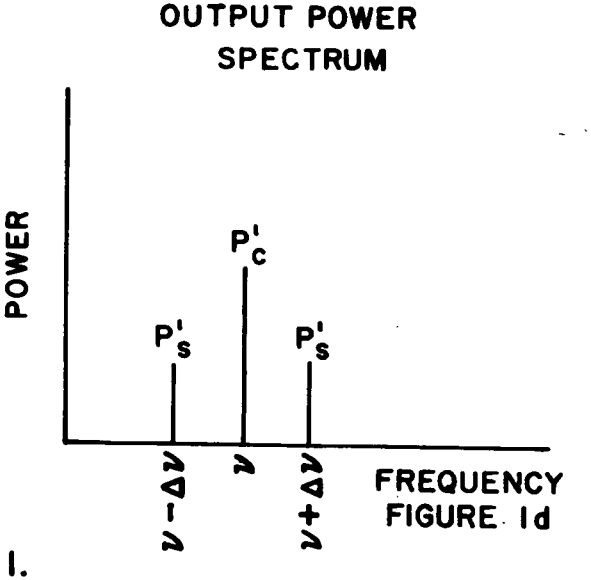

FIGURE 1d

FIGURE 1.
PROPERTIES OF IDEALIZED MEDIUM FOR AMPLITUDE MODULATION

relaxation time of the medium is such that it cannot affect the shape of the high frequency power fluctuations but it can change the maxima in such a way that the output power has the form shown in Fig. 1c.

The peaks of the power fluctuations in Fig. 1c are all lowered with respect to those in Fig. 1b by a constant amount corresponding to the constant absolute power loss in the medium. If we average the power over a time interval long compared to the local oscillator period and short compared to the modulation period we will obtain the identical modulation envelope in both cases, but the transmitted envelope will be lowered by the constant power loss in the medium.

Since the shape of the high frequency power fluctuations have not changed we can represent the output spectrum as a sum of three frequency components as shown in Fig. 1d. Since both the incident and transmitted envelope have the same depth and since the depth is determined by the product of the local oscillator and sideband power, it follows that $P_c P_s = P'_c P'_s$, where primes distinguish the output quantities. This means that P_s in going through the medium is increased by the same ratio that P_c is decreased.

The difference between the CLA and a crystal heterodyne converter is obvious at this point. The output of the crystal converter does not contain microwave frequencies since these are averaged out. In the CLA the microwave frequencies are retained at the output. It is instructive to consider what would happen if the crystal is used to detect the input power and the output power. At first sight it would seem that there has not been any gain in usable signal since the crystal will give rise to a

direct current which does not contain any information and a signal containing information at the frequency $\Delta\omega$ which is proportional to $\sqrt{P_c P_s}$. Since $P_c P_s = P_c' P_s'$ it would seem that there is no gain in this case. However, the reduced carrier at the output of the constant loss medium can be brought up to its original input value without the generation of greater noise in the crystal. The new signal is $\sqrt{P_c P_s'}$ which does show a gain.

Let us now consider the situation when the two sidebands are arranged for frequency modulation of the local oscillator signal. The conditions are shown in Fig. 2. Since the fractional frequency deviation remains the same at the input and the output, it follows that in this case $P_s'/P_c' = P_s/P_c$ or that P_s in going through the medium is decreased by the same ratio as P_c is decreased. That means that frequency modulation sidebands are attenuated, while amplitude modulation sidebands are amplified.

So far we have been discussing the problem from the point of view of power. We will now consider what happens to the electric or magnetic fields in this type of medium. For the case considered in Fig. 1 the fields can be represented mathematically as

$$H(t) = H_c \cos \omega t + \frac{H_s}{2} \cos (\omega + \Delta\omega)t + \frac{H_s}{2} \cos (\omega - \Delta\omega)t$$

and graphically by the projection on the x-axis of a rotating vector

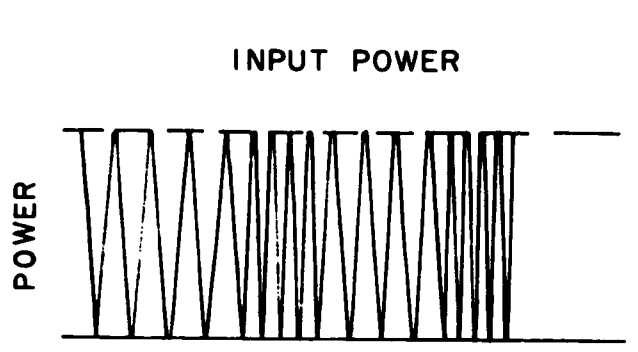

FIGURE 2b.

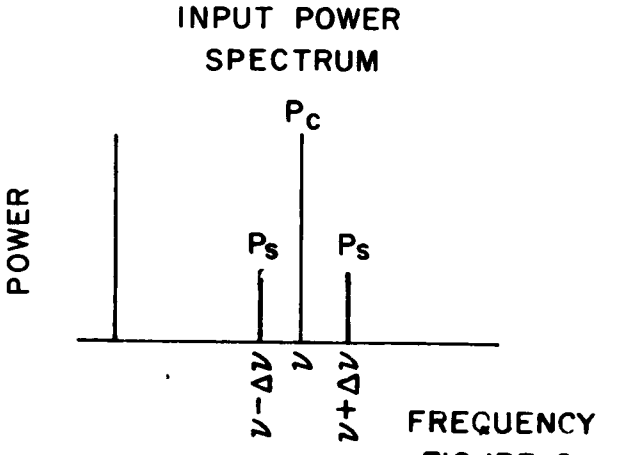

FIGURE 2a

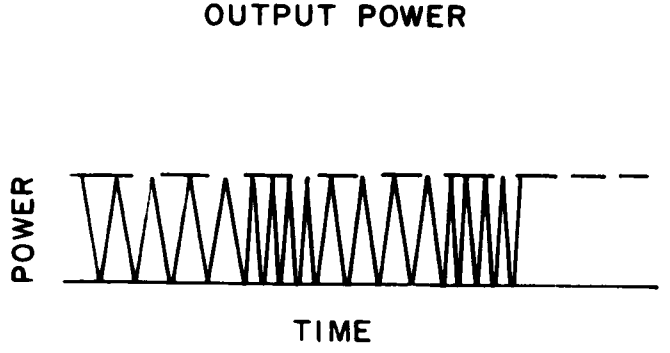

FIGURE 2c.

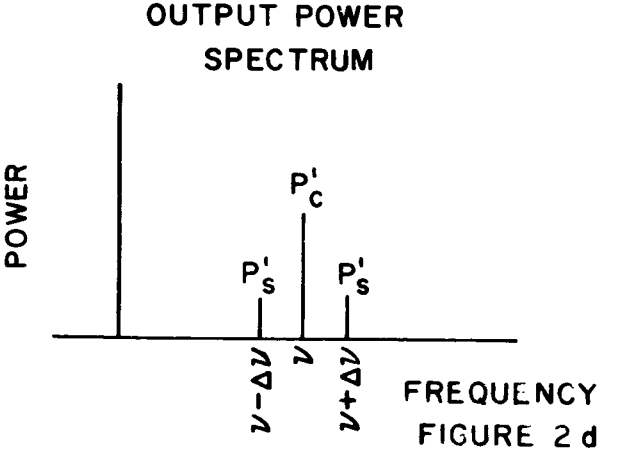

FIGURE 2d

FIGURE 2.

PROPERTIES OF IDEALIZED MEDIUM FOR FREQUENCY MODULATION

with angular velocity ω and magnitude H_c.[3] The length of this vector is constantly changing and this effect can be represented by two smaller component vectors each of constant magnitude $\frac{H_s}{2}$ which are rotating around H_c with angular velocities $+\Delta\omega$ and $-\Delta\omega$, as shown in Fig. 3. The length of the rotating vector is then given by $H_c + H_s \cos(\Delta\omega t)$. After transmission through the medium the length of the vector is given as $\sqrt{H_c^2 + H_s^2 + 2H_cH_s\cos(\Delta\omega t) - H_L^2}$ where the term H_L^2 represents the constant power loss in the medium. To first order in $\frac{H_s}{H_c}$ we can rewrite this as $H_c\eta + \frac{H_s}{\eta}\cos(\Delta\omega t)$ where η is a parameter which is the local oscillator field attenuation and is equal to

$$\sqrt{1 - \left(\frac{H_L}{H_c}\right)^2} \quad .$$

It is noted that the sidebands have been increased and the carrier decreased by the same ratio. This is in accord with the previously stated requirement that the product of the powers in the carrier and the sideband remain constant.

A frequency modulated local oscillator can be represented mathematically by the expression

---

(3) Throughout this report the symbol H will refer to the magnetic field when paramagnetic resonant media are considered and to the electric field when electric dipolar gases (such as HCN) are considered.

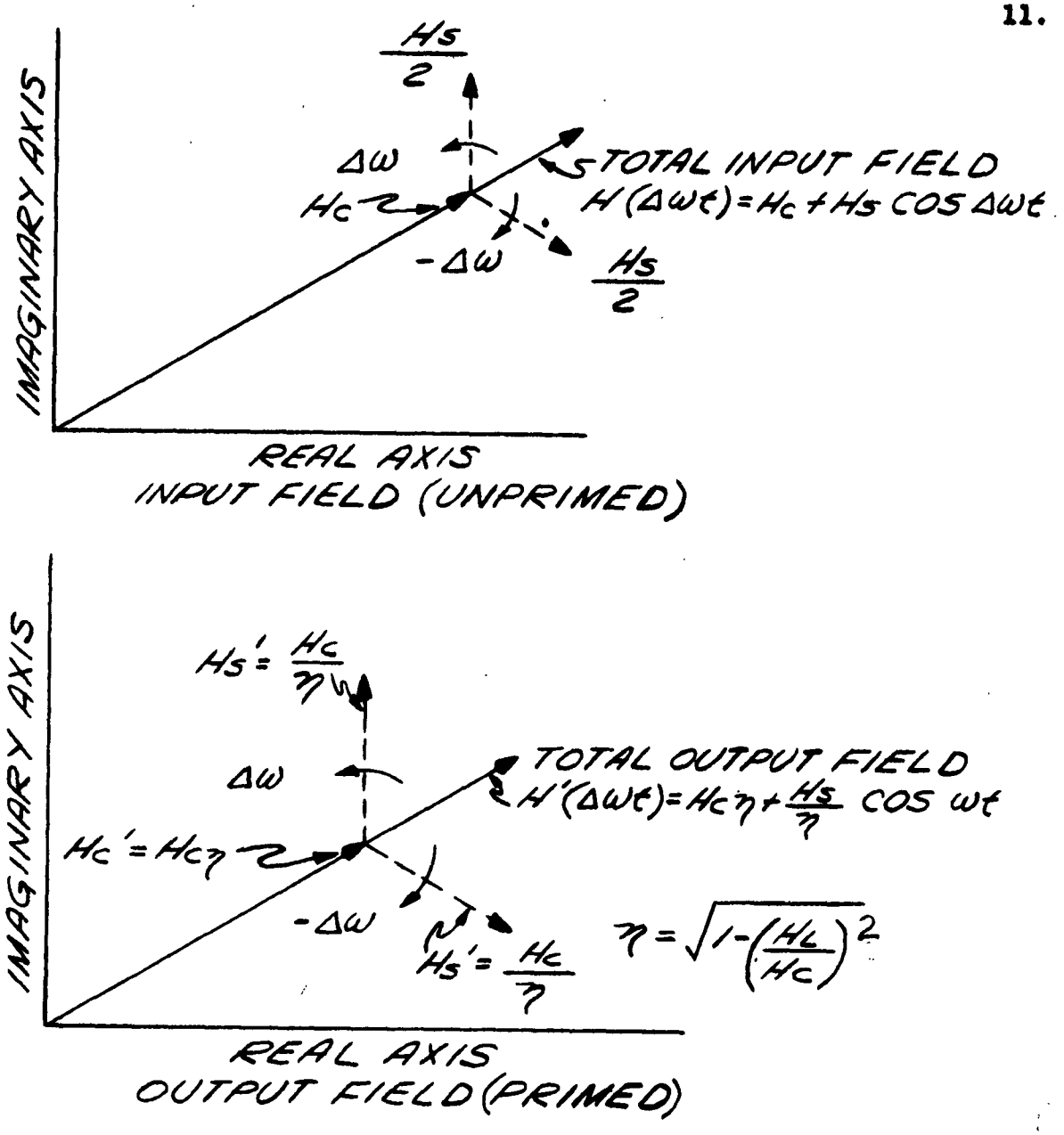

FIGURE 3

Sidebands phased for amplitude modulation.
Relation between input field, H(Δωt), and output field, H'(Δωt) is $H'(\Delta\omega t) = \sqrt{H^2(\Delta\omega t) - H_L^2}$ where H_L^2 represents constant loss in CLA medium.

$$H(t) = H_c \cos \omega t + \frac{H_s}{2} \sin (\omega + \Delta\omega)t + \frac{H_s}{2} \sin (\omega - \Delta\omega)t$$

and graphically by Fig. 4.

The input vector is H_c and wobbles back and forth through an angle $\tan^{-1}(H_s/H_c)$. If we assume that the medium is not dispersive, i.e., it has a propagation constant which is independent of frequency, the output vector will wobble through the same angle and its length will be reduced to $\sqrt{H_c^2 - H_L^2}$ or ηH_c as shown in the bottom half of Fig. 4, and the sideband field will therefore be reduced by the same ratio as the local oscillator field or stated mathematically: $H_s'/H_c' = H_s/H_c$. This is in accordance with the previous statement that the attenuation of the sidebands and local oscillator power is the same for frequency modulation.

We will now consider the case of a single sideband where the input field can be written as

$$H(t) = H_c \cos \omega t + H_s \cos (\omega + \Delta\omega)t \ .$$

We will represent this as a vector in a coordinate system rotating with an angular velocity ω as shown in Fig. 5. Whereas for the amplitude modulation case considered above this vector would retain the same direction, in this case there is some frequency modulation as the input vector moves around a circle. At any given time the magnitude of the output vector is reduced according to the equation

$$H' = \sqrt{H_c^2 + 2H_c H_s \cos (\Delta\omega t) + H_s^2 - H_L^2} \ .$$

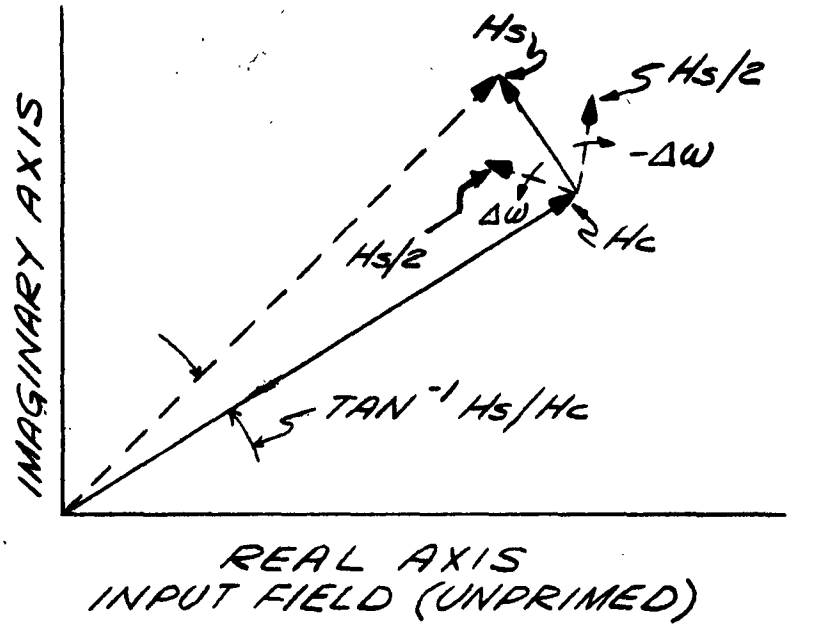

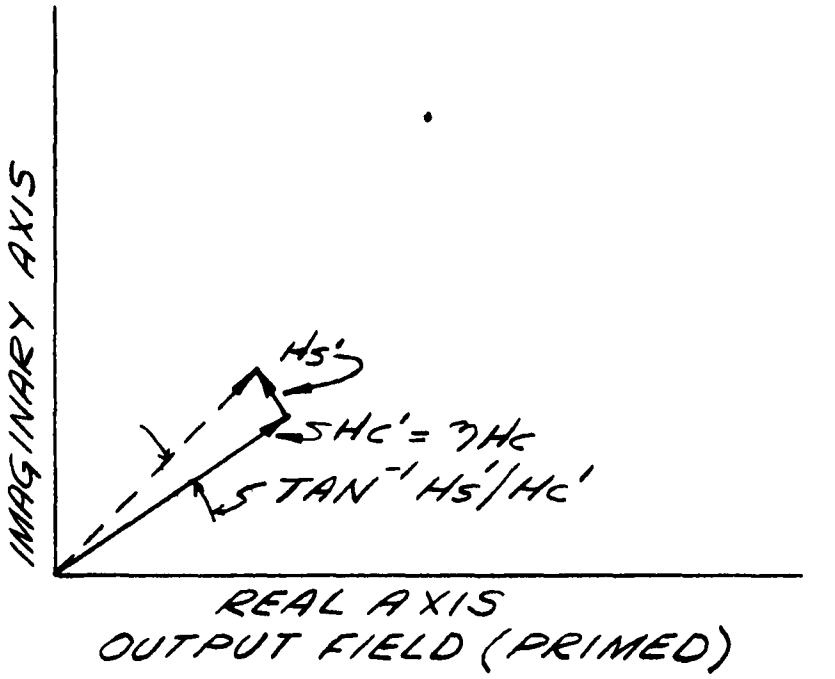

FIGURE 4.

Sidebands phased for Frequency Modulation.
In a non-dispersive medium $\tan^{-1} Hs'/Hc' = \tan^{-1} Hs/Hc$ therefore $Hs' = \eta Hs$.

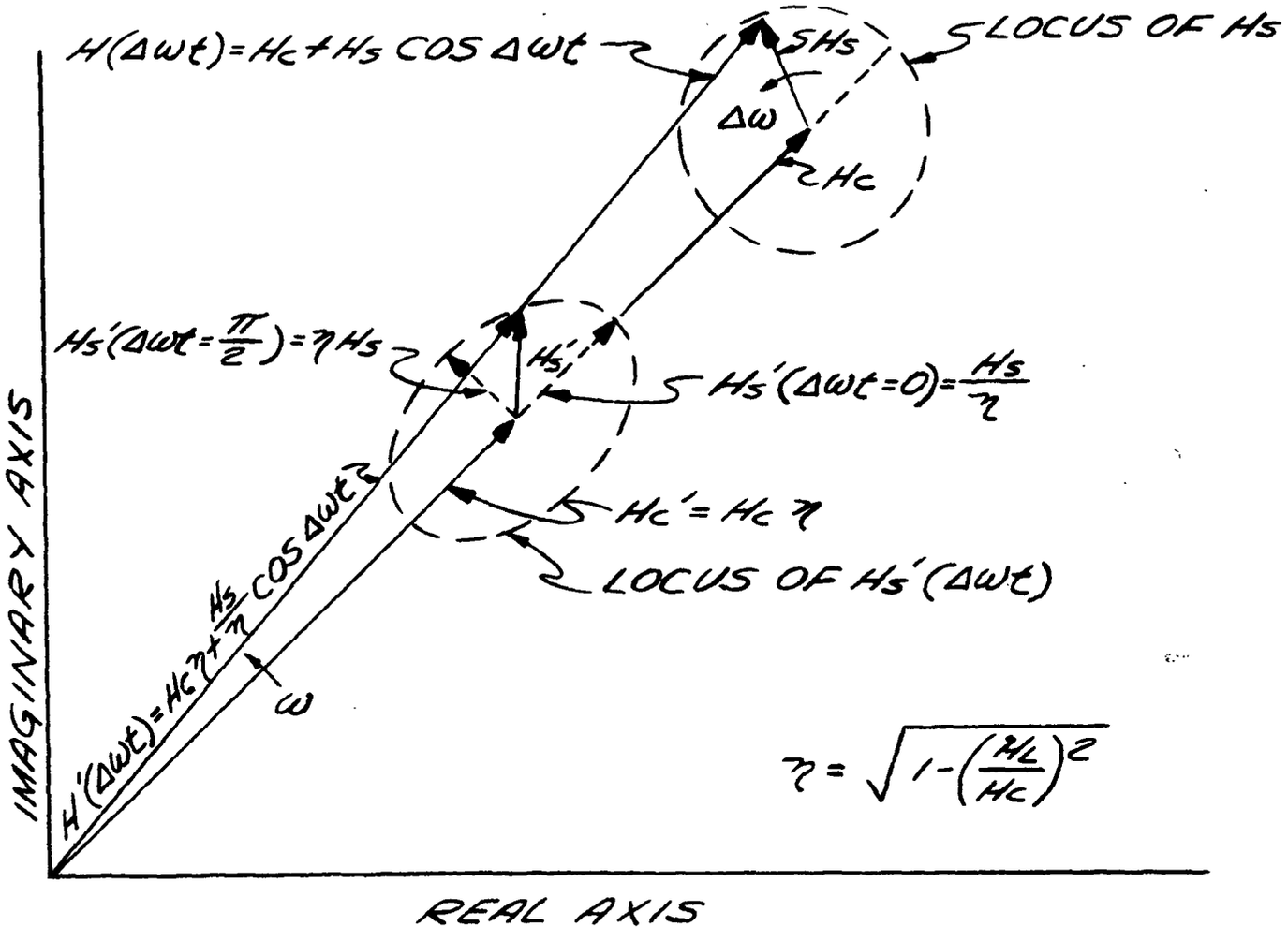

FIGURE 5.

Case of single sideband input fields (unprimed), showing graphical construction of instantaneous output fields after absorption in CLA medium. Relation between input field, $H(\Delta\omega t)$, and output field, $H'(\Delta\omega t)$, is $H'(\Delta\omega t) = \sqrt{H^2(\Delta\omega) - H_L^2}$ where H_L^2 represents constant loss in absorbing medium.

Let us further assume no dispersion so the phase of the vector remains unchanged as a result of going through the non-linear medium. We can find the path of the output vector as shown in Fig. 5. It is seen that the vector H_s' of the output field can no longer be represented by a single Fourier component and,because of its changing magnitude, a second sideband is generated. As a matter of fact, for large amplification ($\eta < 1$) we approach a condition of pure amplitude modulation and the output has two sidebands of equal amplitude. For $\eta = 1$ there is only one sideband. At intermediate values of η we can approximate the two sideband amplitudes by the values $(\frac{1}{\eta} + \eta)\frac{H_s}{2}$ and $(\frac{1}{\eta} - \eta)\frac{H_s}{2}$. This is shown in Fig. 6. As the power loss is increased in the amplifying medium both sidebands increase, but the "image" sideband grows at a more rapid rate until the two sidebands are of equal amplitude and an amplitude modulated output wave results.

An example of a medium which exhibits a constant loss property at low frequencies is a thermistor whose idealized voltage current and power absorption characteristics are represented in Fig. 7. If the thermistor is biased in the saturation region by a dc voltage, V_{dc}, and a small ac voltage, V_s is superimposed as shown in Fig. 8, the relation $V_{dc}V_s = V_{dc}'V_s'$ follows from the graphical considerations of Fig. 9. Another mode of operation which has not received much attention in the past is to bias the thermistor with an rf signal, V_c, as in Fig. 10 and then superimpose small sidebands, V_s, to give an amplitude modulated signal. If the modulation frequency is low enough compared to the thermal relaxation time, T, of the device, Fig. 1 is applicable and the

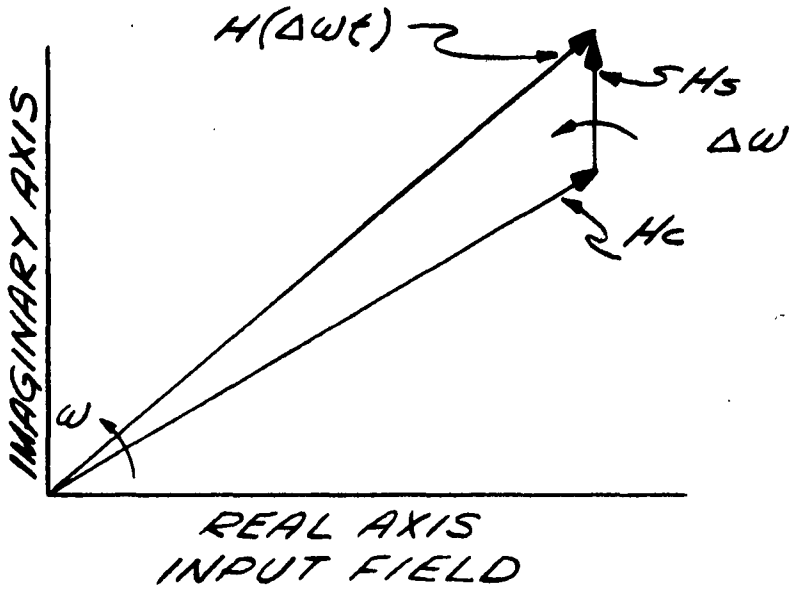

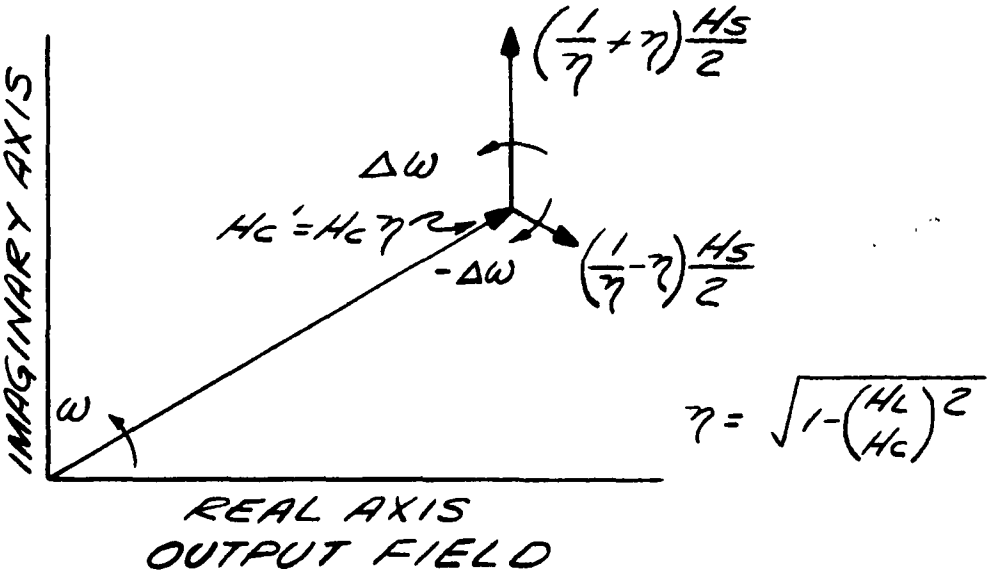

FIGURE 6.

Case of single sideband input signal showing Fourier components of output signal, H'(Δωt). Note generation of second sideband by nonlinear absorption.

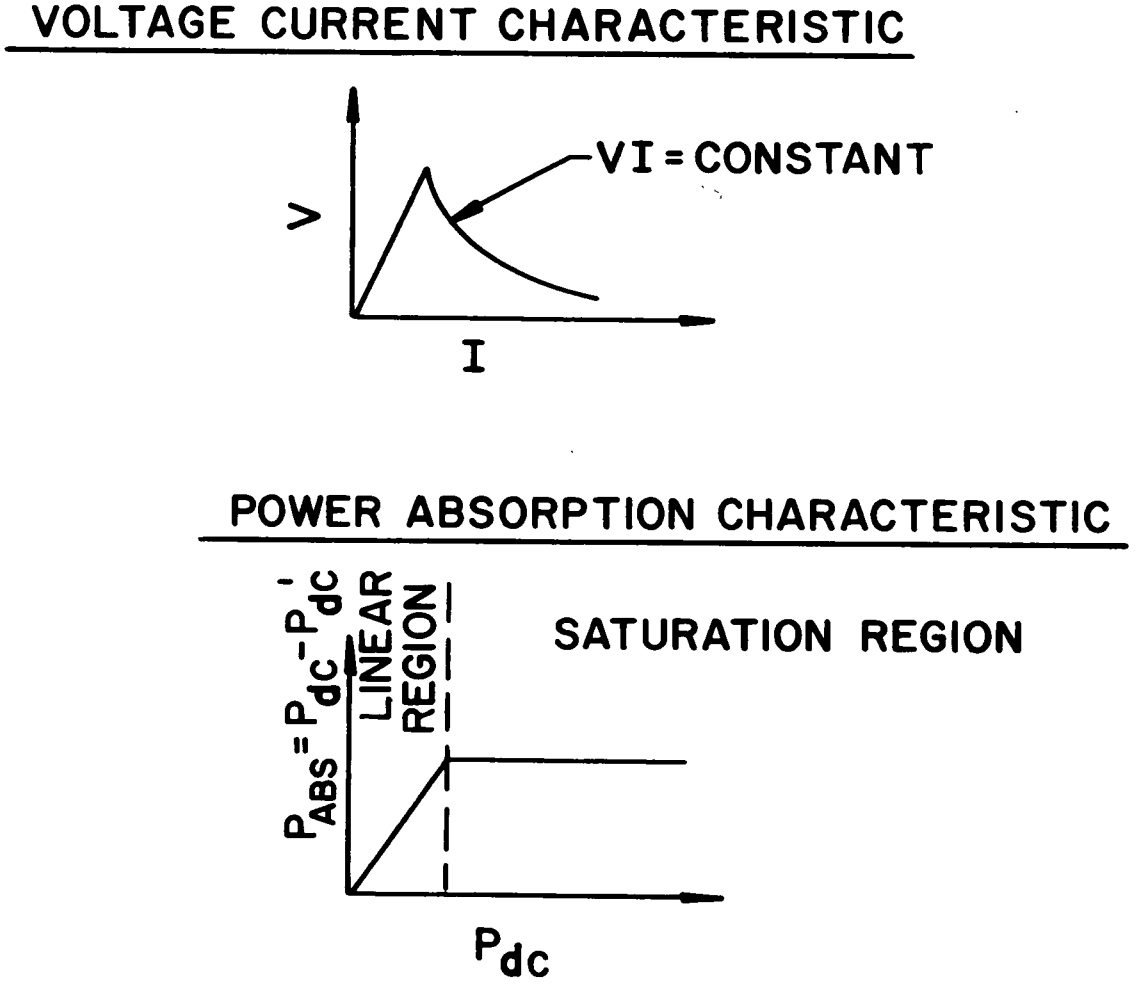

FIGURE 7. Idealized Characteristics of a Thermistor

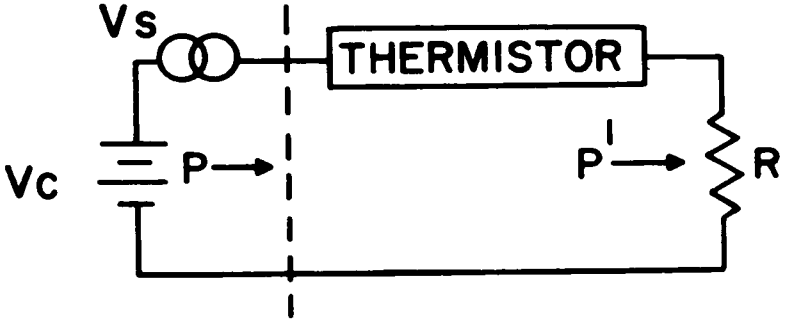

$I_{dc} R >>$ VOLTAGE ACROSS THERMISTOR

$V_s << V_{dc}$

$$P = (V_{dc}^2 + 2 V_{dc} V_s \cos \Delta\omega t)/R$$

$$P' = (V_{dc}'^2 + 2 V_{dc}' V_s' \cos \Delta\omega t)/R$$

IF $\Delta\omega < \frac{1}{T}$ AND V_{dc} SUFFICIENT TO SATURATE,

$$V_{dc}' V_s' = V_{dc} V_s$$

Figure 8. Thermistor Amplifier with dc Bias

Figure 9. Graphical Gain Derivation for Figure 8.

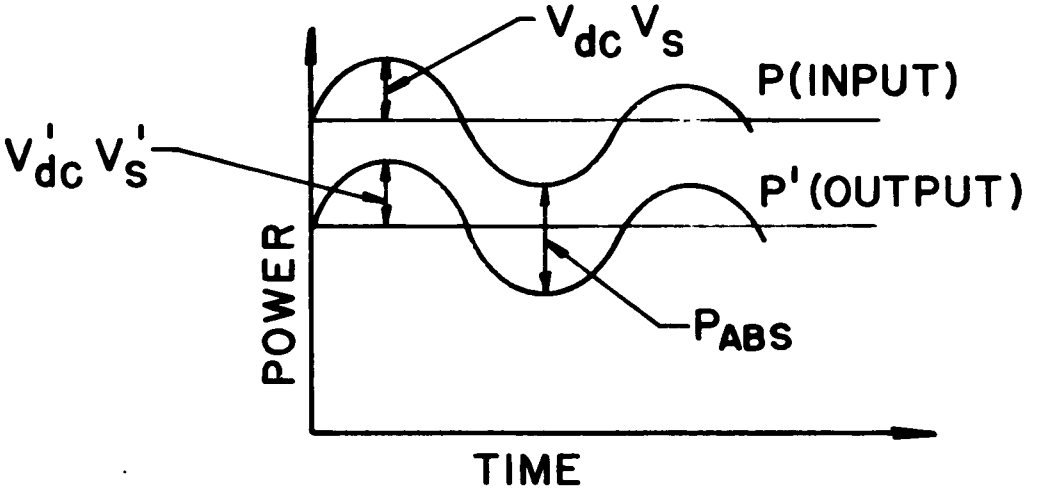

THEREFORE $V_{dc}V_s = V'_{dc}V'_s$ AND $P_{dc}\,P_s = P'_{dc}\,P'_s$

SO THAT

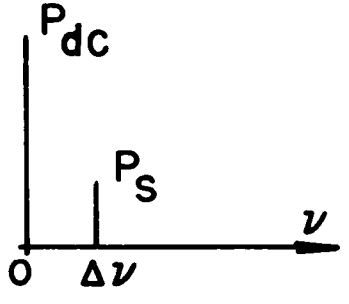

INPUT POWER SPECTRUM

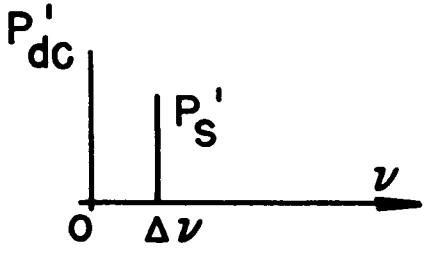

OUTPUT POWER SPECTRUM

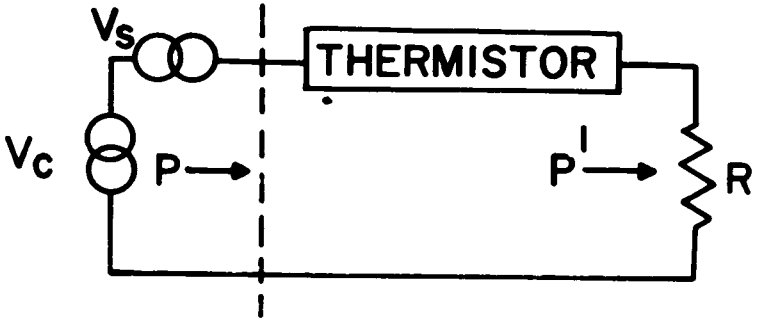

$V_s \ll V_c$

V_c AT FREQUENCY ν AMPLITUDE MODULATED AT $\Delta\omega$

$$P = \left[\left(V_c^2 + 2 V_c V_s \cos \Delta\omega t\right) \cos^2 \omega t\right] / R$$

$$P' = \left[\left(V_c'^2 + 2 V_c' V_s' \cos \Delta\omega t\right) \cos^2 \omega t\right] / R$$

IF $\Delta\omega < \frac{1}{T}$ AND V_c SUFFICIENT TO SATURATE,

$$V_c' V_s' = V_c V_s$$

Figure 10. Thermistor Amplifier with rf Bias

same line of reasoning as used previously yields the result $V_c'V_s' = V_cV_s$. The thermistor is therefore a CLA medium although it is not practical for mm-wave applications.

When the thermistor is operated with rf bias the non-linearity of the medium is only evident when amplitude of the bias signal is changed. The thermistor will not distort an incident sine wave or generate new harmonics. This type of non-linearity, therefore, differs from that encountered in parametric amplifiers.

Another class of media which exhibit a constant power loss are those having atomic and molecular microwave absorption spectra which can be saturated and whose relaxation times are short compared to the modulation period and long compared to the local oscillator period. The saturation of a microwave transition between two energy levels can be briefly described as follows: At equilibrium, in the absence of radiation, we have the Boltzmann condition that there are more atoms in the lower energy state, 0, than in the higher energy state, 1. When the material is irradiated the probability for an atom to make a transition from state 0 to state 1 (induced absorption) is equal to that from state 1 to state 0 (induced emission) so that there will be a net transfer of atoms from the lower to upper state and a net absorption of energy from the electromagnetic field. But as more atoms are transferred to the upper state the population difference is decreased and the medium becomes transparent. It cannot absorb more power than that required to equalize the state populations. Under these conditions the resonance is said to be saturated. This mechanism establishes the constant loss property which is needed to obtain amplification.

In order to obtain a quantitative expression for the effect of the resonant medium on the local oscillator and incoming information signal we will first consider a monochromatic plane wave, with a field (electric or magnetic) $H(t) = H \cos \omega_o t$, propagating in a z-direction through an infinite medium which has a resonant absorption at the frequency ω_o. If the field is weak enough so that it does not disturb the equilibrium populations in the lower and upper state we can apply Poynting's theorem to a differential slab of thickness dz to obtain the expression[4]

$$\frac{1}{H^2} \frac{dH^2}{dz} = - \alpha_\ell \qquad (1)$$

where α_ℓ is an attenuation constant which depends on the parameters of the medium and is independent of the field amplitude. Under these conditions, the power per unit area is attenuated according to Lambert's Law as $\exp(-\alpha_\ell z)$. As the field is increased the resonance begins to saturate and Eq. 1 must be modified[4] to read

$$\frac{1}{H^2} \frac{dH^2}{dz} = - \frac{\alpha_\ell}{1 + H^2/H^2_{sat}} \qquad (2)$$

where H^2_{sat} is a constant which depends on the dipole moment and relaxation times of the medium and is independent of the field amplitude. The

---

(4) C.H. Townes and A.L. Schawlow, Microwave Spectroscopy, (McGraw Hill Book Co.,Inc., New York, 1955), p.371.

saturation properties of the medium are evident from Eq. (2). Keeping in mind that the power is proportional to the field squared, we see that at low fields the expressions (1) and (2) agree but at high fields the power absorbed per unit length is a constant value proportional to $\alpha_\ell H^2_{sat}$. This condition is termed resonance saturation and in this power range the medium has the necessary properties for CLA operation.

Let us now consider the combined incoming radiation consisting of the local oscillator and information signal:

$$H(t) = H_c \cos \omega_c t + (H_s/2)\cos\ (\omega_o + \Delta\omega)t + (H_s/2)\cos\ (\omega_o - \Delta\omega)t. \qquad (3)$$

This expression can be rewritten as

$$H(t) = (H_c + H_s \cos \Delta\omega t) \cos \omega_o t. \qquad (4)$$

If the changes in field amplitude represented by the term in the parenthesis of the above expression are slow enough compared to relaxation time of the medium, Eq. (2) is valid at all times and we have a quasi-static approximation. If $H_s \ll H_c$ we can substitute into Eq. (2)

$$H^2 = H_c^2 + 2H_cH_s\cos \Delta\omega t. \qquad (5)$$

Collecting terms of the same frequency, we obtain, to first order in H_s/H_c

$$\frac{1}{H_c^2}\frac{dH_c^2}{dz} = -\xi^2\alpha_\ell \tag{6}$$

and

$$\frac{1}{H_s^2}\frac{dH_s^2}{dz} = (\xi^2 - 2\xi^4)\alpha_\ell \tag{7}$$

where $\xi^2 = (1 + H_c^2/H_{sat}^2)^{-1}$ is a saturation parameter which varies between one (weak field) and zero (strong field). At weak field ($\xi^2 = 1$) both the local oscillator and sideband signal are attenuated similarly. As the local oscillator field, H_c, is increased the attenuation of the sidebands (Note Eq. (7)) goes through zero ($\xi^2 = \frac{1}{2}$) and becomes a gain. This gain reaches a maximum value at $\xi^2 = \frac{1}{4}$ and then begins to decrease. As $\xi^2 \to 0$, the medium becomes fully saturated and we have from Eq. (6) and Eq. (7),

$$\frac{d}{dz}(H_cH_s) = 0.$$

Therefore, for a finite length $H_c'H_s' = H_cH_s$ or $P_c'P_s' = P_cP_s$ in agreement with our previously derived results. It should be noted that the maximum gain occurs at $H_c^2 = 3H_{sat}^2$ and not at $H_c^2 \gg H_{sat}^2$. The reason for this is that the attenuation approaches one as the input power becomes very large; therefore the gain also approaches one. Thus at very large input powers the medium becomes transparent to all the incident signals.

If the frequency deviation, $\Delta\omega$, is greater than the inverse of the relaxation time, the above analysis is not valid. The Fourier components of the oscillating dipole moment induced by the microwave field must then be calculated by a perturbation method to determine the effect of the medium on the transmitted wave. This type of analysis has been performed for the case of frequency modulated sidebands where the saturating signal field is too weak to alter the Boltzmann population distribution, and thus saturate the resonance.[5] We have extended this analysis in Appendix II to consider the form of Equations (6) and (7) as $\Delta\omega$ is increased. The results are given in Eq. II-14 and II-15 of Appendix II which are reproduced here.

$$\frac{1}{H_c^2}\frac{dH_c^2}{dz} = -\xi^2\alpha_\ell \tag{8}$$

$$\frac{1}{H_s^2}\frac{dH_s^2}{dz} = \frac{x}{\Delta}\xi^2\alpha_\ell \tag{9}$$

where

$$\frac{x}{\Delta} = \frac{y^2 - 1 - \alpha^2\beta^2 - \alpha\beta^2 y}{(1+y)^2 + \beta^2 + \beta^4\alpha^2 - 2\alpha\beta^2 y + \beta^2\alpha^2}$$

where $y = H_c^2/H_{sat}^2$, $\beta = \Delta\omega T_2$ and $\alpha = T_1/T_2$. If $\alpha \gg 1$, we can rewrite

---

(5) A. Karplus, Phys.Rev. 73, 1027 (1948)

the above as

$$\frac{x}{\Delta} \approx \frac{(y^2 - 1) - \alpha^2\beta^2}{(y^2 + 1) + \alpha^2\beta^2} \quad . \tag{10}$$

Since $y^2 - 1$ will be of the order of magnitude of ten for reasonable gains the bandwidth will be limited by the condition $\Delta\omega T_1 < 10$. This implies that the bandwidth will indeed be limited by the long spin lattice relaxation time.

For the case of a molecular gas where $\alpha = 1$, Expression (9) can be rewritten as

$$\frac{1}{H_s^2}\frac{dH_s^2}{dz} = \left(\frac{\xi^2 - 2\xi^4 - \beta^2\xi^4}{1 - 2\beta^2\xi^2 + 4\beta^2\xi^4 + \beta^4\xi^4}\right)\alpha_\ell = \frac{x}{\Delta}\xi^2\alpha_\ell \tag{11}$$

where $\beta = \Delta\omega T$ where T is the collisional relaxation time. The quantity $\frac{x}{\Delta}\xi^2$ is plotted in Fig. 11 as a function of β for several values of ξ^2.

Equation (6) for local oscillator attenuation and equation (7) for information signal gain can be derived in a waveguide filled (or partially filled) with a CLA medium with the following straightforward modifications of the above analysis. In applying Poynting's theorem (Eq. (1) or Eq. (2)), the attenuation, α_ℓ, will be changed by the ratio of the group velocity of the radiation in the infinite medium to that in the waveguide. Furthermore, there will be an extra term, α_w, on the right hand side of Eq. (1) and Eq. (2) to account for the wall losses. Finally, the field will vary over the guide cross section so that the

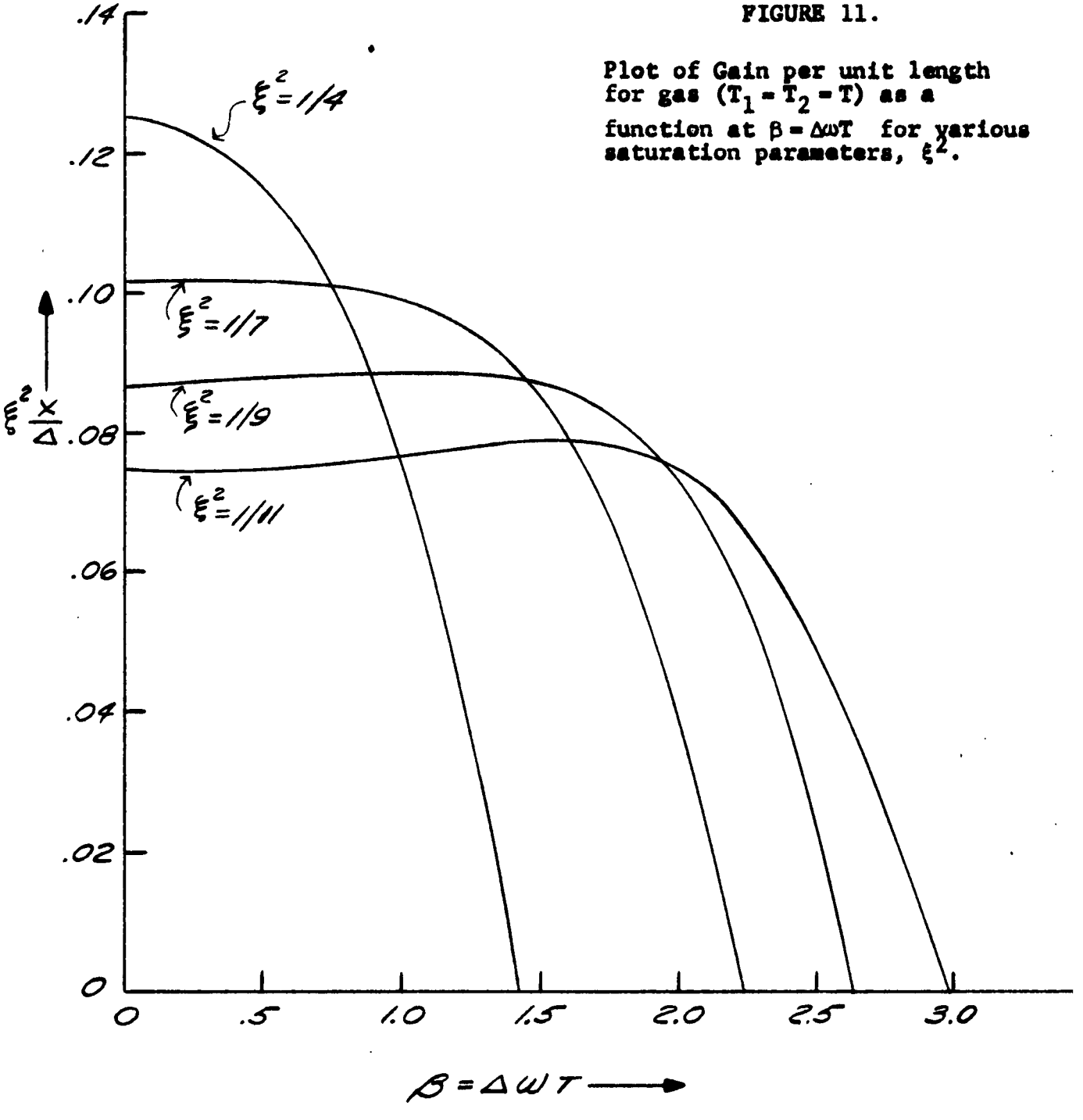

FIGURE 11.

Plot of Gain per unit length for gas ($T_1 = T_2 = T$) as a function at $\beta = \Delta\omega T$ for various saturation parameters, ξ^2.

degree of saturation will be a function of the transverse as well as the longitudinal coordinates in the guide. The local oscillator and information signal power attenuation and gain can be found by integrating Expression (6) and (7) over the guide cross section and length.

When the field at a given guide cross section does not vary across the CLA medium the integrations may be performed explicitly. The quasi-static Equations (6) and (7) including wall losses (α_w) are integrated to obtain

$$-(\alpha_\ell+\alpha_w)z = (\alpha_\ell/\alpha_w)\ell n\left\{\left[(1+\alpha_\ell/\alpha_w)(P_{sat}/P_c)+P_c'/P_c\right]\left[(1+\alpha_\ell/\alpha_w)(P_{sat}/P_c)+1\right]^{-1}\right\}+\ell n(P_c'/P_c) \tag{12}$$

which yields the local oscillator attenuation P_c'/P_c as a function of $(\alpha_\ell+\alpha_w)z$, α_ℓ/α_w and P_c/P_{sat} where $P_c/P_{sat} = H_c^2/H_{sat}^2$. The information signal gain becomes

$$P_s'/P_s = (P_c'/P_c)(1+P_c/P_{sat})^2(1+P_c'/P_{sat})^{-2}(1+\alpha_\ell/\alpha_w+P_c'/P_{sat})^2 \times (1+\alpha_\ell/\alpha_w+P_c/P_{sat})^{-2} \tag{13}$$

These equations are plotted for various values of $(\alpha_\ell+\alpha_w)z$ and α_ℓ/α_w in Fig. 12 and Fig. 13.

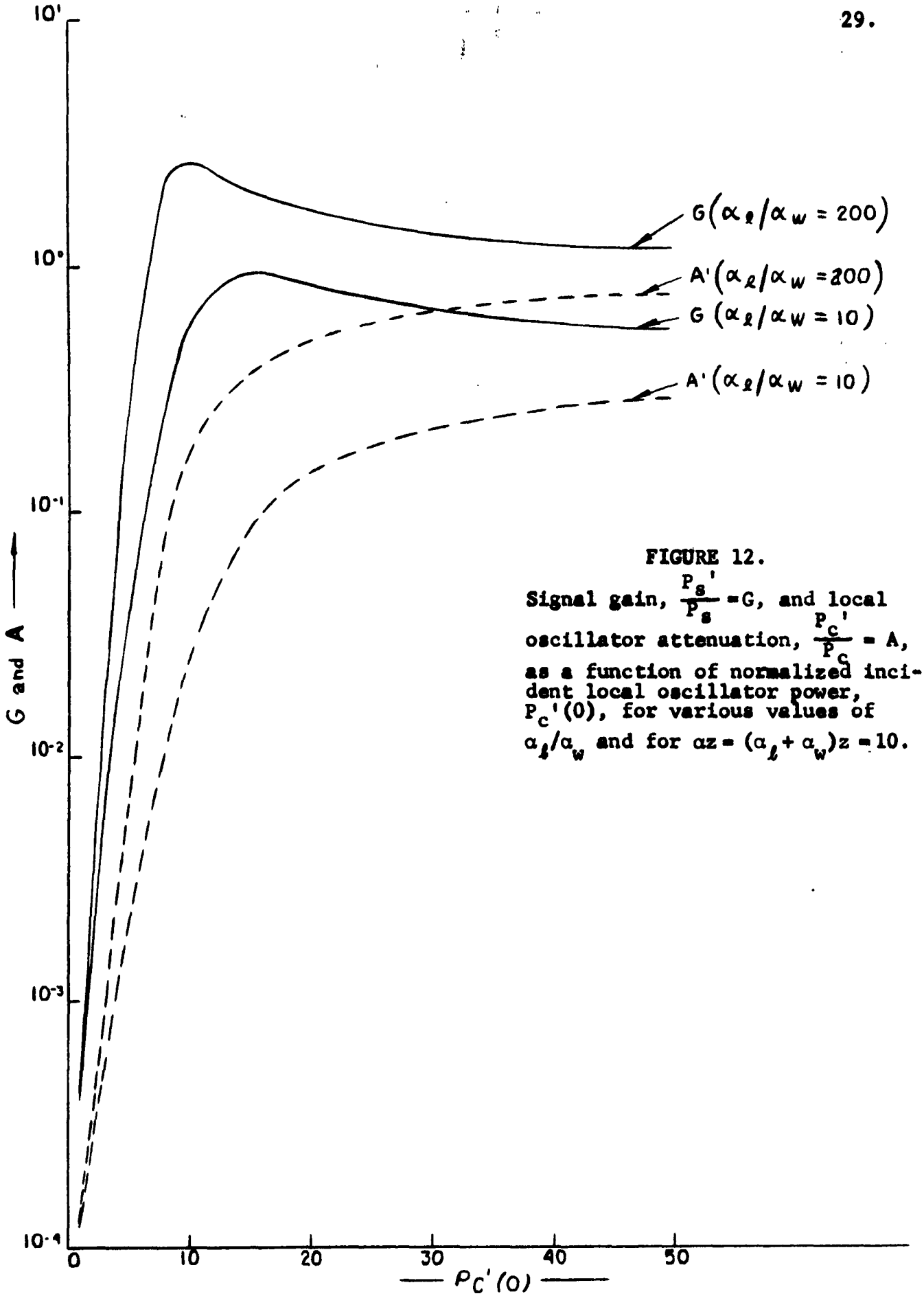

FIGURE 12.

Signal gain, $\frac{P_s'}{P_s} = G$, and local oscillator attenuation, $\frac{P_c'}{P_c} = A$, as a function of normalized incident local oscillator power, $P_c'(0)$, for various values of α_ℓ/α_w and for $\alpha z = (\alpha_\ell + \alpha_w)z = 10$.

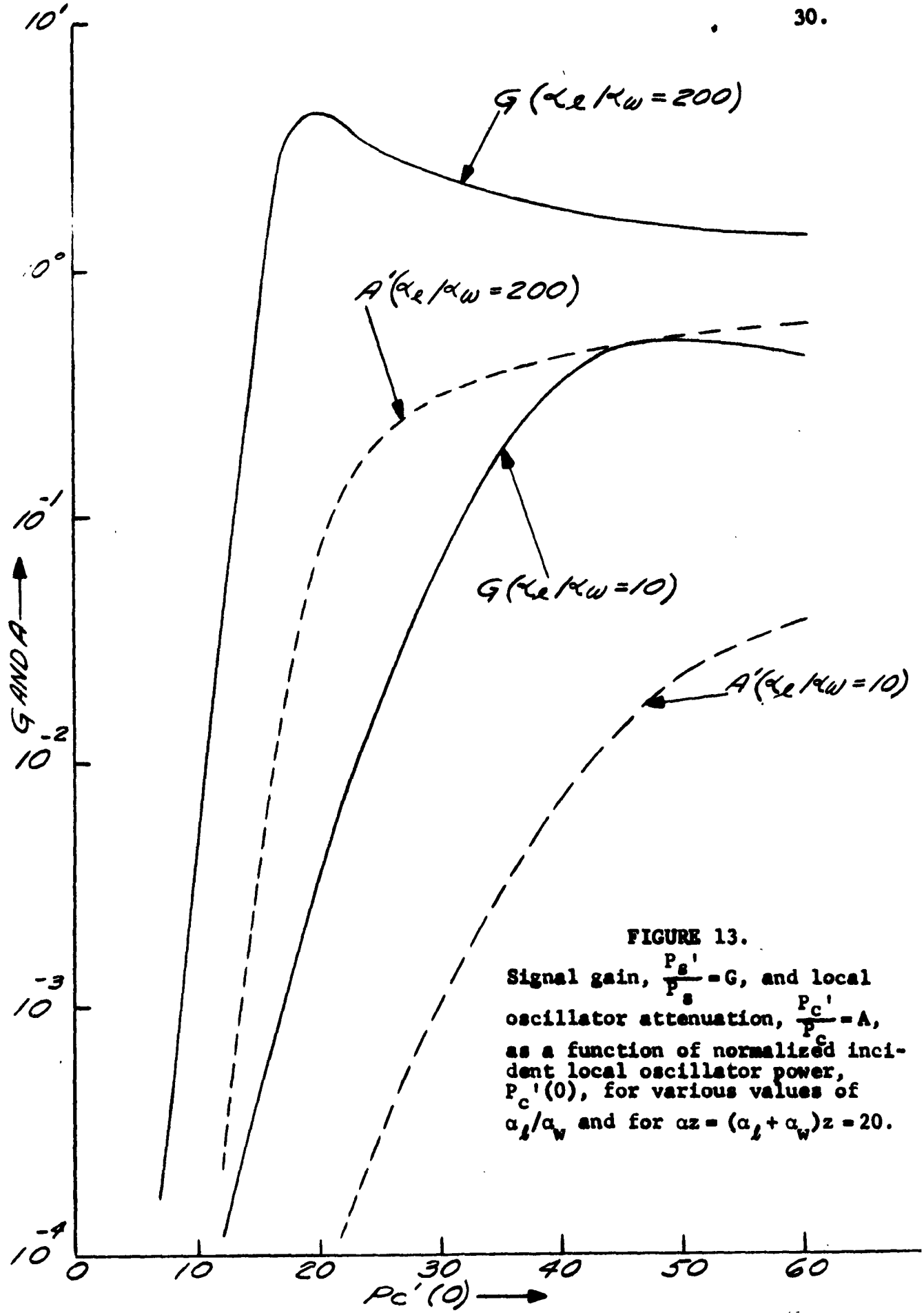

FIGURE 13.

Signal gain, $\frac{P_s'}{P_s} = G$, and local oscillator attenuation, $\frac{P_c'}{P_c} = A$, as a function of normalized incident local oscillator power, $P_c'(0)$, for various values of α_ℓ/α_w and for $\alpha z = (\alpha_\ell + \alpha_w)z = 20$.

As $(\alpha_\ell + \alpha_w)z$ is increased, the signal gain increases until P_s'/P_s reaches a maximum value of $\alpha_\ell/(16\alpha_w)$ and then begins to decrease. This is due to the fact that as the guide is made longer and longer the input power has to be increased accordingly to maintain saturation and when this input power becomes too large the gain per unit length is insufficient to compensate for the linear losses.

When the field at a given guide cross section does vary over the guide cross section the Equations (6) and (7) must be integrated numerically.[1]

3. Amplifier Structure

The experiment was performed using iron doped rutile as the active material in a travelling wave structure. Before discussing the amplifier design let us briefly consider the energy levels of the material. The electronic configuration of the outer shell of the Fe^{+++} ion is $3d^5$, which on application of Hund's Rule, yields a $^6S_{5/2}$ ground state. Since an odd number of electrons are involved, each energy level under the influence of the crystalline electric field must be at least doubly degenerate according to Kramer's Rule. In the particular case of Fe^{+++} in TiO_2 the ground state is composed of three Kramer's doublets. The energy level diagram has been previously investigated(6) and the two upper doublets are shown in Figure 14. The different quantum states are designated by S_m, the component of spin angular momentum (in units of Planck's Constant) along the crystal field symmetry axis. The three doublets are characterized by the values $S_m = 5/2$, $3/2$ and $1/2$. In Figure 14 the energy levels are designated by their "weak" (magnetic) field quantum numbers. Thus at weak fields the magnetic dipole transitions, which determine the microwave absorption spectrum, obey the selection rule $S_m = \pm 1$. At strong (magnetic) field, where curvature of the levels in Figure 14 is evident, the above selection rule breaks down. The rate at which the frequency changes with the field in the linear Zeeman region is 296 Mc/gauss which is somewhat greater than the 2.80 Mc/gauss of the free electron. This difference is due to the perturbing influence of the crystalline electric field.

---

(6) D. Carter and A. Okaya, Phys. Rev. 118, 1485 (1960).

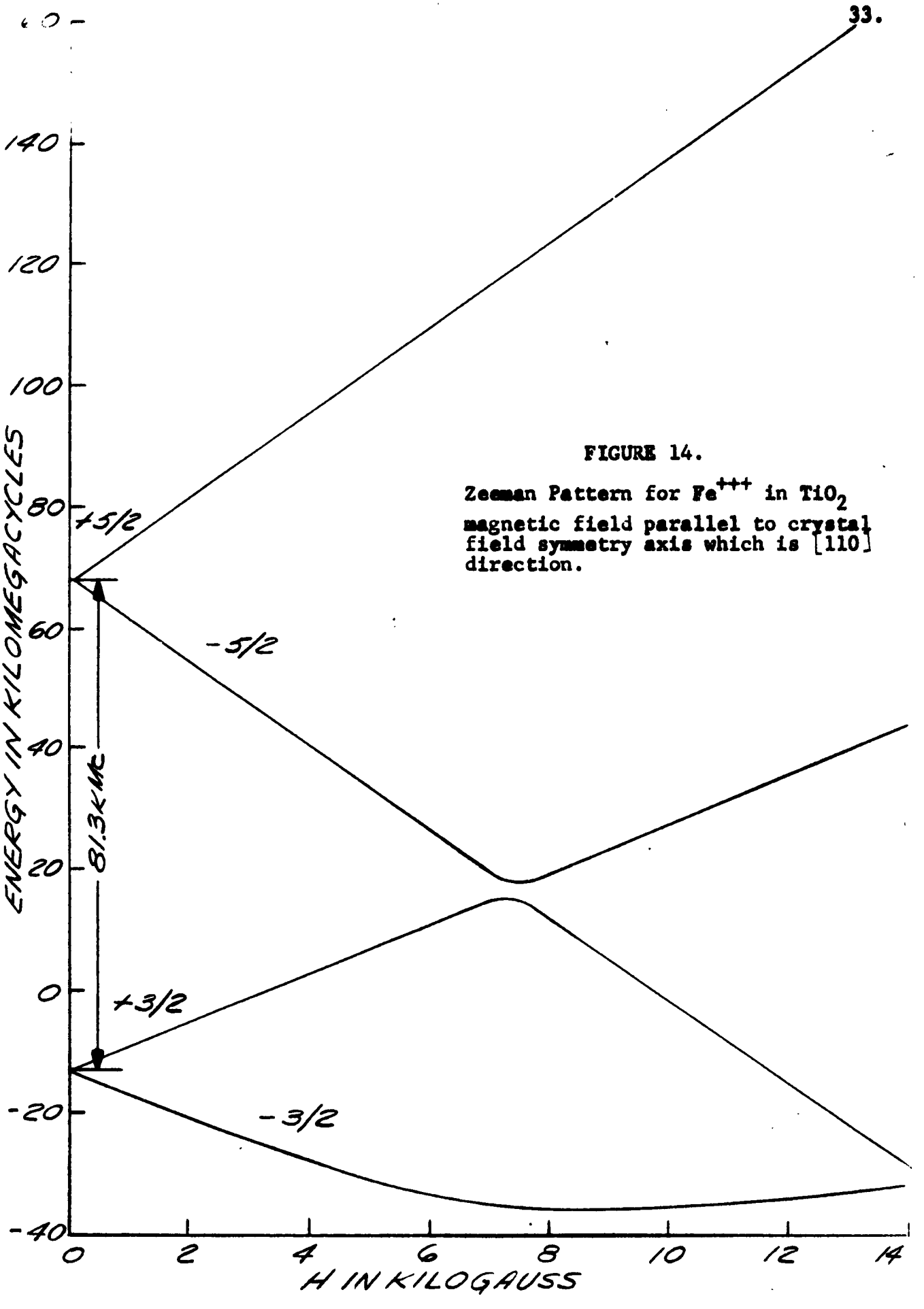

FIGURE 14.

Zeeman Pattern for Fe^{+++} in TiO_2 magnetic field parallel to crystal field symmetry axis which is [110] direction.

The active medium consists of a slab of iron doped rutile in between two slabs of clear rutile. The entire sandwich is located in a rectangular guide as shown in Figure 15. A photograph in the y-direction is shown in Figure 16. The match to air-filled guide is accomplished with quartz and clear rutile transition sections as is shown in Figure 17. A picture of a unit encapsulated in a metal waveguide is shown in Figure 18. The dimensions of the center (amplifier) section are 0.400 x 0.015 x 0.007 inches.

In order to facilitate the testing of this principle and to achieve a tunable device, a superconducting electromagnet was built to provide a maximum field of 8 kilogauss over the active amplifier region with a magnet current of approximately 3 amperes.

Since the amplifier section is small a rather small magnet gap can be used. The magnet gap width is determined by the 0.007 inch amplifier dimension and is 0.030 inch in magnitude. This will then reduce the number of ampere turns required to establish the magnetic field. A schematic of the magnet design is shown in Figure 19. Four hundred turns of 0.003" Niobium wire are used for the winding. This type of magnet with a 1/4 inch gap was originally proposed by S. Autler[7] at Lincoln Laboratory. The Niobium wires can be insulated with 0.002" of nylon coating. The magnet dimensions are given in Figure 19. The gold coating was required to avoid corrosion which is a considerable problem in light of the exposure to moisture

---

(7) S. H. Autler, Rev. Sci. Inst. 31, 369 (1960).

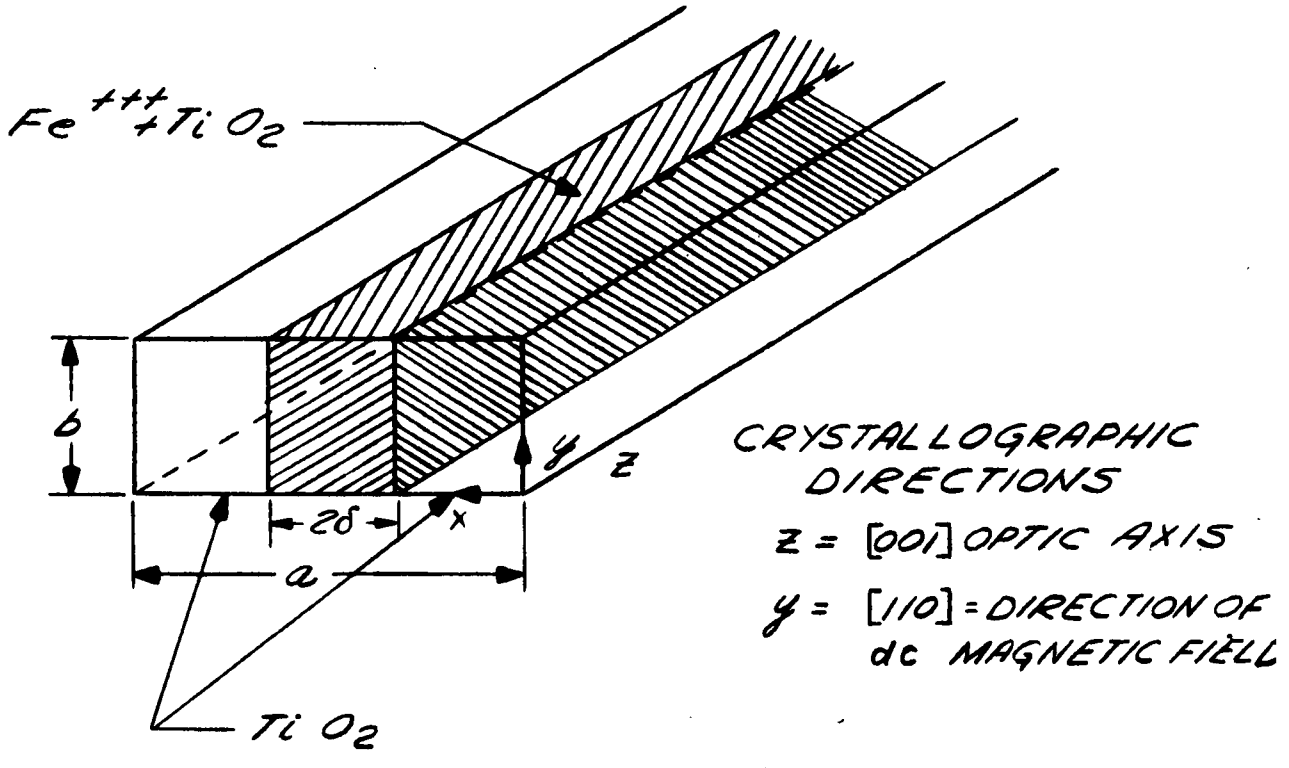

FIGURE 15.

Rutile-filled waveguide cross-section showing the iron doped region and the crystallographic directions.

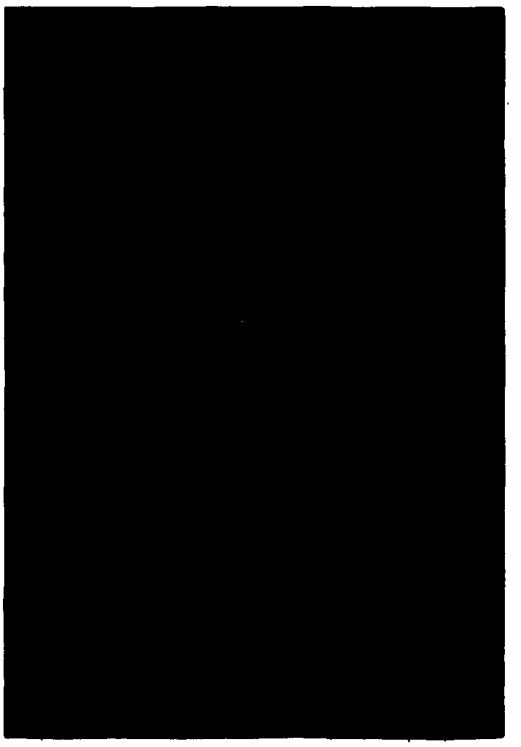

Fig. 16

Plan view of rutile amplifier section
Total width is .015 inches

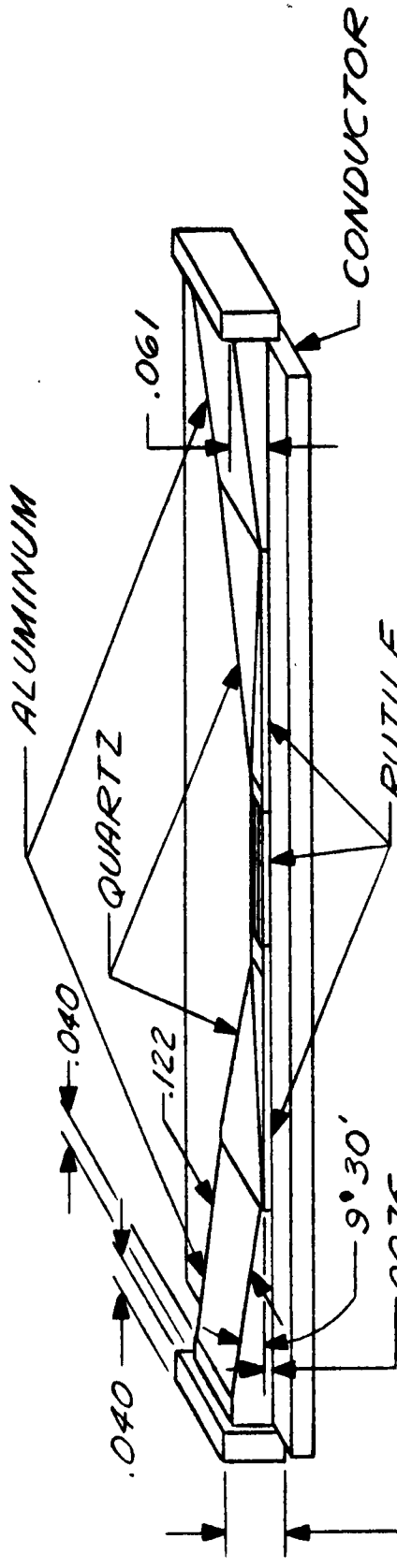

FIGURE 17.

Schematic of CLA Test Unit. (All dimensions in inches.)

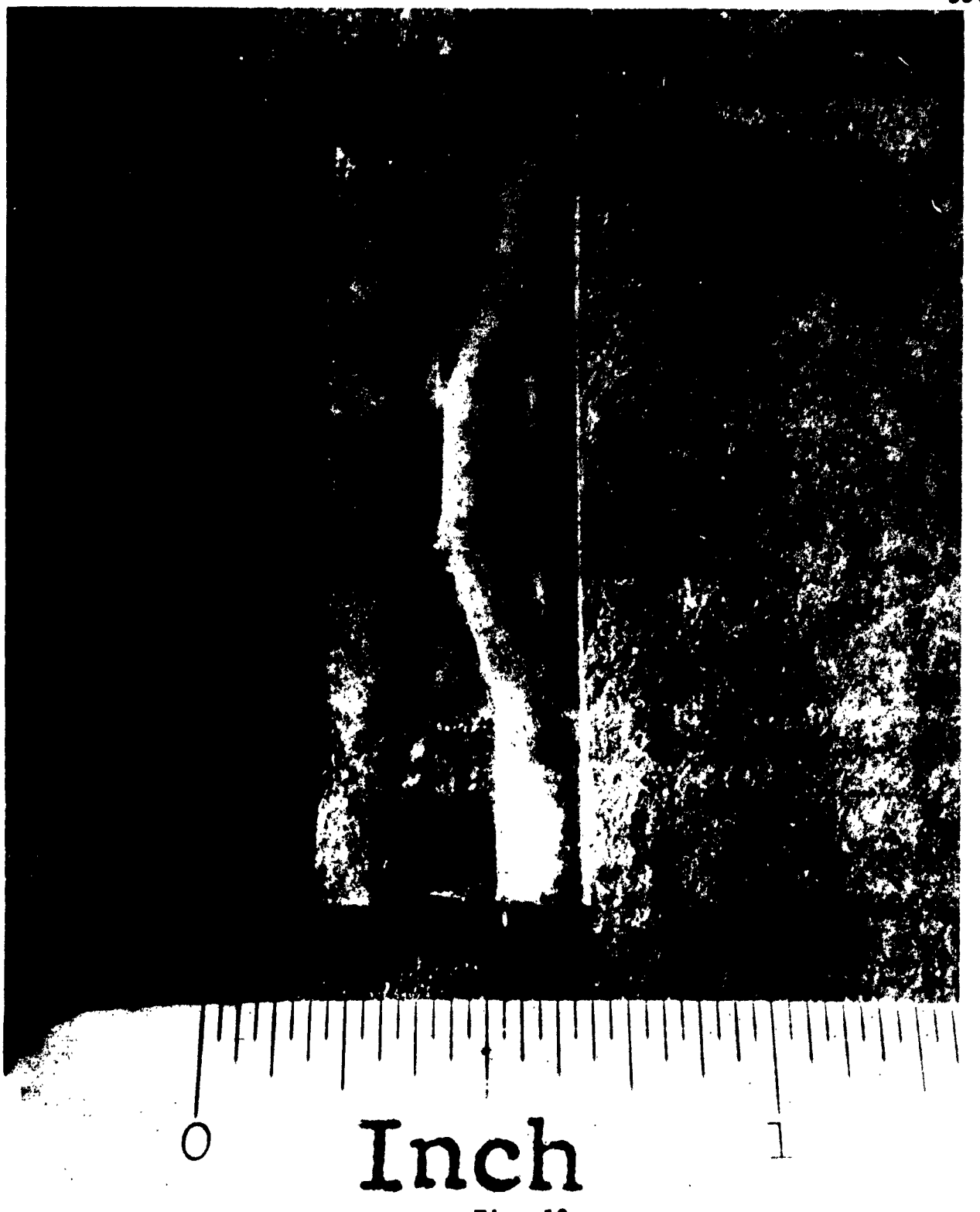

Fig. 18

Encapsulated Amplifier

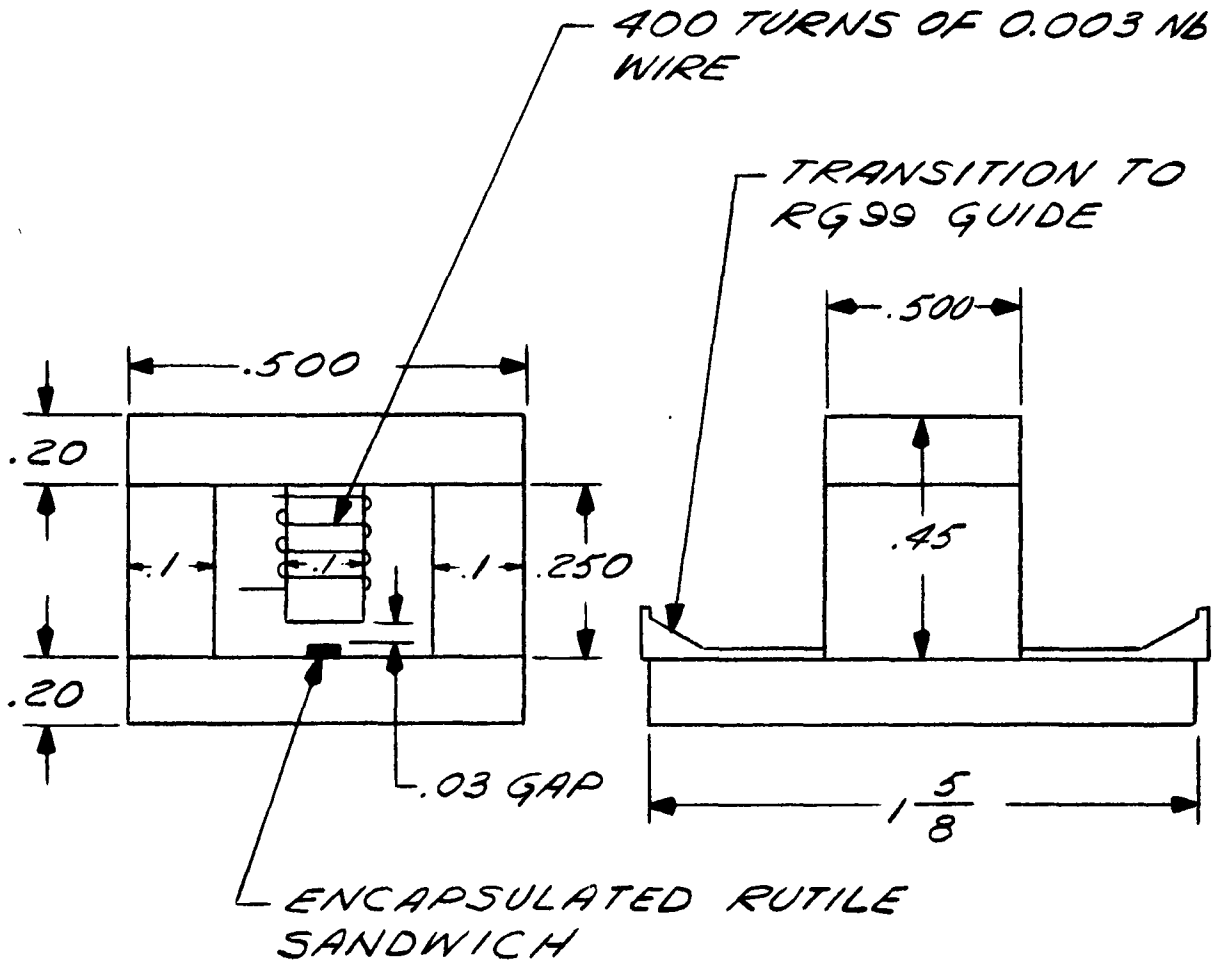

FIGURE 19.

Schematic of Magnetically Tuned CLA

when the magnet is removed from its liquid helium container. To achieve the required degree of homogeneity of the magnetic field stringent tolerances requirements must be met. The magnet gap faces are ground to an optical one wavelength flat as was checked by light interference techniques. Parallelism was controlled by auto-collimation techniques which have a precision of 20 seconds of arc.

The resultant magnetic field vs. current was measured at room temperature using a Hall Effect Meter with a 0.020" probe which can be inserted in the gap. Since the susceptibility at low temperatures[8] is smaller than the room temperature susceptibility, the above result can only be used as a guide. The estimated sensitivity is 3 gauss/ma. This was checked at low temperatures using both the magnet and the amplifier. Since the g value of rutile is known[6], the Zeeman frequency splitting gave a confirmation of the magnetic field as a function of current at liquid helium temperatures.

Since the sensitivity of the magnet is about 3 gauss/ma and the spectral line to be used for amplifier operation moves at the rate of approximately 3 Mc/gauss the amplifier tuning factor was 9 Mc/ma.

The encapsulated unit and magnet in position are shown in Figure 20. The large coil around the waveguide (covered with glass wool sleeving) is a heater which is used to bake out the CLA device in the dewer.

---

(8) R. M. Bozorth, Ferromagnetism (D. Van Nostrand Co., N.Y. 1951).

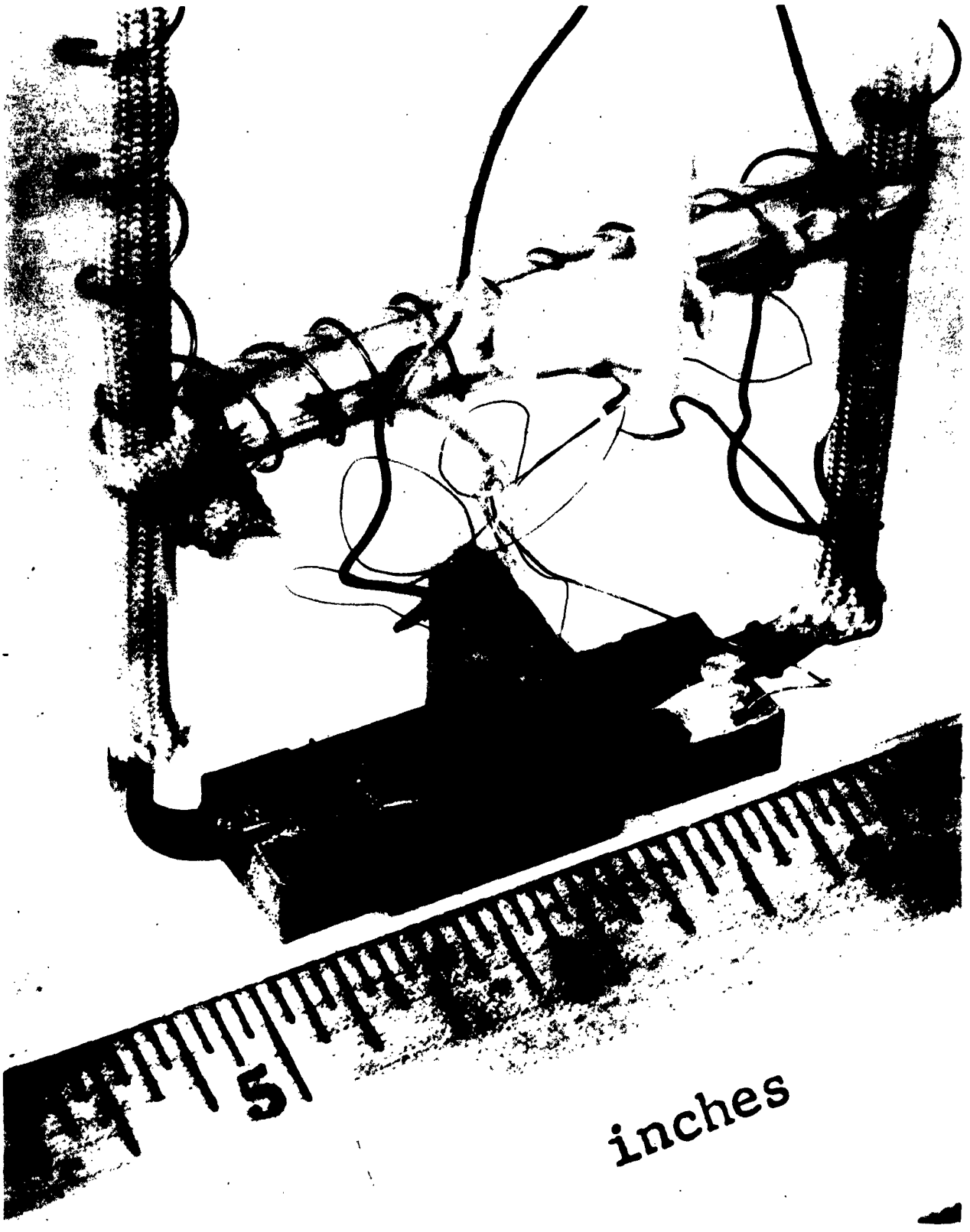

Fig. 20
Amplifier and Tuning Magnet Assembly

4. Experimental Results

In order to measure the amplifier gain and local oscillator attenuation the microwave circuit shown schematically in Figure 21 and pictorially[9] in Figure 22 was used. The frequency generator consists of a stabilized ($1:10^7$) klystron which delivers about 20 mw of power at 81.3 kMc. The generator supplies the local oscillator power P_c through a variable precision attenuator. A side arm with a 70 cps audio amplitude modulated switch supplies the information signal components P_s and the unwanted carrier P_c''. Since the local oscillator power P_c is at least 20 db greater than P_c'' the signal entering the amplifier is composed of the local oscillator signal P_c and the information signal sidebands P_s separated from the local oscillator by the frequency $\Delta\omega$. The phase shifter in the side arm permits the sidebands to be phased for either amplitude modulation ($\phi = 0$) or frequency modulation ($\phi = \pi/2$) of the local oscillator signal. After passing through the CLA the microwave energy is detected by homodyning with the signal P_H in a square law detector (barretter) to yield an output $\sqrt{P_H P_s'}$ at a frequency of 70 cps. To facilitate our discussion we will call this signal H_s' since it is actually proportional to the field. The attenuation of the local oscillator was measured by disconnecting the signal arm and switching the incoming pump, P_c, on and off at the rate of 70 cps by a ferrite switch. The outgoing pump, P_c', is then combined with the homodyne

---

(9) All components in this picture were made under the supervision of A. Simmons of the Component Group of TRG in Boston. In the experiment the balance arm was not used and the crystal modulator was replaced by a ferrite switch.

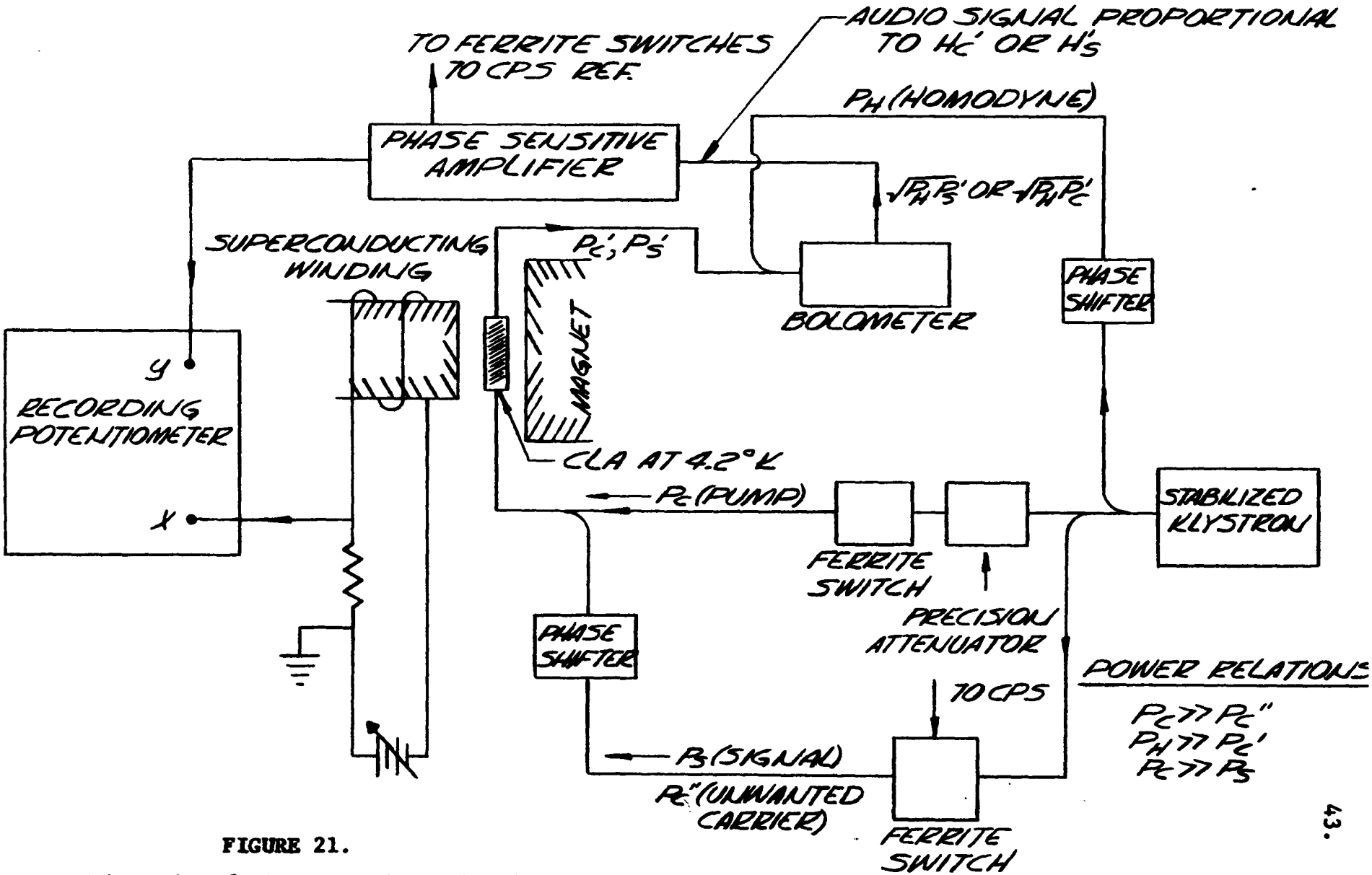

FIGURE 21.

Schematic of Microwave Test Circuit

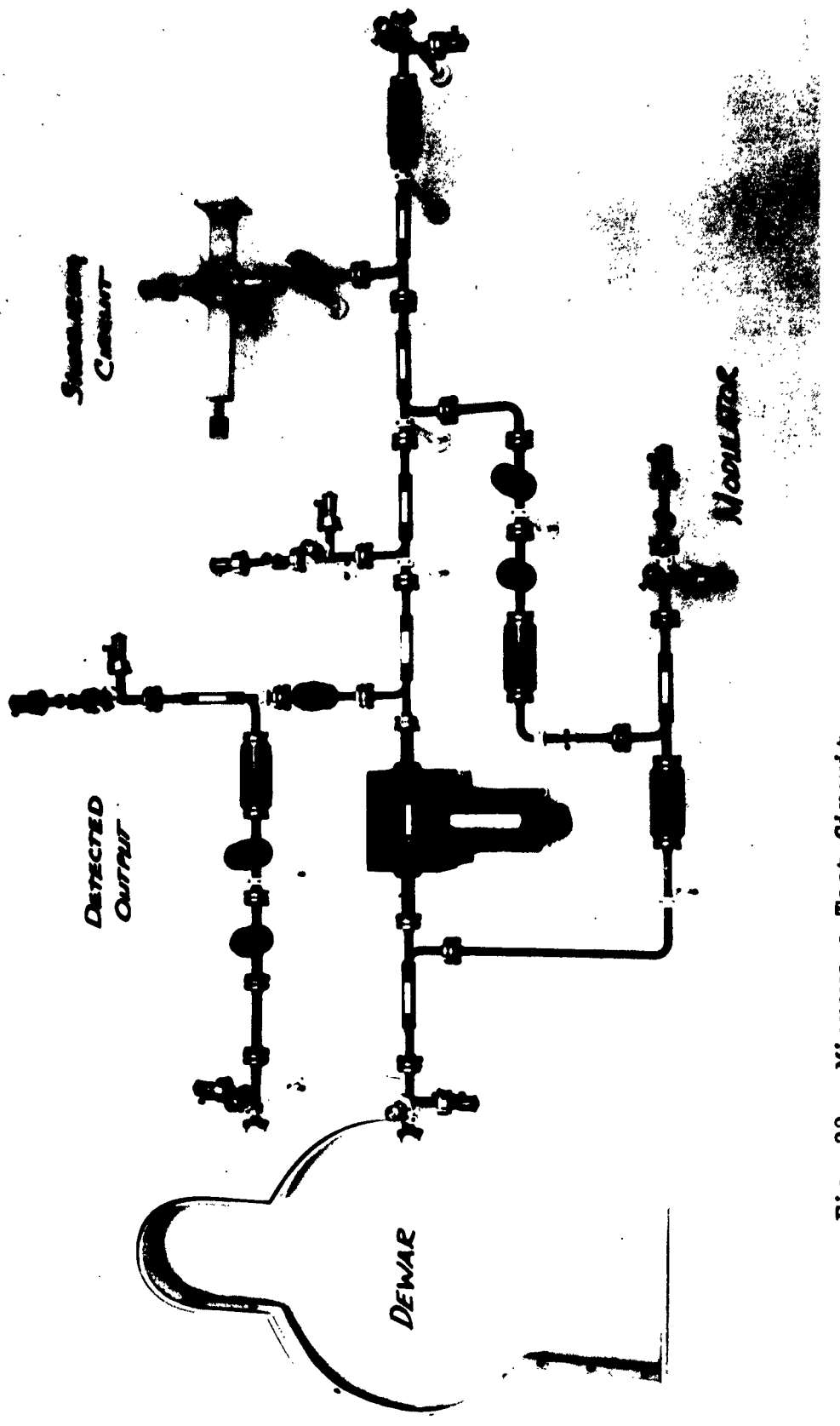

Fig. 22. Microwave Test Circuit

signal P_H, which is several orders of magnitude larger, to obtain a 70 cps audio beat whose amplitude is proportional to $\sqrt{P_c' P_H}$. We will refer to this signal as H_c'.

The frequency of the klystron is detuned from the zero field resonance which is 81.3 kMc to 80.2 kMc. As the magnet current is varied, H_c' goes through a minimum as shown in Figure 23a due to the resonance absorption of the -3/2 to -5/2 level (Fig. 14). Increasing the input power by a factor of 10 so that H_c = 36,600* thoroughly saturates the resonance as is shown in Figure 23c. Let us consider the case where the incoming information signal is in the form of sidebands which are phased for amplitude modulation. We will designate the amplitudes of sidebands phased in this manner as $H_s(\phi = 0)$. In the linear absorption region the behaviour of the local oscillator (Fig. 23c) is identical to the information signal (Fig. 23b). In the saturated absorption region the behaviour of the local oscillator is markedly different from the information signal as seen in Figure 23c and Figure 23d. As the magnetic field sweeps through resonance both local oscillator and information signal show attenuation but then the information signal shows a relative gain before being attenuated again. This is in agreement with theory, since off resonance the degree of saturation decreases and is too small to cause an amplification. Therefore two troughs and one peak are seen in Figure 23d. This measurement was repeated several times with substantially the same result. It was also repeated over a range of input powers where the gradual changes in the line shapes could be noted.

---

* arbitrary units

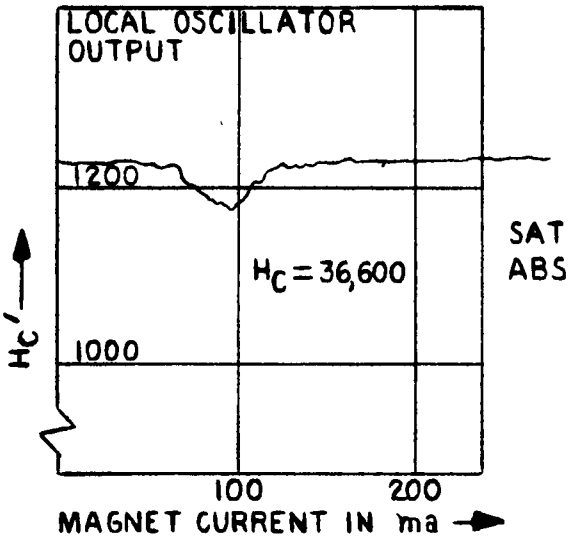

Fig. 23c

SATURATED
ABSORPTION

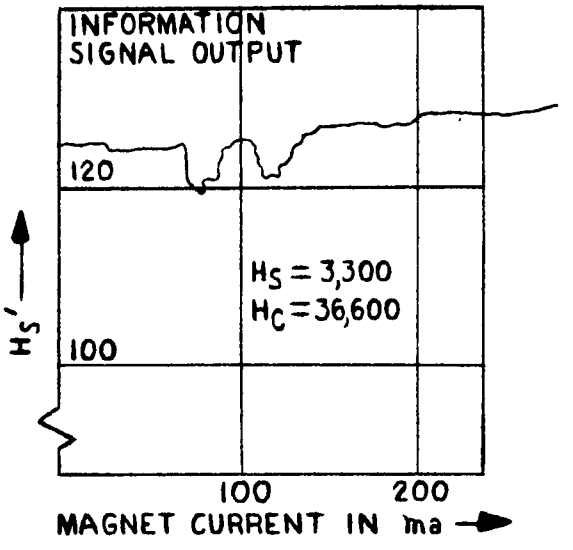

Fig. 23d

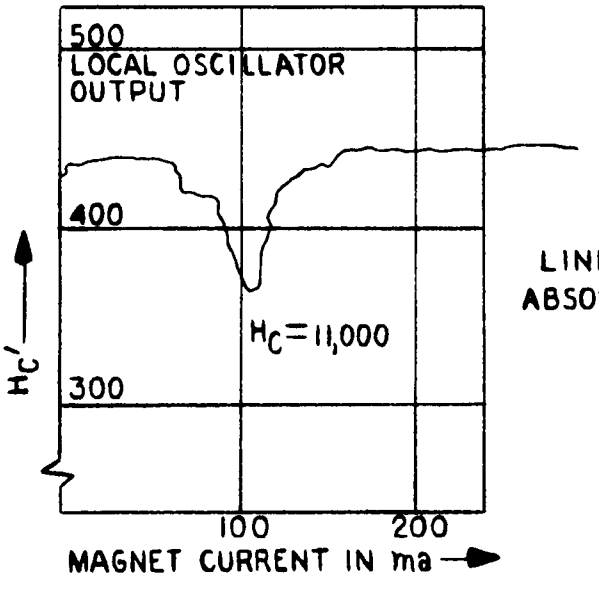

Fig. 23a

LINEAR
ABSORPTION

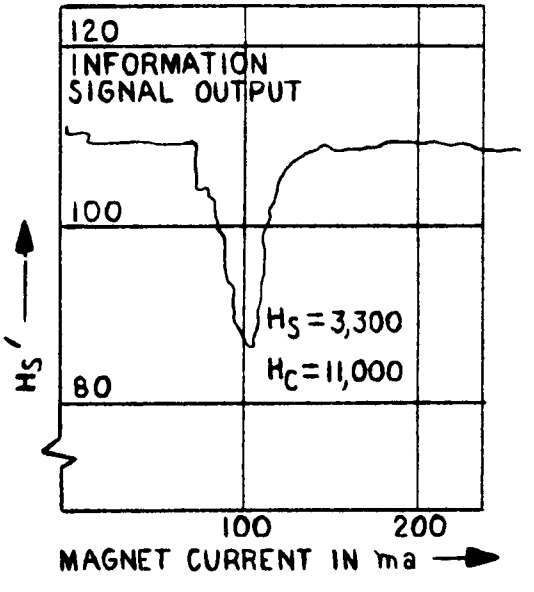

Fig. 23b

FIGURE 23.

Demonstration of Gain in the CLA

Recorder output, in arbitrary units, of the transmitted microwave pump field, H_c', and microwave signal field, H_s' ($\phi = 0$), as a function of the d.c. magnetic field. Unprimed quantities refer to the microwave input fields. Operating frequency 80.2 kMc.

Another unit was tested at zero field at a frequency of 81.3 kMc. Both amplitude ($\phi = 0°$) and frequency ($\phi = \pi/2$) modulated sidebands were used. Each individual trace in Figure 24 is a plot of the relative field attenuation as the magnet current is varied from 0 to 100 ma (corresponding to a frequency variation of about one kMc). The three traces on the left are taken when the medium exhibits linear absorption. As expected, the relative field attenuation is identical for the local oscillator, H_c', frequency modulated sideband, H_s' ($\phi = 90°$) and amplitude modulated sideband, H_s' ($\phi = 0$). When the medium is saturated as in the three traces on the right the behaviour is again markedly different. The attenuation is identical for the local oscillator field, H_c', and frequency modulated sidebands H_s' ($\phi = 90°$) but the amplitude modulated sideband shows considerably less attenuation. This is in good accord with the above analysis which clearly indicates that the behaviour for FM sidebands and local oscillator is identical in both the linear and saturated absorption regions. The power saturation in Figure 24 is apparently not sufficiently great to give relative signal gain as in Figure 23.

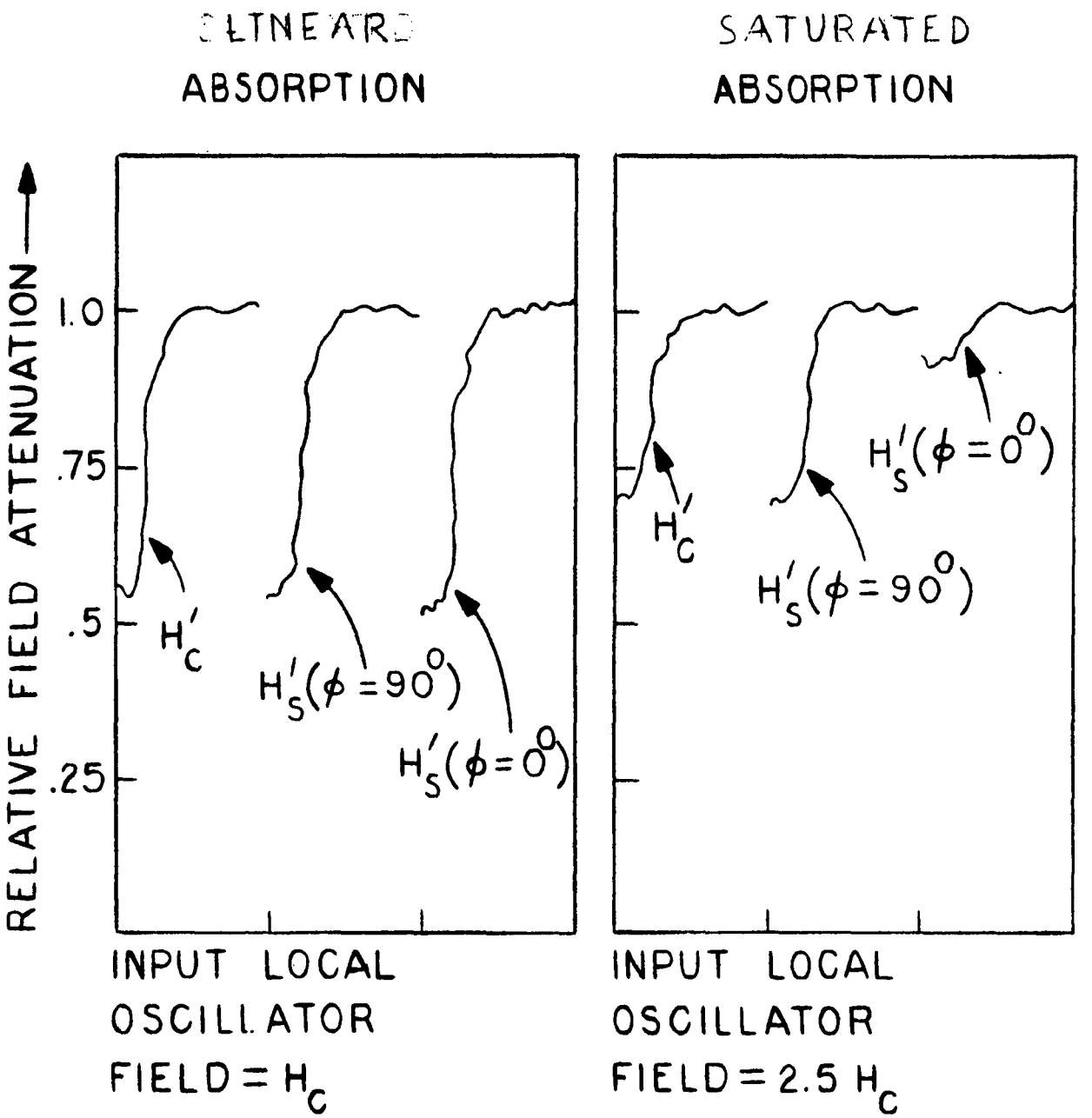

FIGURE 24.

Relative Field Attenuation as a function of magnet current increasing towards right for local oscillator field, H_c' frequency modulated sideband $H_s'(\phi = 90°)$ and amplitude modulated sideband $H_s'(\phi = 0°)$. Operating Frequency is 813KMc.

5. Discussion

In order to compare the observed results with theory we will first write an expression for the attenuation constant in the center (amplifier) section;

$$\alpha_\ell = \frac{8\pi}{c} \frac{h'}{k} \frac{\sqrt{\epsilon}}{\eta} \omega T_2 \, P_\epsilon(\mu^2) F$$

where F = Filling factor

k = propagation vector of a plane wave in medium with dielectric constant ϵ.

h' = propagation vector for TE_{10} mode in wavequide, $\sqrt{k^2 - (\pi/a)^2}$

P_ϵ = population difference between 3/2 and 5/2 state

and (μ^2) is the matrix element of the dipole moment for the transition of interest. For the $|3/2|$ and $|5/2|$ levels in Fig. 14 this would be $5\mu_o^2$ (where μ_o is the Bohr magneton) if the states at zero field were pure. Because of the slight mixing[10] of states this value is $5.6\ \mu_o^2$. The pertinent experimental parameters are

N = concentration of iron ions = $2 \times 10^{16} cm^{-3}$

F = Filling factor = 1/3

Operating temp. = 4.2°k

a = .43 mm

b = .28 mm

z = length of active section = 1 cm.

ϵ = 120 (for electric field perpendicular to optic axis)

---

(10) Private Communication from D. Carter.

The value of T_2 is determined from the measured linewidths in Figures 23 and 24 to be 10^{-9} sec. P_ϵ is computed from the Boltzman population distribution. Since there are two equivalent lattice sites in rutile, whose local symmetry axes are mutually perpendicular, only one half the number of atoms, N, are effective in the absorption spectrum shown in Fig. 23. The resultant value of $\alpha_\ell = 0.5$ cm^{-1} is in agreement with the value obtained for the absorption (50%) in the linear region in Fig. 23.

The total wall and material attenuation of the unit in Fig. 23 is high. It is 27 db as can be seen from the value of the input and output fields. This value is considerably higher than the theoretical value predicted from the computed wall losses.

This discrepancy may be due to the following:

a) Small air gaps where two rutile pieces of crossection .015 x .010 inches come in contact present the appearance of a waveguide beyond cutoff - a several mil gap can attenuate the signal by more than 3 db.

b) Some plating can take place in the gap giving rise to an iris in the waveguide which will reflect some power (this will then be absorbed so that it will not be measured at either end of the unit).

c) It is difficult to make a perfect quartz or rutile knife edge thus giving rise to further reflections.

d) Because of a lifting of the copper coat at an inside corner in the rutile amplifier section the corner was soft-soldered —soft solder can give rise to an attenuation constant which is three or four times that of copper.

e) The quartz which was used was Brazilian natural quartz which although optically flawless may have a rather high impurity concentration which can raise the loss tangent.

f) Data on the loss tangent of the adhesive is not available at the frequency of interest, although it is available at 35 kMc. Nevertheless there may be a sharp rise of the loss tangent due to the particular mode of curing or due to the increase of frequency.

6. Conclusion

The experimental data described above has indicated the general validity of the CLA principle as applied to a paramagnetic solid. The main drawbacks have been a) the high linear losses encountered b) the narrow amplification bandwidths obtainable.

On the basis of this experience the molecular gas[1] definitely seems to be a superior CLA medium.

Appendix I -- MOLECULAR AMPLIFIERS BASED ON MASER PRINCIPLES

During the preliminary phase of RADC Contract Number AF30(602)2033, an investigation was made of molecular amplifiers based on the MASER principle. A list of molecular amplifiers was given in the First Quarterly Memorandum of this contract. A revised list with some references is given below.

3 level MASERs optically pumped by:

- Resonance radiation in a paramagnetic atomic gas.

  Optical pumping by polarized light in the alkali vapors (see N. Knable, Bull.Am.Phys.Soc. 6, 67 (1961)). This is a narrow bandwidth device.

- Concident atomic spectral line acting on a paramagnetic molecular gas.

  Optical pumping by polarized light from the lower ground state to an excited electronic state, and subsequent decay to an upper ground state. This is a narrow band device.

3 level MASERs microwave pumped

- Paramagnetic ions in crystals with Zeeman splitting.

  This is the most familiar type of MASER. Its performance and limitations are well known.

- Electric dipolar molecular gas with Stark splitting.

  Similar to above. See Basnov, N.G. and Prokhorov, A.M., J. Exptl. Theoret. Physics (U.S.S.R.) 27, 431 (1954); 28, 249 (1955).

2 level MASERs using field separation of upper and lower states

- Molecular beam through electric field gradient

  The first (Ammonia) MASER was based on this principle. Recently D. Marcuse (J.A.P. 32, 743 (1961)) obtained amplification using HCN at 3.4 mm wavelength. Narrow bandwidth and mechanically involved structures are the practical drawbacks of this type of device.

- Atomic beam through a magnetic field gradient

  A variation of the above. Paramagnetic (alkali) vapors and atomic hydrogen may be passed through a magnetic field and focussed in a cavity. See Goldenberg, H.M., Kleppner, D. and Ramsey, N.F., Phys. Rev. Lett. 5, 361 (1960) and Singer, J.R., I.R.E. Trans. on Microwave Theory Tech. MTT, 7, (1959).

- Differential diffusion out of electric field gradient after thermal equalization of populations.

  A method of providing continuous physical separation in a gas without using a beam. Experimental attempts were unsuccessful; see RCA Reports on Signal Corp. Contract DA 36-039-SC-73031.

- Differential diffusion out of electric field gradient after microwave equilization of populations.

  A variant of above. Question of experimental feasibility.

MASERs pumped by collisions between

- Hot electrons and atomic gas (Hydrogen).

  In a hydrogen discharge, population of the $2^2P_{3/2}$ can exceed that of the $2^2S_{1/2}$ (metastable) as noted by W.E. Lamb and R.C. Retherford, Phys. Rev. 79, 570 (1950). This amplifier output would have to be "shielded" from the hot electrons to avoid excessive noise.

- Mono-energetic electrons and atomic gas (Hydrogen).

  A varient of above where an electron beam is used to selectively excite certain levels. Depends on the fact that inelastic collision cross sections are much greater for allowed electric dipole radiation transitions than for the forbidden transitions. Getting sufficient populations to amplify or oscillate is always a problem when beams are used.

Inversion of level population by

- 180° resonant pulse in electric dipolar or paramagnetic molecular gas.

  Depends on application of the proper intensity and duration pulse to invert the upper and lower state populations. This

technique requires large microwave powers which at present are unavailable in the mm-wave region.

- Adiabatic fast passage in a paramagnetic molecular gas.

  Requires a field reversal slow compared to existing precessional motions (adiabatic) but rapid compared to the relaxation times. A paramagnetic molecular gas with a long relaxation time is Iridium Hexafluoride (IrF_6). Because of the shielding effect of the fluorine on the iridium this has a long relaxation time.

- Sudden field reversal in paramagnetic solid, electric dipolar molecular gas and paramagnetic gas.

  Depends on reversing the field (non-adiabatically) to obtain an inversion. Weak interactions are required so that the field can be reversed rapidly compared to the existing precessional motions. This experiment has been performed by Purcell, E.M. and Pound, R.V., Phys. Rev. 81, 279L (1951), using nuclear magnetic resonance phenomena. This type of inversion is not favorable for extension to higher frequencies.

- Non-random relaxation in resonant fields.

  This technique is similar in principle to the 180° pulse inversion except that the pulse "duration" is controlled by a coherence interrupting process, such as a wall collision. Consider a gas in a multitude of small containers

where the collision time is determined by the enclosure. By a suitable choice of rf power and container dimension a 180° pulse inversion can be obtained.

Work on the investigation of the above amplifiers was discontinued when the CLA principle was discovered.

Appendix II - BANDWIDTH AND GAIN COMPUTATION

The quasi-static analysis of the constant loss amplifier is based upon a theory which gives the resonance spectrum of a dipole system irradiated with a single frequency external field. An expansion in terms of a small amplitude modulation of such a field then provides a solution to the problem at hand if the modulation frequency is small, i.e. if the frequency representing the information signal to be amplified is close to the local oscillator frequency (which is on resonance). We are here concerned with the solution to the problem when the above restriction is removed. Thus we must examine the gain as a function of the relaxation and operating parameters, these being the local oscillator and information signal amplitudes and frequencies. In particular we require the quantum mechanical solution to the problem of a dipole system irradiated by an external field consisting of several frequencies.

The two types of coherence interrupting mechanisms are specified by the spin-lattice relaxation time, T_1, and the spin-spin relaxation time, T_2. The spin-lattice interaction not only interrupts the radiative process but also tends to restore the spin system to thermal equilibrium through its interaction with the crystal lattice. On the other hand the spin-spin interaction does not alter the population distribution of the various states. These characteristics will be evident in the manner in which they are introduced into the equations for the density matrix used for the solution of the problem. The relaxation time T_2 is a measure of the resonance line width of the system. Since it is related to spin-spin interactions its value

is determined by the relative distance of the individual spin systems to one another.

The quantum mechanical problem of irreversible processes (due to relaxation phenomena) can be effectively handled by the methods of statistical quantum mechanics. This makes use of statistical theory to obtain information about a macroscopic system by a suitable averaging over the possible states of the microscopic system. To this end we use the properties of the density matrix.* This formulation will be outlined here in order to understand more clearly the nature of the solution obtained. The mean expectation value of any observable operator in quantum mechanics for an ensemble of systems which can be specified by pure states can be given in terms of the density matrix. The matrix elements are related to the total Hamiltonian of the system by the differential equation of motion of the density matrix which is obtained using Schrödinger's equation. Given the complete Hamiltonian the problem can in principle be solved. However, the explicit form of the Hamiltonian for a system in which relaxation phenomena are involved is too complicated to permit a simple solution. In this case those terms in the Hamiltonian involving the spin-spin interaction and spin-lattice interaction are lumped together in simple expressions involving the relaxation times. This is done as follows:

In an energy representation the diagonal elements of the density matrix are proportional to the populations of the various

---

* For a discussion of the use of the density matrix see U. Fano, "Description of States in Quantum Mechanics by Density Matrix and Operator Techniques", Rev. Mod. Phys., 29, (January 1957).

possible states. Thus in the absence of external fields these elements will decay exponentially with time to their thermal equilibrium values. Further, since only the longitudinal relaxation phenomenon alters the population of states this decay time must be the longitudinal relaxation time, T_1. The transverse relaxation interactions are introduced by assuming that the off diagonal terms decay to zero with the relaxation time T_2. Thus the relaxation processes are introduced phenomenologically into the differential equation for the density matrix while the externally applied fields are written explicitly in the Hamiltonian.

The applied field perturbation is in the form of a dipole interaction between the atomic or molecular dipole and the electromagnetic field which we will write as μH. When this perturbation is written in the expression for the Hamiltonian, μ is an operator which for a two level system can be written as

$$\mu = \begin{pmatrix} 0 & \mu_{12} \\ \mu_{21} & 0 \end{pmatrix} . \qquad \text{(II-1)}$$

Similarly we can write for the density matrix

$$\rho = \begin{pmatrix} \rho_{11} & \rho_{12} \\ \rho_{21} & \rho_{22} \end{pmatrix} . \qquad \text{(II-2)}$$

The macroscopic dipole moment per unit volume M can be written as

$$M = \mathrm{Tr}(\mu\rho) = \mu_{12}\rho_{21} + \mu_{21}\rho_{12} \qquad \text{(II-3)}$$

when $\mathrm{Tr}(\rho) = N$, where N is the (II-4)

total number of microsystems in the ensemble which in this case will be taken as number of spins or molecules per unit volume.

The equation of motion of the density matrix is

$$\dot{\rho} = -\frac{1}{i\hbar}\left[\rho\mathcal{H}\right] \tag{II-5}$$

where commutator brackets are used and $\mathcal{H}$ is the total Hamiltonian. The part of the Hamiltonian composed of the unperturbed energy operator of the isolated microsystems (an ion in a crystal field or a molecule in field free space) will not contribute to the right hand side of Eq.(II-5) because this part of the Hamiltonian is diagonal. The remaining terms in the Hamiltonian will yield the following set of equations

$$\begin{aligned}
\frac{\partial\rho_{11}}{\partial t} &= \frac{1}{i\hbar}\left(\mu_{12}\rho_{21} - \rho_{12}\mu_{12}\right)H + \frac{(\rho_{22}-\rho_{11})}{2T_1} - \frac{(\rho_{22}-\rho_{11})_\epsilon}{2T_1} \\
\frac{\partial\rho_{22}}{\partial t} &= -\frac{1}{i\hbar}\left(\mu_{12}\rho_{21} - \rho_{12}\mu_{21}\right)H - \frac{(\rho_{22}-\rho_{11})}{2T_1} + \frac{(\rho_{22}-\rho_{11})_\epsilon}{2T_1} \\
\frac{\partial\rho_{12}}{\partial t} &= \frac{1}{i\hbar}\left(\rho_{22}-\rho_{11}\right)\mu_{12}H + i\omega_o\rho_{12} - \frac{\rho_{12}}{T_2} \\
\frac{\partial\rho_{21}}{\partial t} &= -\frac{1}{i\hbar}\left(\rho_{22}-\rho_{11}\right)\mu_{21}H - i\omega_o\rho_{21} - \frac{\rho_{21}}{T_2}
\end{aligned} \tag{II-6}$$

where the two relaxation times T_1 and T_2 are introduced. From the definition of the density matrix, ρ_{11} and ρ_{22} are the populations of the lower and upper state. The ϵ subscript indicates the equilibrium populations. If the external field is zero, $(\rho_{22}-\rho_{11})$ approaches $(\rho_{22}-\rho_{11})_\epsilon$ exponentially with time constant T_1, and ρ_{12} and ρ_{21} approaches zero with time constant T_2.

The above equations can now be written in terms of the macroscopic parameters, M and P where $P = (\rho_{22} - \rho_{11})$, the population difference per unit volume,

$$\ddot{M} + \frac{2}{T_2}\dot{M} + (\omega_o^2 + \frac{1}{T_2^2})M = \frac{2\omega_o}{\hbar}|\mu|^2 PH$$
$$\dot{P} + \frac{P - P_\epsilon}{T_1} = -\frac{2}{\hbar\omega_o}(\dot{M} + \frac{M}{T_2})H \quad . \tag{II-7}$$

Let us consider the applied field as the real part of

$$H = H_c e^{i\omega_c t} + \frac{H_s}{2} e^{i\omega_+ t} + \frac{H_s}{2} e^{i\omega_- t} \tag{II-8}$$

where $\omega_c = \omega_o$ and $\omega_\pm = \omega_c \pm \Delta\omega$.

Let us assume solutions of the form

$$P = P_o + P_1 e^{i\Delta\omega t} + P_1 e^{-i\Delta\omega t} \tag{II-9}$$

and for M

$$M = M_c e^{i\omega_c t} + \frac{M_{s+}}{2} e^{i\omega_+ t} + \frac{M_{s-}}{2} e^{i\omega_- t} \tag{II-10}$$

We have neglected terms of frequency $2\Delta\omega$, $3\Delta\omega$, etc. because of our small signal assumption ($H_s << H_c$) and we will also neglect high frequency terms in P.* The solution for M is straightforward but lengthy. We obtain

---

* Snyder, H.S. and P.I. Richards, Phys. Rev., 73, 1178, (1949)

$$M_c = -iAH_c = \chi_c H_c$$

$$M_{s+} = iA\left(\frac{x-iL}{\Delta}\right) H_s = \chi_{s+} H_s \qquad \text{(II-11)}$$

$$M_{s-} = iA\left(\frac{x+iL}{\Delta}\right) H_s = \chi_{s-} H_s \ .$$

where

$$A = \frac{\mu^2 T_2 P_\epsilon}{\hbar(1+y)}$$

$$y = H_c^2/H_{sat}^2$$

$$H_{sat}^2 = (\hbar^2)(\mu^2 T_1 T_2)^{-1}$$

$$x = y^2 - 1 - \alpha\beta^2 y - \alpha^2\beta^2$$

$$\beta = \Delta\omega T_2$$

$$L = \beta(2y\alpha + y - 1 - \beta^2\alpha^2)$$

$$\alpha = T_1/T_2$$

$$\Delta = (1+y)^2 + \beta^2 + \beta^4\alpha^2 - 2\alpha\beta^2 y + \beta^2\alpha^2 \ .$$

Writing the complex susceptibility as $\chi = \chi' - i\chi''$ the effect of the medium on the radiation can be characterized by three complex susceptibilities which may be written as follows

$$\chi_c = 0$$

$$\chi_c'' = A$$

$$\chi'_{s+} = -\chi'_{s-} = \frac{AL}{\Delta} \qquad \text{(II-12)}$$

$$\chi''_{s+} = \chi''_{s-} = -\frac{Ax}{\Delta}$$

Using Poynting's Theorem, one can write for any field component

$$\frac{1}{H^2}\frac{\partial H^2}{\partial Z} = -\frac{8\pi^2}{\lambda}\chi'' \qquad \text{(II-13)}$$

where λ is the wavelength in the medium.

This will yield the two equations

$$\frac{1}{H_c^2}\frac{dH_c^2}{dZ} = -\frac{8\pi^2}{\lambda}\chi_c'' = -\xi^2\alpha_\ell \qquad \text{(II-14)}$$

$$\frac{1}{H_s^2}\frac{dH_s^2}{dZ} = \frac{x}{\Delta}\xi^2\alpha_\ell \qquad \text{(II-15)}$$

The above equations are the generalized forms of Eq. 6 and 7 in the text when the restriction $\beta \ll 1$ is removed.

Appendix III - DESIGN OF A WAVEGUIDE TAPERED MATCHING TRANSITION

The amplifier section consists of a rectangular waveguide completely filled with rutile. Since rutile has a dielectric constant of approximately several hundred, the waveguide dimensions in the amplifier section are much smaller than those of the air filled guides which serve as input and output lines. It is therefore necessary to design an impedance matching transition between the guides. As a first approximation we may assume that the amplifier section is uniformly filled with undoped rutile. We will consider matching sections formed of linear tapers only and for which the waveguide dimensions taper gradually from one waveguide size to the other. We further make use of a linear tapered layer of dielectric so as to form a smooth transition from the air filled guide to the rutile filled guide. The plan view of the matching section is shown in figure III-1. The tapers are made in both E and H planes where these are over different intervals along the axis of transmission. The dielectric taper extends only over one such interval and is chosen so that the dielectric-air interface is parallel to the incident E sector and thus excites only a TE mode. This assures a smoother transition between the lowest order TE modes in the air filled guide and the rutile filled guide. Within the rutile filled guide, the TE mode has only a transverse electric field which is perpendicular to the crystal axis. Thus although rutile has anisotropic properties only that component of the dielectric constant parallel to this electric field is of interest.

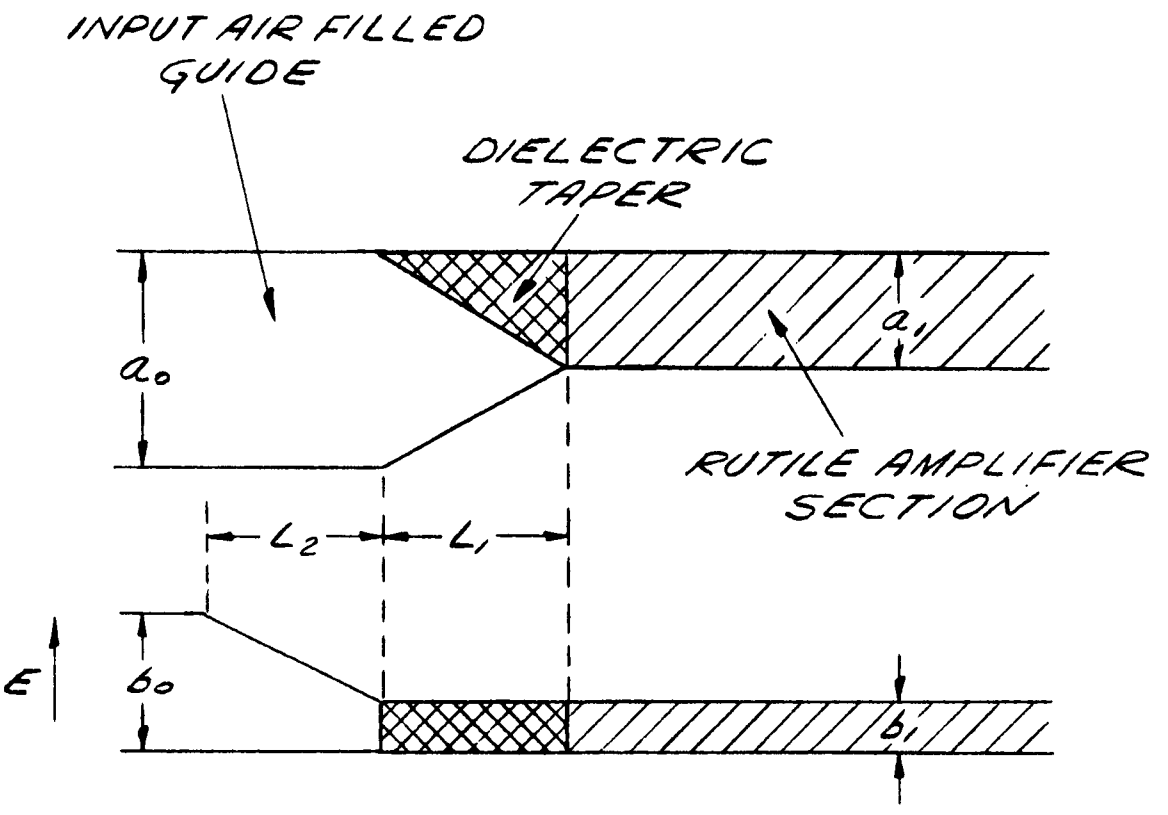

FIGURE III-1. Tapered Matching Section

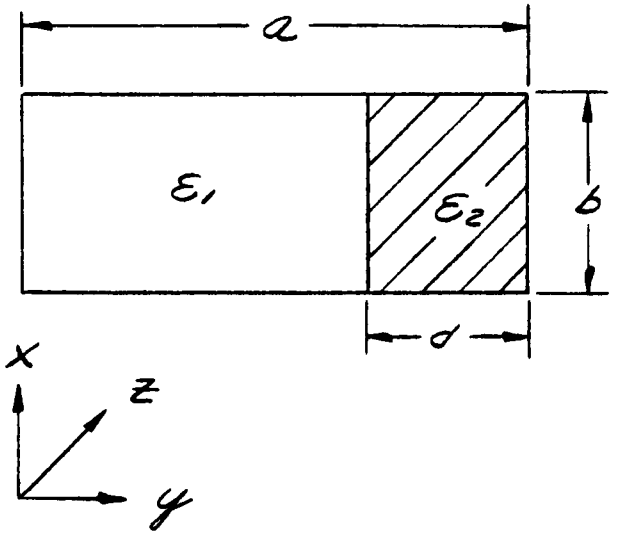

FIGURE III-2. Cross Section of Tapered Section

The design of tapered matching transitions has been discussed in a number of places*. We shall follow here a formulation given by Johnson†. The assumptions made are (1) only the lowest TE_{10} mode propagates and (2) the taper is gradual with a continuous change from the impedance of the input guide to the impedance of the amplifier section waveguide. As a consequence of condition (2) we assume that all reflections are small and that therefore multiple reflections can be neglected. The tapered region can be divided into a set of stepped transition sections, each section of which has a propagation constant and impedance corresponding to the local geometry at that section. The reflection at each step is added together to form a summation consisting of first order reflection terms. On passing to the limit of the continuous taper transition an expression is obtained for the reflection coefficient. This is given as, †

$$\Gamma = \left[\frac{1}{4ih}\ \frac{d}{dz}\ (\ell n\ Z)\right]_o - \left[\frac{1}{4ih}\ \frac{d}{dz}\ \ell n\ Z\right]_L \exp - \left[2i\int_o^L h\ dz\right]$$

$$+\int_o^L \frac{d}{dz}\left[\frac{1}{4ih}\ \frac{d}{dz}\ \ell n\ Z\right] \exp - \left[2i\int_o^z h\ dz\right] dz \qquad \text{(III-1)}$$

---

* S. A. Schelkunoff, "Electromagnetic Waves", D. Van Nostrand Co., Inc. New York, 1943.
G. L. Ragan, "Microwave Transmission Circuits", Radiation Laboratory Series, McGraw-Hill, 1948.

† R. C. Johnson, "Design of Linear Double Tapers in Rectangular Waveguides", IRE Trans. on Microwave Theory and Techniques, MIL-7 pp. 374-378, July 1959.

where h is the propagation constant in the transmission direction, z and Z is the impedance. h and Z are both functions of z. The brackets indicate the values of the appropriate quantities at the values z = o and L corresponding to the extremities of the taper. The VSWR is given by

$$\text{VSWR} = r = \frac{1 + |\Gamma|}{1 - |\Gamma|} \qquad \text{(III-2)}$$

It can be shown that the last term in (III-1) can be neglected. In addition we note that for the remaining terms the impedance at the extremities only need be known.

The values for h and Z are found, according to the assumptions previously made, from the local cross sectional geometry at the appropriate points. Thus at a given position of z it is necessary to solve the field problem for a waveguide where cross sectional geometry is as shown in figure III-2. When inserting the values of h and Z into equation (III-1), the parameters a, b, and d will depend upon z. The solution to the waveguide problem is a standard one and will not be given here. Upon evaluation of the propagation constant and impedance, eq. (III-1) becomes

$$\Gamma = \frac{\lambda_o}{\varepsilon\pi} \frac{1}{\sqrt{1-\left(\frac{\lambda_o}{2a_o}\right)^2}} \frac{1-\sqrt{\varepsilon_2}}{\sqrt{\varepsilon_2}} \left[\frac{1}{L_2} + \frac{1}{L_1\left(1-\frac{\lambda_o}{2a_o}\right)^2} e^{i4\pi\ell}\right] \qquad \text{(III-4)}$$

where the parameters a_o, b_o, ε_2, L_1, L_2 are defined in the figures and λ_o is the free spare wavelength. We have taken $_1 = 1$, $a_1 = \frac{a_o}{\sqrt{\varepsilon_2}}$, $b_1 = \frac{b_o}{\sqrt{\varepsilon_2}}$. The parameter ℓ is given by

$$\ell = \frac{1}{2\pi}\int_{-L_2}^{L_1} h(z)dz$$

For a practical design knowledge of the value of ℓ is not needed. Inserting the complete function Γ into r results in an oscillatory curve with an envelope whose amplitude is decreasing. While a design at one of the minima of this function would give the lowest VSWR it is extremely sensitive to the parameters. A more practical design consists in merely requiring the envelope of the VSWR to be sufficiently low. This is obtained by increasing the total length of the taper. For the case $L_1 = L_2$ figure III-3 shows the envelope of VSWR as a function of L/λ_o (i.e. we ignore the oscillations which give lower VSWR at specific points of L/λ_o.)

In the actual structure an additional wedge of quartz was used for support in the interval containing the rutile taper. Since the dielectric constant of quartz is low it was not expected that this support will not cause any difficulty. The previous computed results will remain essentially the same.

FIGURE III-3. VSWR vs. taper length for taper design shown in fig. III-1 with $L_1 = L_2$.

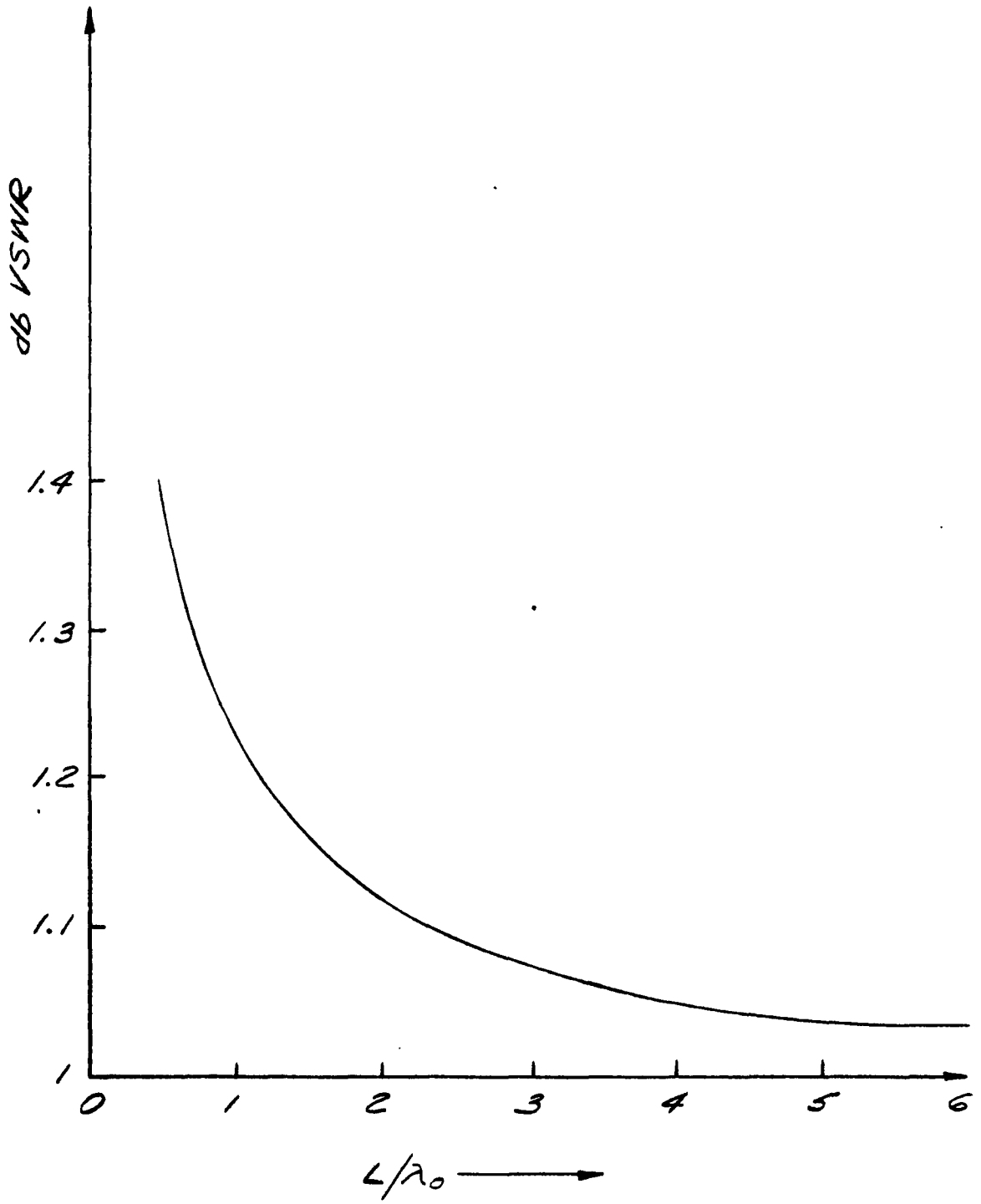

Appendix IV - FABRICATION

It is desirable to operate the rutile amplifier and its transition section so that only the fundamental mode will propagate. This requires rather minute dimensions and considerable deviations from existing fabrication procedures.

In Step 1, Figure IV-1, wafers of quartz and rutile are lapped down on block I, Figure IV-2 with silicon carbide 600 grit powder. Coarser grit is unsatisfactory because it forms deep cracks below the surface of the rutile. In Step 2, Figure IV-1, wedges of quartz and rutile are cemented together as shown. In Step 3, Figure IV-3, material is lapped down to form a knife edge. Step 4, Figure IV-3, indicates the sandwich from which the amplifier will be constructed. The adhesive layers used must have certain electrical, mechanical and thermal properties. A variety of cements, all requiring oven curing, were tested and a Buna S adhesive* was chosen as the most satisfactory. Steps 5 and 6 of Figure IV-4, are self explanatory. Step 7, Figure IV-5, was performed with the aid of a jig which keeps pressure applied along the slanted face of the 18°28' quartz wedge. The problem originally encountered in Step 8 was that the bond failed as the material is lapped thinner than 20 mils. This problem was solved by a clamping jig. Step 9, in Figure IV-6 shows the final assembly as in Figure 17 of the text. The purpose of the machined temporary aluminum mandrel on either end of the assembly in this step is to supply the final taper to the

---

* Emerson and Cumming Eccomold L-70

Figure IV-1

Fabrication Procedure - All dimensions in inches

① CUT .380 x 150 x .020 WAFERS (2) RUTILE (2) QUARTZ
LAP ON BLOCK I FIG. III-2 TO OBTAIN:

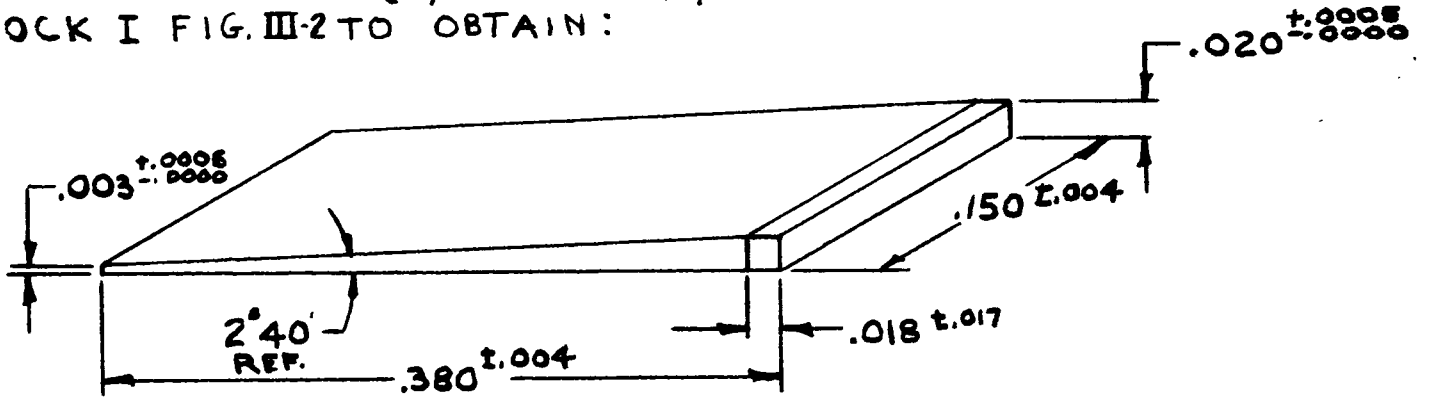

② CEMENT QUARTZ TO RUTILE AS SHOWN

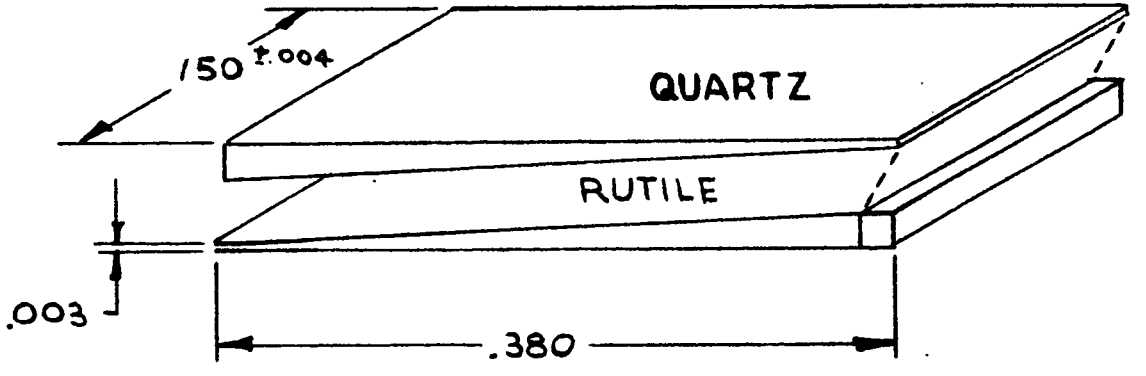

Figure IV-2

Lapping Blocks

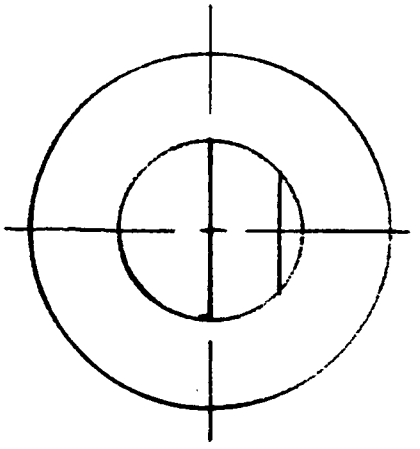

BLOCK I

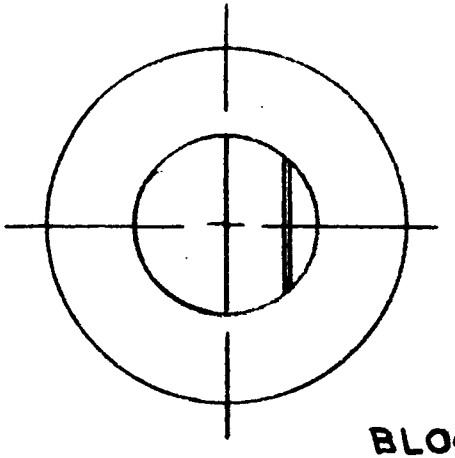

BLOCK II

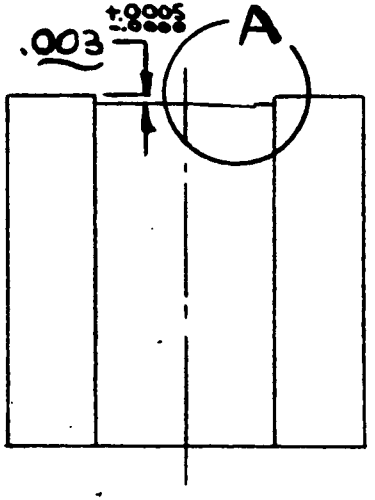

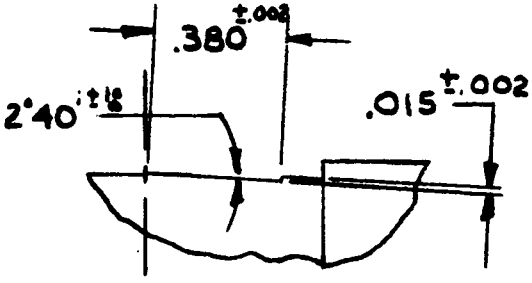

A
2-1

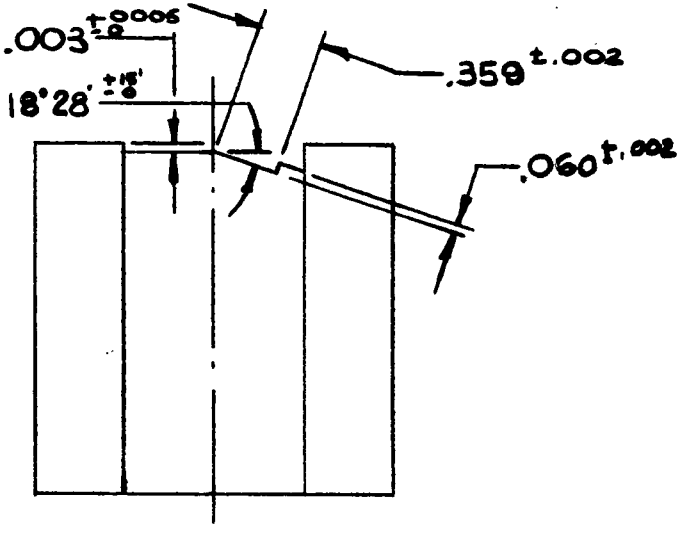

③

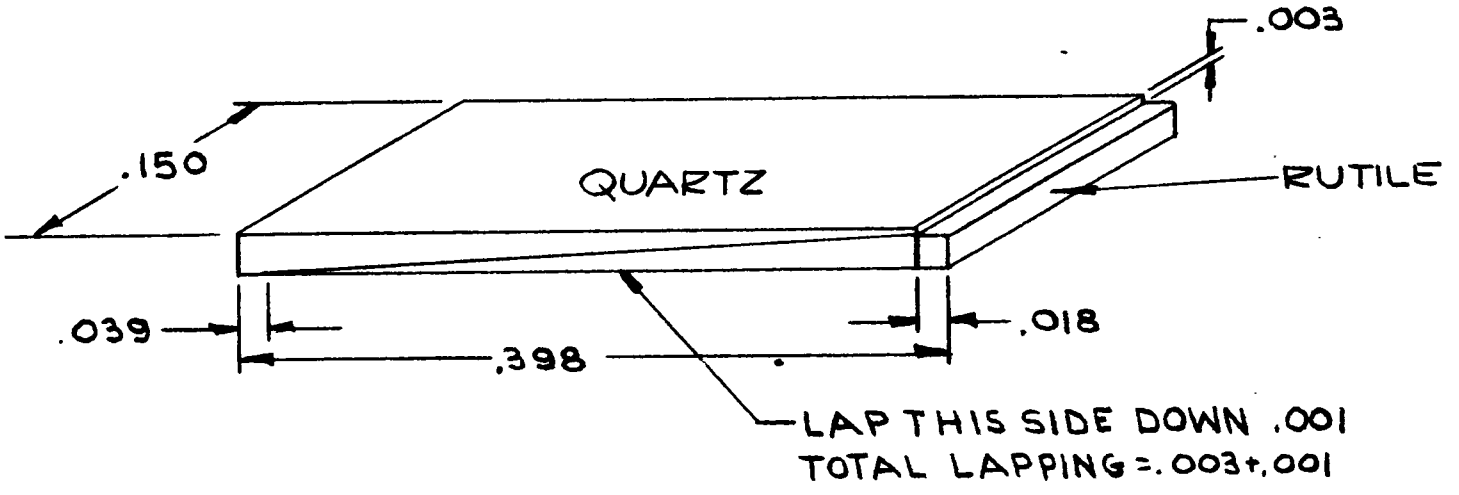

④ MAKE SANDWICH AS SHOWN

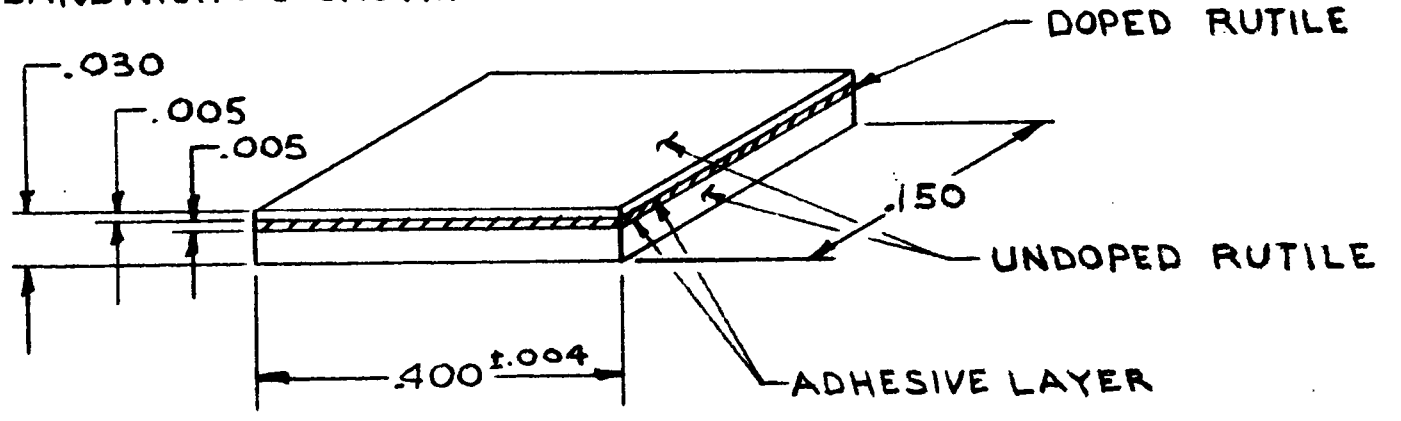

Figure IV-3

Fabrication Procedure - All dimensions in inches

⑤ WAX ON BACKING AS SHOWN

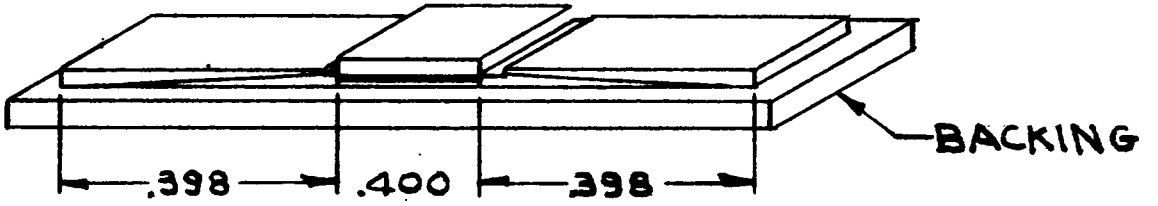

⑥ LAP AND POLISH TO .015 AS SHOWN

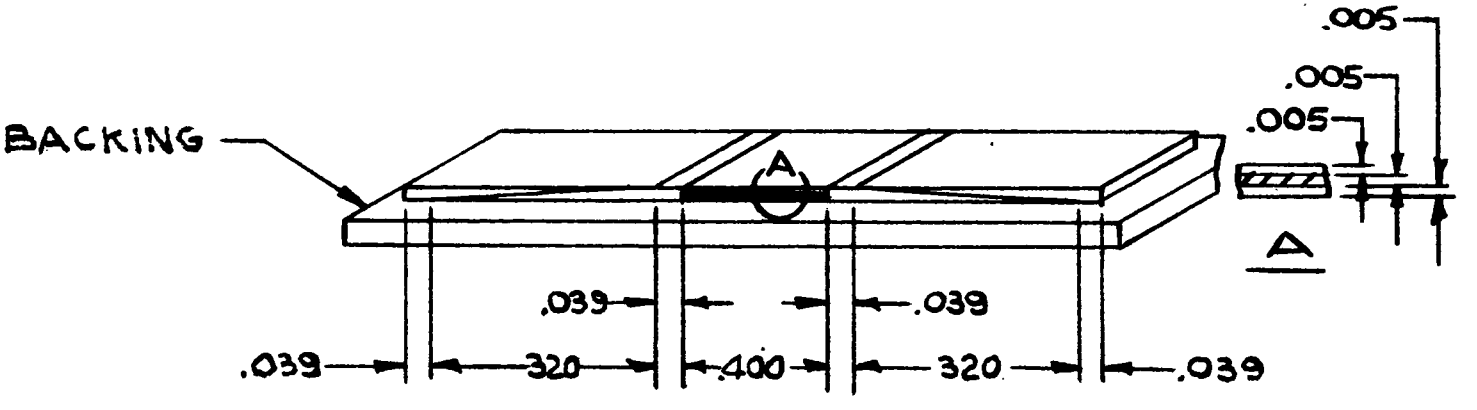

Figure IV-4
Fabrication Procedure - All dimensions in inches

⑦ PLACE .107 x .150 x .359 QUARTZ WAFER ON BLOCK II FIG III-2 LAP DOWN AND CEMENT AS SHOWN

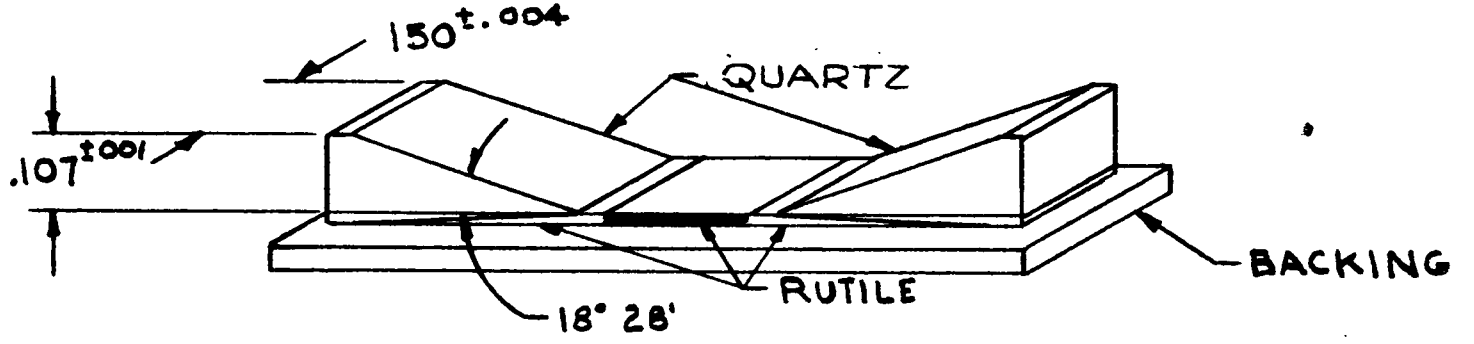

⑧ CUT .015 WAFERS FROM ⑦ LAP AND POLISH ONE SIDE THEN REVERSE AND CEMENT ON TO CONDUCTOR. LAP AND POLISH DOWN TO .0075

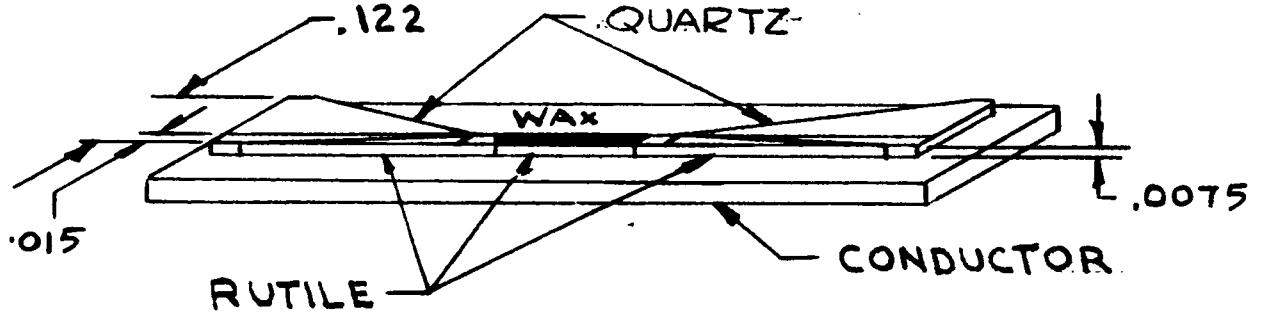

Figure IV-5

Fabrication Procedure - All dimensions in inches

⑨ MACHINE ALUMINUM MANDREL AND POSITION AS SHOWN

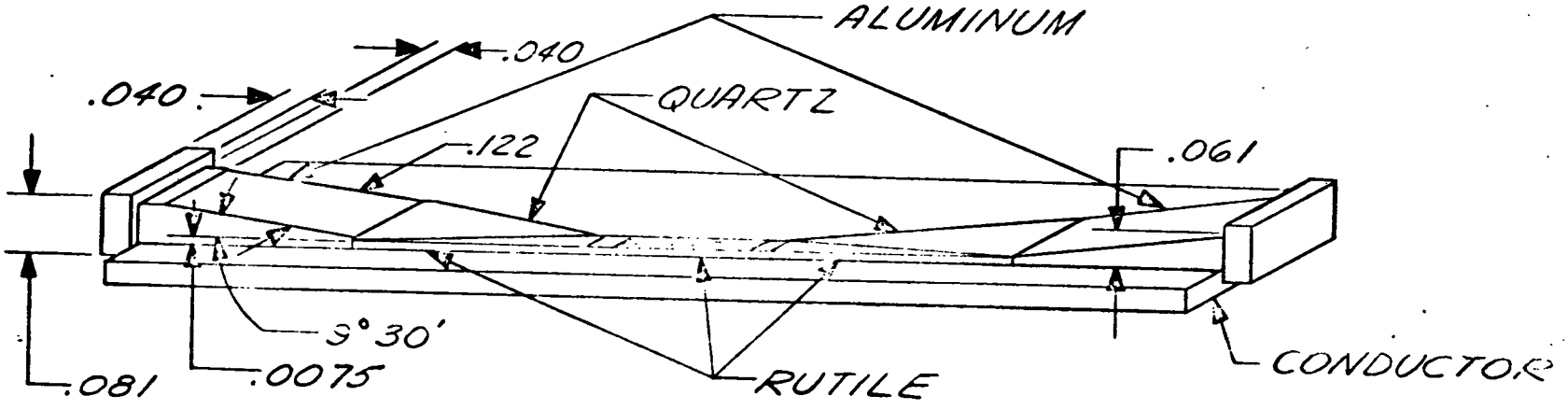

⑩ VAPORIZE SUITABLE METALLIC COAT

⑪ ELECTRO-FORM TO ENCAPSULATE

⑫ ETCH OUT THE ALUMINUM

Figure IV-6

Fabrication Procedure - All dimensions in inches

.061 x .122 inch air-filled waveguide and to provide a means of soldering the amplifier assembly to the bottom of the waveguide shown in Figure V-2.

The assembly shown in Step 9 has a thin copper or gold conducting coat vaporized on it (Step 10), and the coat thickness was then increased to .050" by electrodeposition in Step 11. Two kinds of plating baths were tried: A periodic reversal copper cyanide bath and a periodic reversal copper sulfate bath. The latter was found to be superior because it did not attack the Buna S (rubber) adhesive.

The final Step 12 was to etch out the aluminum with hot concentrated hydrochloric acid. It may be of interest to note that originally quartz mandrels were not used - all mandrels were made out of aluminum, including the one in the H plane taper shown in Figure IV-5 Step 8. The problem encountered was the inability to etch out the aluminum in the apex of the taper. This was due to a formation of gas which could not escape from the minute aperture and which blocked further etching action. When permanent quartz mandrels were used this problem did not arise.

Appendix V - CRYOGENIC CONTAINER

The liquid helium dewar is shown in Figures V-1 and V-2. At the high frequencies used in this experiment, the waveguide leading to the CLA device in the dewar must be absolutely moisture-free. In order to accomplish this the gas handling system in Figure V-3 was used. The operating instructions for this system follow:

1) Evacuate dewar. Starting with all valves closed, open valves 2,3,4,5,6 and 1 and evacuate.

2) Flush helium and nitrogen connecting lines. Ⓕ and Ⓖ if necessary.

a) Nitrogen line Ⓖ. Close 2 and 3. Open 8, wait one minute, close 8, then open 2 and 3 to evacuate. Repeat above operation.

b) Helium line Ⓕ. Close 2 and 3. Open 7, wait one minute, close 7, then open 2 and 3 to evacuate. Repeat above operation then close 2 and 3 and open 7.

3) Fill outer dewar jacket Ⓒ with liquid nitrogen and cool system down.

4) Flush the helium dewar vacuum chamber Ⓑ with nitrogen.

a) Close 4 and 7 and open 3 to evacuate. Close 3.

b) Open 8, close 8, open 3, close 3, open 8, close 8, open 3 and evacuate thoroughly. Close 6,5 and 3.

5) Connect liquid helium chamber Ⓐ to gaseous helium supply. Open 4 and 7. Remove part Ⓓ and insert pre-cooled transfer tube. Open 9 slowly and close 7. Apply helium pressure to storage dewar to effect transfer.

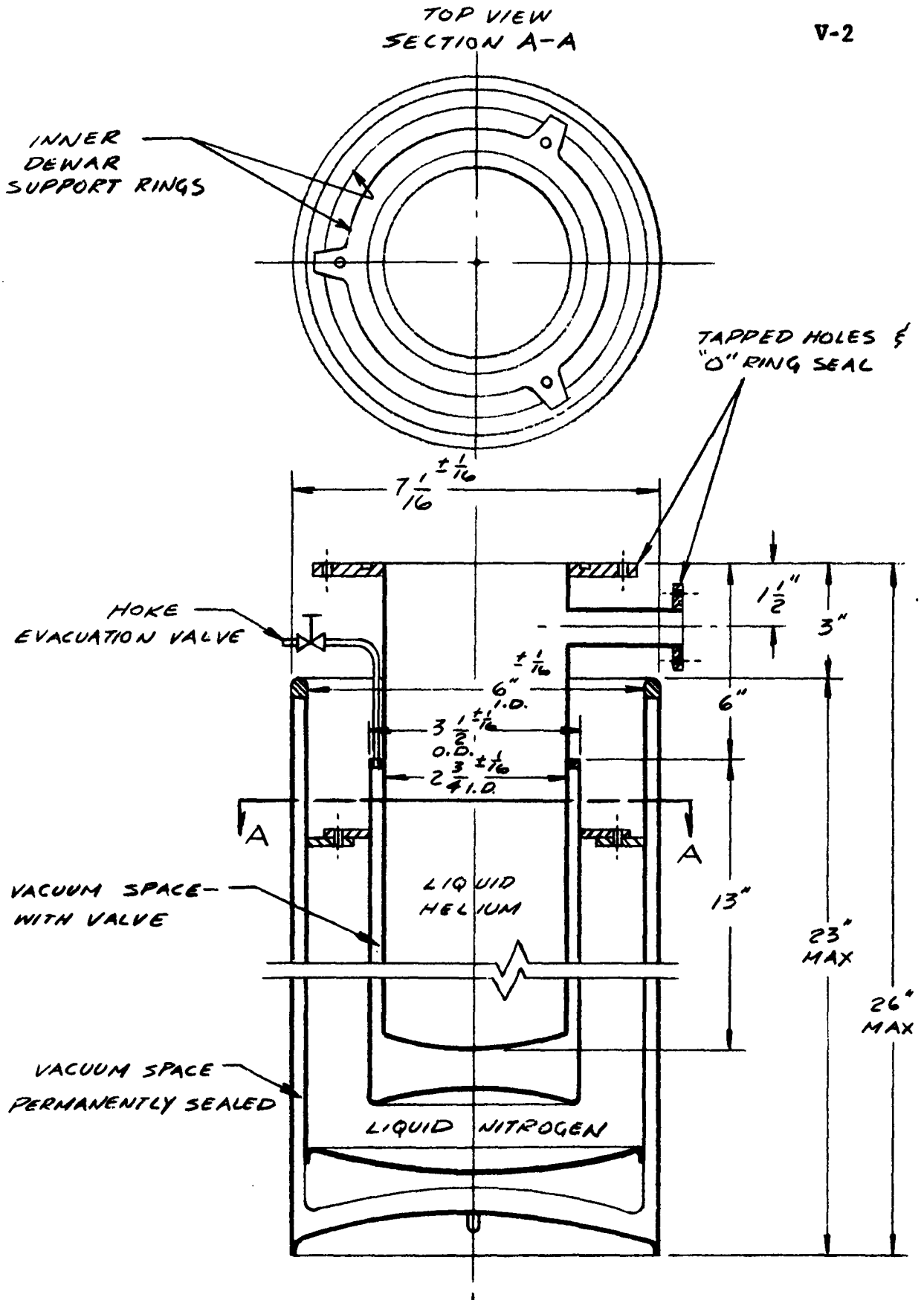

FIGURE V-1

Liquid Helium Dewar

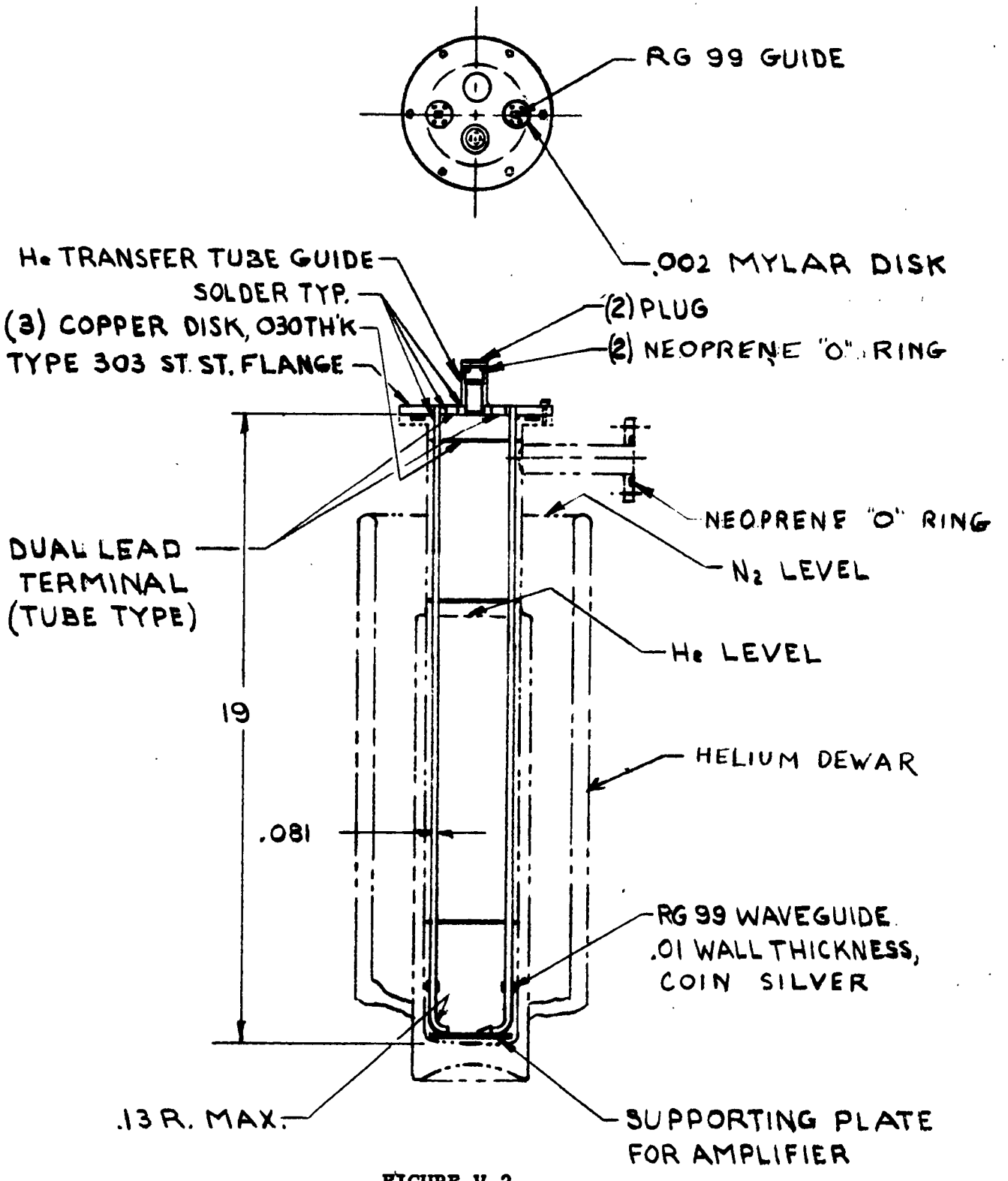

FIGURE V-2

Waveguide in dewar

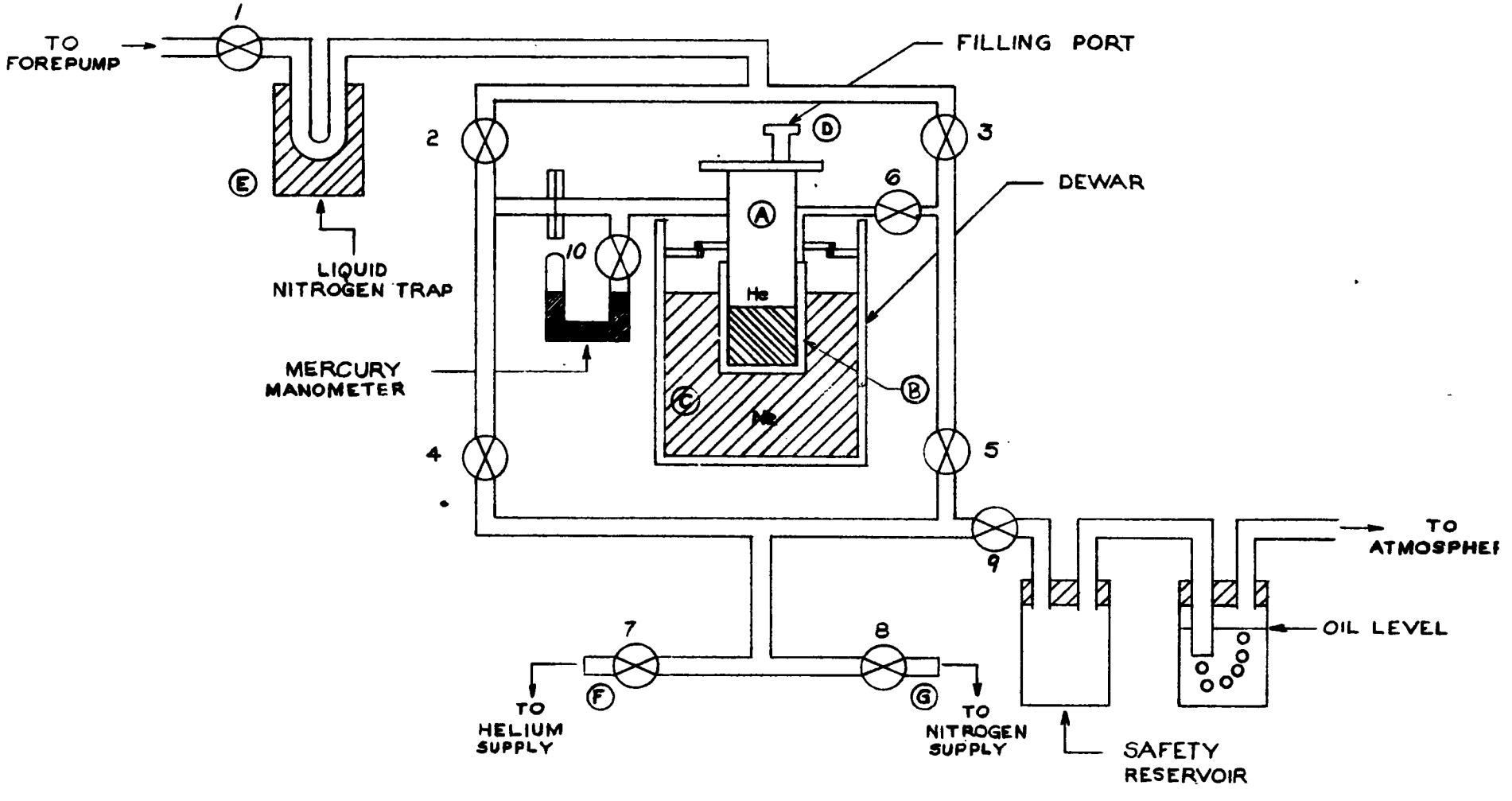

Figure V-3

Liquid Helium Dewar

6) Transfer required amount of liquid helium. Remove transfer tube-close port (D).

7) Dry out system. After liquid helium is evaporated close 9 and open 5,6 and 7. Open 9. Blow out the liquid nitrogen in (C) and apply heat for one hour. Fill trap (E) with liquid nitrogen. Close 7 and 9 and open 2 and 3. After several hours remove heat and close 2,3,4,5,6 and 7. Blow liquid nitrogen from trap (E) and close 1.

Appendix VI - STABILIZATION CIRCUIT FOR GENERATOR

A schematic of the stabilization circuit is shown in Figure VI-1. The mm-wave Raytheon QKK 606 klystron is stabilized against the 6th harmonic of the K_u band LFE klystron. The difference frequency between the 6th harmonic of the K_u band klystron and the fundamental of the mm-wave klystron is obtained at the output of a crystal mixer which will be described below. The 10 Mc output of the crystal mixer is fed into a phase or frequency discriminator (Schomandl FDS-3) which feeds the error signal to the mm-wave klystron power supply. When a greater degree of stabilization is required the phase of the 10 Mc difference frequency is compared by the Schomandl FDS-3 with a 10 Mc standard generated by the General Radio Type 1213 D oscillator.

As shown in the block diagram of the stabilized klystron system (Figure VI-1) the harmonic generator and mixer are separate units. In practice it has been found that both of these operations can be performed more efficiently in a single crystal. This device, shown in Figure VI-2, called the harmonic-mixer, consists, essentially, of a piece of RG 91/U waveguide and a piece of RG 99/U waveguide set at 90° with respect to each other with a common wall separating them in a cross-guide configuration. Arranged in a line perpendicular to the plane of intersection of waveguides and passing through a hole in the center of the common wall are: a differential screw mechanism, a post, germanium crystal, cat-whisker, and coaxial connector. When assembled, the top surface of the

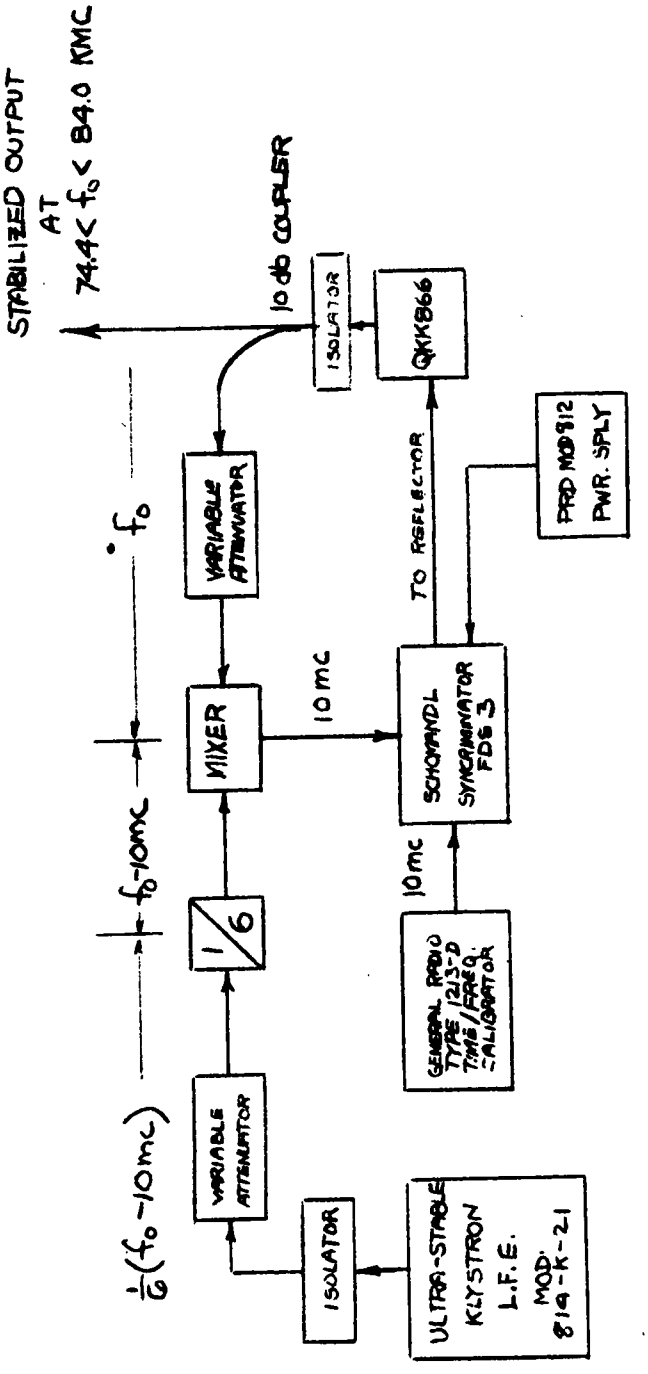

FIGURE VI-1

STABILIZED KLYSTRON SYSTEM

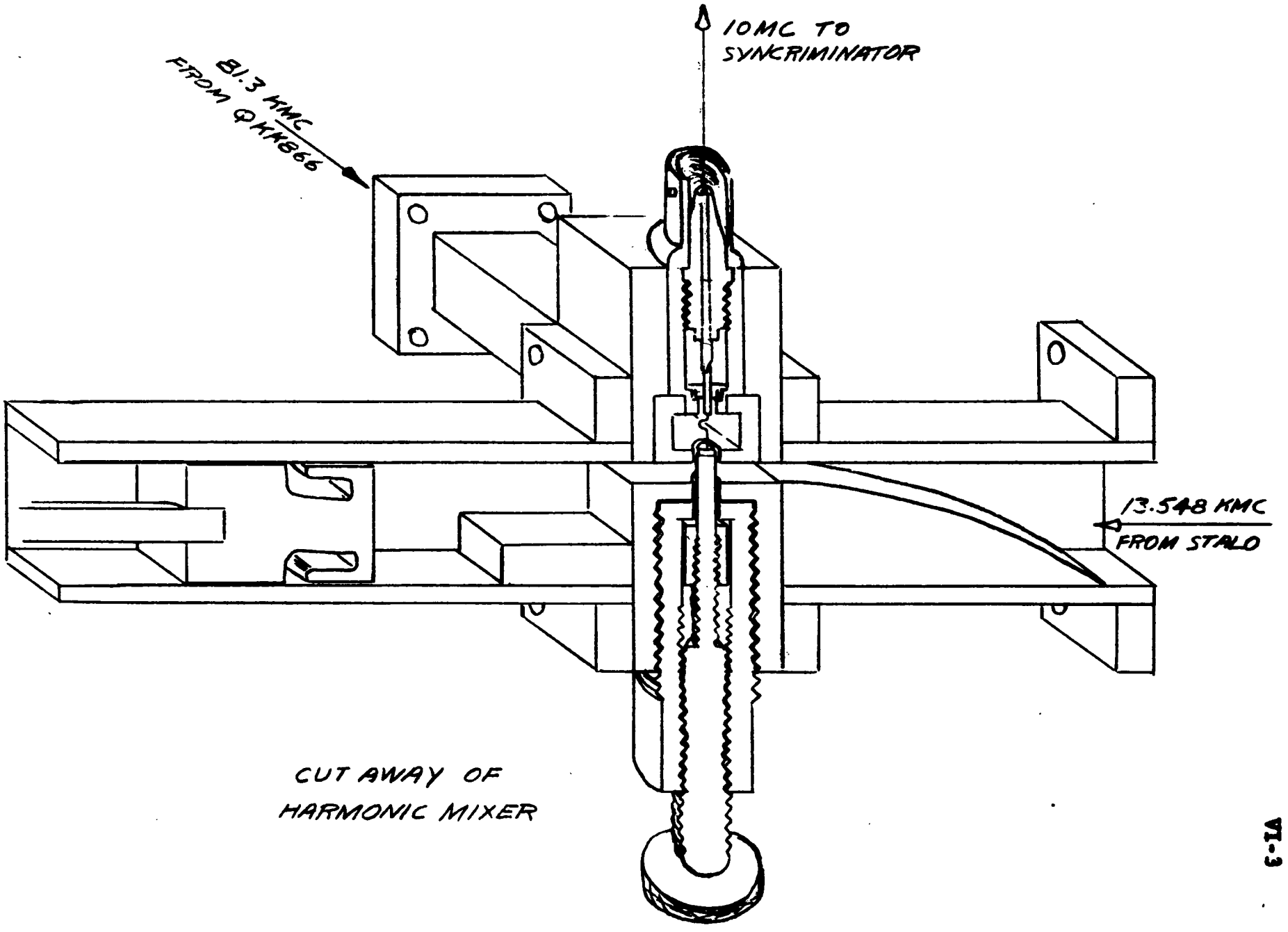
10MC TO
SYNCRIMINATOR
81.3 KMC
FROM QKM866
13.548 KMC
FROM STALO
CUT AWAY OF
HARMONIC MIXER

FIGURE VI-2

crystal is approximately flush with the bottom of the RG 99/U guide. The post to which the crystal is soldered is driven by the differential screw mechanism. This allows one to bring the crystal into contact with the cat-whisker very slowly without damage to either. The other end of the cat-whisker is connected to a coaxial connector where the difference frequency is extracted. The unit is ruggedly constructed to minimize the effects of normal shock and vibration. Included, also, are sliding shorts and a ramp for matching.

Using the above stabilization circuit the width and stability of the mm-wave klystron spectrum output were determined by placing a Lavoie Laboratories LA 18 Spectrum Analyzer in parallel with the Schomandl Syncriminator FDS-3 shown in Figure VI-1. The spectrum analyzer trace from 9.5 Mc to 10.5 Mc is shown in Figure VI-3. The upper trace represents the spectrum of the unstabilized klystron which actually drifted in a period of several seconds over the entire one megacycle band shown. The lower trace represents the output of the stabilized klystron and indicates a spectral linewidth of 10 Kc with a short term (several seconds) stability of the same magnitude. The klystron output therefore had a short term stability and spectral purity of one part in 10^7.

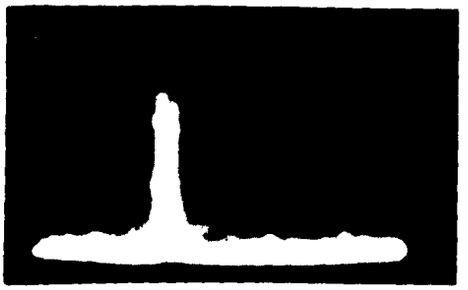

Unstabilized

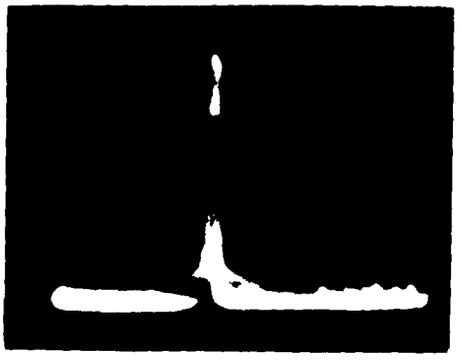

Stabilized

Fig. VI-3

QKK 866 Spectrum

Appendix VII - AUDIO FREQUENCY DETECTION SIGNAL TO NOISE ANALYSIS

A schematic of the detection circuit is given in Figure VII-1. The microwave power is incident on the E991 bolometer which is manufactured by T.R.G. and has the following specifications:

Sensitivity: 100 ohms/mw

Bias: 0.5 ma

Resistance: 1000 ohms

Time Constant: 10^{-4} sec

Diameter: 10 microinch.

The total microwave signal which consists of the homodyne signal, P_H, and information signal, P_s, is demodulated to give an audio signal which is proportional to $\sqrt{P_H P_s}$. This signal is then fed thru the UTC H 291 chopper transformer which matches a 1000 ohm impedance in the primary to the 300,000 ohm input impedance of the Tektronix 122 pre-amplifier. The latter operates best with a well regulated dc plate and filament supply. Under these conditions the noise voltage in a 10 cps bandwidth at 70 cps is about 0.4 μv. The output of the Tektronix pre-amplifier feeds into a Sanborn amplifier Model 150-1200 and then into a recorder or voltmeter. The Sanborn amplifier is a phase sensitive detector whose averaging time can be adjusted for various overall transmission bandwidths. We will perform our signal to noise calculations for an averaging time of 0.03 sec which corresponds to a 10 cps transmission bandwidth, for a signal power $P_s = 10^{-11}$ watts and a homodyne power $P_H = 10^{-3}$ watts.

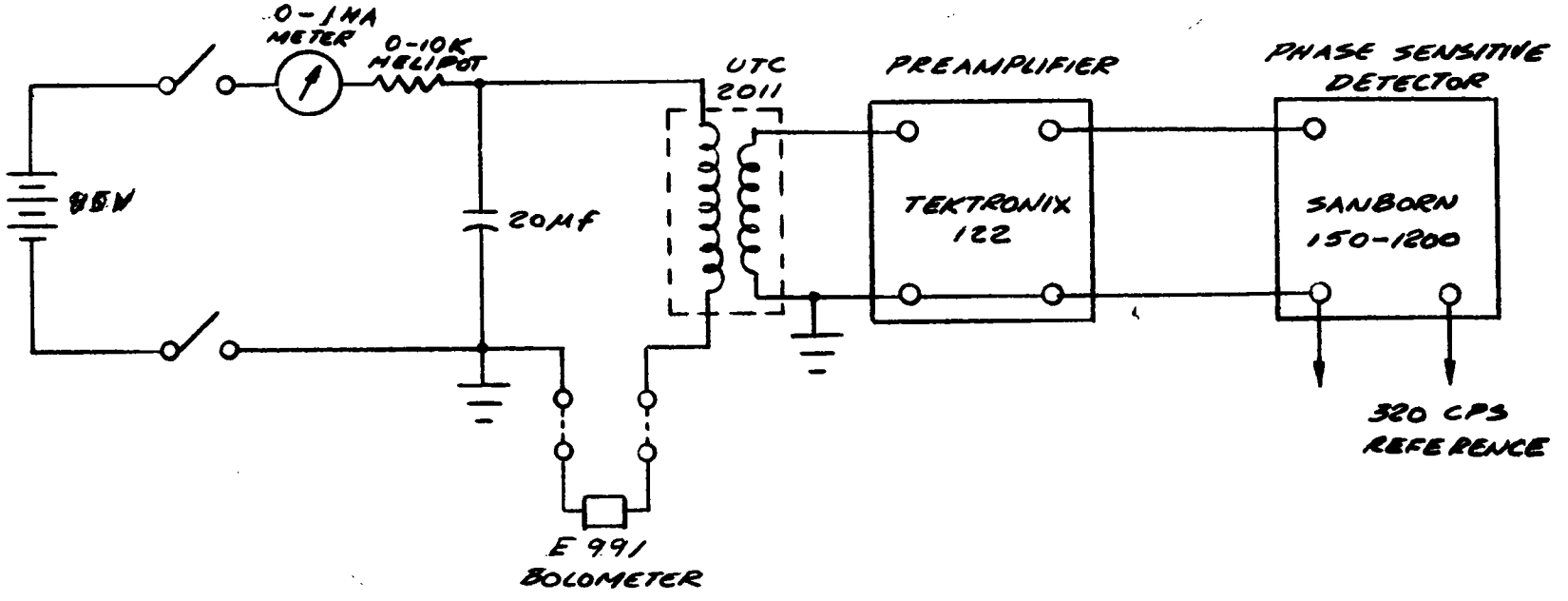

Figure VII-1

SCHEMATIC OF DETECTION CIRCUIT

An analysis will now be made of the signal to noise ratio to be expected using the microwave test circuit shown in Figure 21 in conjunction with the audio detection circuit of Figure VII-1. The total current in the bolometer wire in the waveguide consists of the sum of currents induced by the microwave field in the waveguide and the current resulting from the applied e.m.f. of the biasing battery which is external to the waveguide. The resistance of the bolometer can be considered as the sum of two components: the cold resistance of the wire and the change in resistance due to the ohmic heating effects of the total current. In computing the resistance change of the wire we must keep in mind that only frequency components less than $(2\pi\tau)^{-1}$ where τ is the thermal relaxation time of the wire will cause resistance fluctuations. The product of the total current and total resistance will give rise to a voltage signal containing many frequency components. We will compute only the components in a narrow bandwidth, $\Delta f = 10$ cps, at a frequency $\Delta\nu = 70$ cps.

Three sources of noise will be included in this analysis: fluctuations due to the biasing battery current which in the limit of an ideal battery would be shot noise, thermal fluctuation current in the bolometer wire and current fluctuations due to local oscillator noise.

The voltage generated across the bolometer wire in the waveguide is

$$V = I(R_o + \Delta R) \qquad \text{(VII-1)}$$

where I is the total current induced by the microwave fields and the battery emf, R_o is cold resistance and ΔR is the resistance change of the wire due to ohmic heating. The resistance change can be expressed as

$$\Delta R = SI^2 (R_o + \Delta R). \qquad \text{(VII-2)}$$

This expression can be written as an infinite series in SI^2. By keeping only the first term we will be making an estimated 30% error. We will make this approximation and rewrite VII-2 as

$$\Delta R = SI^2 R_o$$

so that

$$V = I(R_o + SI^2 R_o). \qquad \text{(VII-3)}$$

We will now express I as the sum of coherent and incoherent currents

$$I = I_H e^{i2\pi\nu_c t} + (I_S + I_{CN} + I_{HN} + I_{TN}) e^{i2\pi(\nu_c \pm \Delta\nu)t} \qquad \text{(VII-4)}$$

$$+ I_{DC} + (I_{BN} + I_{TN}) e^{i2\pi\Delta\nu t}$$

where

I_H - current induced by the local oscillator homodyning field

I_S - current induced by information signal field

I_{HN} - fluctuations in current due to local oscillator noise

I_{BN} - noise in biasing current

I_{DC} - biasing current

I_{TN} - thermal fluctuation current.

Where

$I_{BN} = (2eI_{DC}\,\Delta f)^{\frac{1}{2}}$ where e is the electronic charge and

$I_{TN} = \left(\frac{KT\Delta f}{R_o}\right)^{\frac{1}{2}}$ where K is the Boltzmann constant and T is the absolute temperature. The term representing local oscillator noise is defined in the following manner:

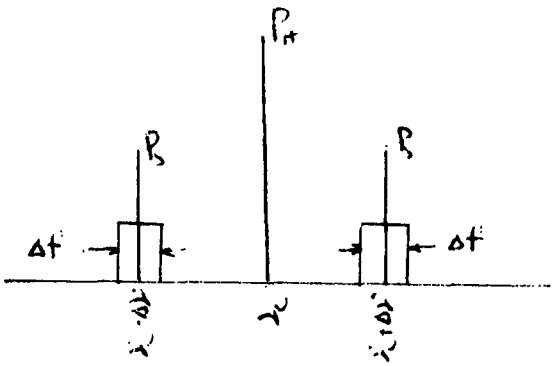

Referring to the above figure, if the local oscillator noise power in a bandwidth Δf at a frequency $\nu_c \pm \Delta\nu$ is P_{HN}. We will define

$$I_{HN} \equiv \sqrt{\frac{P_{HN}}{R_o}}\ .$$

Inserting VII-4 into VII-3 and keeping only those terms which contain at least two first order factors I_{DC} or I_H we attain at frequency $\Delta\nu$

$$V = SR_o \left[I_{DC}I_H\,(I_S + I_{HN} + I_{BN} + I_{TN}) + I_{DC}^2\,(I_{BN} + I_{TN})\right] + (I_{BN} + I_{TN})\ R_o \qquad \text{(VII-5)}$$

The sensitivity of the detector is defined as

$$\frac{V_S}{I_S} = SR_o I_{DC} I_H \qquad \text{(VII-6)}$$

where V_S is the voltage signal due to the microwave sidebands. From VII-6 it is obvious that greatest sensitivity is achieved when $I_{DC}I_H$ is maximized. Since the total power input to the bolometer is limited we can write the equation

$$(I_{DC}^2 + I_H^2)\, R_o = \text{Constant.} \qquad \text{(VII-7)}$$

We can now maximize the product $I_{DC}I_H$ subject to the condition VII-7 to attain $I_{DC} = I_H$ for maximum sensitivity. The resultant signal of the amplifier input will therefore be

$$V = SR_o \left[I_{DC}^2 \, (I_S + I_{HN} + 2I_{BN} + 2I_{TN}) \right] + (I_{BN} + I_{TN})\, R_o$$

The signal to noise ratios will now be considered for the case where the signal power $P_s = 10^{-11}$ watts. Considering the noise due to the biasing current we can write

$$\frac{I_S}{I_{BN}} = \sqrt{\frac{P_s}{R2eI_{DC}\Delta f}} \approx 3\times10^3 \text{ for the signal to noise ratio}$$

so that this noise component may be neglected. The thermal noise is also negligible because

$$\frac{I_S}{I_{TN}} = \sqrt{\frac{P_s}{KT\Delta f}} \sim 3\times10^4.$$

The noise due to the local oscillator presents a somewhat more difficult problem. Only a rough estimate can be made. According to data on lower frequency klystrons* the noise power per cycle within a given repeller mode is less than 10^{-16} of the coherent klystron power output. This implies that for a homodyne power $P_H = 10^{-3}$ watts, P_{HN} equals 10^{-18} watts. Therefore we can write that

$$\frac{I_S}{I_{HN}} = \sqrt{\frac{P_s}{P_{HN}}} \approx 3\text{x}10^3$$

so that the signal will be about 35 db above local oscillator noise component.

We will now compare the voltage signal for $P_s = 10^{-11}$ watts with the amplifier input noise voltage. Equation VII-6 can be rewritten as

$$V_S = SI_{DC} \sqrt{(I_H^2 R_o)(I_S^2 R_o)}$$

$$= SI_{DC} \sqrt{P_H P_s}$$

which yields a value for V_S of 10 μv. Therefore the signal input to the Tektronix 122 pre-amplifier will be about 10^{-4} volts. Using the estimated amplifier noise voltage of 0.4 μv yields a signal to noise ratio of about 23 db. Comparison with the other signal to noise ratios indicates that the limiting noise for this detection scheme is the amplifier noise.

---

* M.W.P. Strindberg, Microwave Spectroscopy (John Wiley and Sons, New York, 1954) p. 89

Appendix VIII - PROPAGATING MODES IN THE AMPLIFIER SECTION

The cross section of the amplifier waveguide is shown in Figure 15. Rutile is an anisotropic medium and as such the dielectric constant is a tensor quantity. An analysis of waveguide modes in such a medium shows that in general the TE and TM modes are mixed. However, in the case of rutile which has a symmetry such that two of the dielectric components are equal we will show that a preferred direction exists (Optic Axis) along which pure TE or TM modes can propagate. For the crystal orientation in Figure 15, this preferred direction coincides with the usual waveguide propagation direction.

If in general the dielectric constant $\bar{\varepsilon}$ is given as

$$\bar{\varepsilon} = \varepsilon_o \begin{vmatrix} \varepsilon_x & 0 & 0 \\ 0 & \varepsilon_y & 0 \\ 0 & 0 & \varepsilon_z \end{vmatrix}$$

and we consider the magnetic permeability μ to be a complex scalar quantity, then we can derive second order inhomogeneous wave equations for H_z and E_z which couple these field components. These are

$$\left(\frac{\varepsilon_x}{k_x^2}\frac{\partial^2}{\partial x^2} + \frac{\varepsilon_y}{k_y^2}\frac{\partial^2}{\partial y^2} + \varepsilon_z\right)E_z = -\frac{\beta\omega\mu(\varepsilon_x - \varepsilon_y)}{k_x^2 k_y^2}\frac{\partial^2 H_z}{\partial x \partial y}$$

$$\left(\frac{1}{k_y^2}\frac{\partial^2}{\partial x^2} + \frac{1}{k_x^2}\frac{\partial^2}{\partial y^2} + 1\right)H_z = \frac{-\beta\omega\varepsilon_o(\varepsilon_x - \varepsilon_y)}{k_x^2 k_y^2}\frac{\partial^2 E_z}{\partial x \partial y}$$

where we have assumed a solution $e^{i(\omega t - \beta z)}$. The transverse field components are given in terms of derivatives of E_z and H_z.

The propagation constants can be written as

$$k_x^2 = \omega^2 \varepsilon_o \mu_x - \beta^2$$

$$k_y^2 = \omega^2 \varepsilon_o \mu_y - \beta^2$$

We note that if $\varepsilon_x = \varepsilon_y$ there is no coupling between the field components. If in addition the boundary conditions do not couple the components (as is the case for the cylindrical structure) then the pure TE or TM modes do exist.

Based on the above equations it can be shown that the lowest mode is a TE mode which is identical to the lowest order mode in a waveguide filled with an isotropic medium whose dielectric constant has the value of the component $\varepsilon_\perp = \varepsilon_x = \varepsilon_y$. That this result is reasonable can be seen by considering the effect of the anisotropic medium in the lowest order waveguide mode. This is a TE mode with a single component E_y (see Figure 15) and therfore only the dielectric component ε_y is of importance. With the orientation used, the component $\varepsilon_y = \varepsilon_\perp$ where $\varepsilon_\perp$ is that component perpendicular to the optic axis.

The solution for the fields in a waveguide containing a doped layer of dielectric as shown in Figure 15 are

$$H_x = A \sin \gamma_1 x \, e^{-i\beta z}$$

$$E_y = -\frac{\beta \omega \mu_1}{k_{y_1}^2} A \sin \gamma_1 x \, e^{-i\beta z} \qquad \text{for } 0 \leq x \leq \frac{a}{L} - \delta$$

$$H_z = \frac{i\gamma_1 \beta}{k_{y_1}^2} A \cos \gamma_1 x \, e^{-i\beta z}$$

$$H_x = A \sin \gamma_1(a - x)e^{-i\beta z}$$

$$E_y = -\frac{\beta\omega\mu_1}{k_{y_1}^2} A \sin \gamma_1(a - x)e^{-i\beta z} \qquad \text{for } a/2 + \delta \leqslant x \leqslant a$$

$$H_z = -i\frac{\gamma_1\beta}{k_{y_1}^2} A \cos \gamma_1(a - z)e^{-i\beta z}$$

and

$$H_x = B \cos \gamma_2(x - a/2)e^{-i\beta z}$$

$$E_y = -B\frac{\beta\omega\mu_2}{k_{y_2}^2} \cos \gamma_2(x - a/2)e^{-i\beta z} \qquad \text{for } a/2 - \delta \leqslant x \leqslant a/2 + \delta$$

$$H_z = -B\, i\frac{\gamma_2\beta}{k_{y_2}^2} \sin \gamma_2(x - a/2)e^{-i\beta z}$$

where $\mu_1 = \mu_o$, $\mu_2 = (1 - i\mu'')\mu_o$. The subscripts 1,2 refer to the appropriate quantities in the undoped and doped regions respectively. Also $B = A\frac{\mu_1}{\mu_o}\frac{\sin \gamma_1(a/2 - \delta)}{\cos \gamma_2\delta}$. The propagation constant β is determined by the solution of the equations

$$\beta^2 = k_o^2 \varepsilon_\perp - \gamma_1^2 = k_o^2 \varepsilon_\perp \mu_2 - \gamma_2^2$$

$$\frac{\tan \gamma_1(a/2 - \delta)}{\gamma_1} = \mu_2 \frac{\cot \gamma_2\delta}{\gamma_2} \quad .$$

For the case $\mu'' = 0$, the structure corresponds to the uniformly filled waveguide and the above equations provide the usual solution $\gamma = \pi/a$. In the case of small μ'', as is the case in the CLA amplifier, the

equatior can be solved by means of a power series solution in μ''. For the parameters used, i.e. $\delta/a = 1/6$, such a solution is given by

$$\gamma_1 a = \pi + i(.0970\ \sigma - .8667\mu'' + (.000188\ \sigma^2 - .0623\ \sigma + .503)\mu''^2$$

where $\sigma = (k_o a)^2\ \varepsilon_\perp$. To first order, for the appropriate value of $\sigma \approx 60$, $\gamma_1 a \approx \pi + i5.35\ \mu''$. Computation of the guide wavelength based upon this solution shows that for the range of μ'' considered, the guide wavelength may be appropriated by that corresponding to the uniformly filled undoped guide to better than 0.1%. Since the propagation constants are only slightly perturbed by the doped region, the fields are essentially those of the uniform guide and the approximations of Section 5 of the text are valid.

Appendix IX - EVALUATION OF LINEAR ATTENUATION LOSS, α_w.

At high frequencies and low temperatures, the electric and magnetic fields at a conductor boundary are no longer simply related by the frequency and dc conductivity. At high temperatures the mean free path of the electrons is much smaller than the skin depth and the electron relaxation time is smaller than the period of the impressed microwave field. Under these circumstances the Maxwell equations in the conductor can be written in terms of a well defined electrical conductivity which is the same as the dc conductivity. In the extreme of low temperature, high frequency operation, which is the region of interest for this experiment, the material cannot be characterized by a simple conductivity because the electrons, during a mean free path, are subject to a field that varies both in space and time. The exact analysis of this situation is quite involved and will not be given here. Rather, a simple argument*, which does not take into account the temporal variation of the field during the electron relaxation time will be given to illustrate the difference.

Assume that the electronic mean free path, ℓ, is greater than a certain depth of field penetration, δ_r. Only those electrons which remain in the field for a considerable fraction of the lattice relaxation time, τ, will give an appreciable contribution to the conductivity. Call this fraction, $1/\beta$, the electrons which contribute to the conductivity are those with a velocity normal to

---

* Pippard, "Advances in Electronics and Electron Physics", Vol. 6, 17, (1954)

the surface less than $\beta\delta_r/\tau$. The fraction of electrons which satisfy this requirement can be found by integrating the degenerate Fermi-Dirac electron velocity distribution with the appropriate integration limits. This fraction is $(3\beta\delta_r)/(2\ell)$. The effective conductivity is then reduced by this factor and δ_r is found, on application of the usual skin depth formula, to be (Gaussian units)

$$\delta_r = \left(\frac{c^2 \ell}{12\pi\omega\beta\sigma} \right)^{1/3} \qquad \text{(IX-1)}$$

A more exact theory* indicates that, using $\beta = 9.8$, the above expression for δ_r is valid in the limit $\ell/\delta \gg 1$, where δ is the normal skin depth. In the classical limit $\ell/\delta \ll 1$ the usual expression for the normal skin depth

$$\delta_r = \frac{1}{2} \left[\frac{c^2}{2\pi\sigma\omega} \right]^{1/2} = \frac{\delta}{2} \qquad \text{(IX-2)}$$

results.

To find δ_r, the ℓ/δ parameter is first obtained on the basis of the free electron theory of conductivity. This is done using the measured dc conductivities and assuming one free electron per atom. From the magnitude of this parameter, the applicability of Equation (IX-1) or (IX-2) can be determined. The results are given in Table IX-1. Where available, experimental data is used and corrected for frequency. The experimental values, in general, agree with values computed from (IX-1) to within a factor of two.

---

* Pippard, "Advances in Electronics and Electron Physics", Vol. 6, 17, (1954)

TABLE IX-1. Low Temperature High Frequency Conductivity for Various Metals

TEMP / Metal	300°K			77°K			20.4°K		14.2°K		4°K		
	ℓ/δ	δ_r	Method	ℓ/δ	δ_r	Method	δ_r	Method	δ_r	Method	ℓ/δ	δ_r	Method
		$cm \times 10^{-6}$			$cm \times 10^{-6}$		$cm \times 10^{-6}$		$cm \times 10^{-6}$			$cm \times 10^{-6}$	
Ag	.236	11.3	1	2.6	3.61	2	4.10	3			1360	3.94	3
Au	.135	14.1	1	16.8	3.61	2	5.33	3				5.25	3
Cu		11.9	1	11.0	3.47	2	3.38	3	3.38	3		3.38	3
Al		15.3	1	9.1	2.97	2	2.69	3	2.69	3		2.70	3
Pt	.0137	28.2	1	.206	11.6	1						3.52	2
Ti	.0012	80.0	1	.0074	35.8	1					.013	29.6	1

Method 1 - Computed from the known dc conductivities and the normal skin depth formula.

Method 2 - Computed from the known dc conductivites and anomalous skin depth formula with $\beta = 9.8$.

Method 3 - Computed from measured values of anomalous skin depth and related to the frequency of interest by formula 3.3-2.

From the point of view of attenuation in the waveguide, there is not much difference between the various metals considered, with the exception of Ti which gives an order of magnitude greater attenuation.

An estimate of the wall losses to be expected in copper can be made by considering a TE_{10} mode of propagation in the waveguide. For the TE_{10} mode we have

$$\alpha_w' = \frac{4\delta_r(\frac{\pi}{a})\left[\frac{q^2}{2b} + \frac{1}{a}\right]}{\sqrt{q^2 - 1}} \qquad \text{(IX-3)}$$

where $q = \omega/\omega_c$ and is the ratio of the impressed frequency to the waveguide cutoff frequency. For a $\delta_r = 4 \times 10^{-6}$ cm, a = 0.04 cm, b = 0.02 cm and q = 2, we obtain an $\alpha_w' = .1\ \text{cm}^{-1}$.

The above value is correct if the surface roughness is small compared to the skin depth. This requires a high optical polish, better than 1/10 wavelength of light. As the roughness is increased a theoretical analysis by S. P. Morgan* indicates that the attenuation constant may double when the surface roughness is considerably larger than the skin depth. When the roughness is equal to the skin depth there is a 60% increase in the attenuation constant. In light of this, a more realistic appraisal of the attenuation constant (in the absence of a highly polished surface) would be $\alpha_w' = 0.2\text{-}0.3\ \text{cm}^{-1}$.

---

* S. P. Morgan, J.A.P. 20, 352 (1949) Figures 3 and 4.

The complete linear, non-saturating loss can be expressed as:

$$\alpha_w = \alpha_w' + \alpha_d + \alpha_\zeta \qquad (IX\text{-}4)$$

where α_w' represents the ohmic wall losses, α_d the dielectric losses and α_ζ the loss in the bonding cement.

The second term in equation IX-4 represents the dielectric loss in the clear rutile. This may be expressed as

$$\alpha_d = \frac{\epsilon_i}{\epsilon_r} \frac{K^2}{h'} \quad . \qquad (IX\text{-}5)$$

Where the complex dielectric constant $\epsilon = \epsilon_r + i\epsilon_i$, K is propagation vector in free space and h' is the guide propagation vector.

The loss tangent, ϵ_i/ϵ_r, can be inferred from Q measurements* on solid rutile cavities. Values of Q greater than 10^4 have been reported at 50 kMc and 4°K. This implies that the ratio $\frac{\epsilon_i}{\epsilon_r} = 10^{-4}$ for some crystals. If we consider a ratio five times this value as representative of the average crystal, i.e. $\frac{\epsilon_i}{\epsilon_r} = 5 \times 10^{-4}$, we obtain $\alpha_d = 0.1\ cm^{-1}$, which is still somewhat less than the value of α_w' considered above.

The third term in equation (4) represents the loss in the cementing material. The following analysis has been performed which gives an estimate of this loss.

Since the adhesive layer is thin compared with the other regions we employ a perturbation scheme for the solution to the electromagnetic problem, i.e., where possible approximations are made which are valid due to the small layer thickness and the

---

* Seventh Quarterly Progress Report Contract DA-36-039-sc73279, Columbia Radiation Laboratory (1959).

solution is obtained to a first order correction term as a function of this thickness.

A cross section of the waveguide system is shown in Figure IX-2a, the doped region in the center of thickness 2δ, the adhesive layers of thickness ζ each, and the undoped rutile outer layers of thickness η each. For the purpose of the present problem it is reasonable to neglect the paramagnetic loss in the doped region. Further since we are dealing with the lowest mode, the anisotropic character of the rutile need not be considered since for this mode only $\epsilon_\perp$ (i.e., the dielectric constant perpendicular to the crystal optic axis) has any effect, there being an electric field corresponding to this direction only.

We can immediately write the equation for the propagation constant by using the transverse equivalent circuit for the waveguide system as shown in Figure IX-2b. For the lowest mode, a symmetric one, we need consider only one half the guide and place an open circuit at the guide mid-plane. ($\chi = a/2$) and a short circuit at the guide wall. The equation for the propagation constant is given by

$$Z_1 \tan\beta_1\eta = Z_2 \frac{Z_1\cot\beta_1\delta - Z_2\tan\beta_2\zeta}{Z_2 + Z_1\cot\beta_1\delta\tan\beta_2\zeta} \qquad \text{(IX-6)}$$

where β_1, β_2 are the transverse propagation numbers for the rutile and adhesive layer regions respectively, and Z_1, Z_2 are the characteristic impedances for these respective regions. These quantities are related by

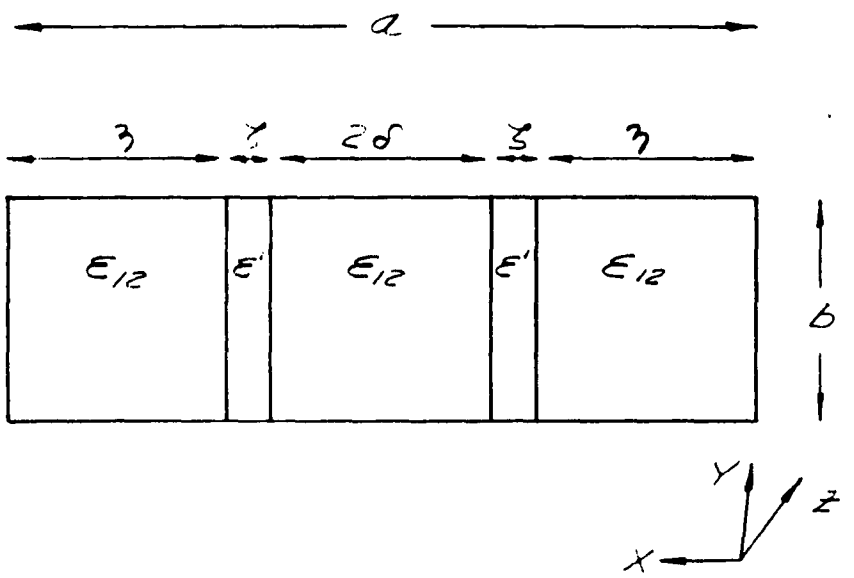

FIGURE IX-2a.

RUTILE ADHESIVE LAYER WAVEGUIDE CROSSECTION

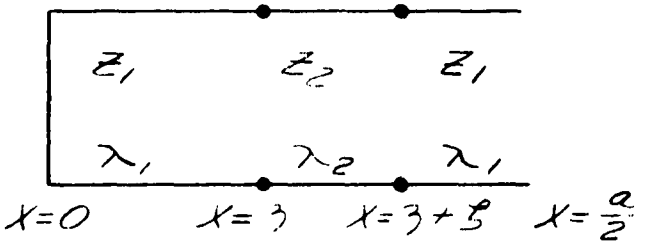

FIGURE IX-2b

TRANSVERSE EQUIVALENT CIRCUIT FOR SYSTEM IN FIGURE IX-2a.

$$\frac{Z_2}{Z_1} = \frac{\beta_1}{\beta_2} = \sqrt{\frac{\epsilon_r - \left(\frac{\lambda_o}{\lambda_g}\right)^2}{\epsilon' - \left(\frac{\lambda_o}{\lambda_g}\right)^2}} \qquad \text{(IX-7)}$$

$$\text{and } \beta_2^2 = \beta_1^2 + k_o^2 (\epsilon' - \epsilon_r) \qquad \text{(IX-8)}$$

where λ_o is the free space wavelength, λ_g the guide wavelength, and $k_o = \frac{2\pi}{\lambda_o} = \frac{K^2}{\epsilon_r}$. For small ζ, IX-6 can be approximated by

$$\tan\beta_1\eta - \cot\beta_1\delta \approx - \beta_2\zeta \left(\frac{Z_2}{Z_1}\right) \left[1 + \left(\frac{Z_1}{Z_2}\right)^2 \cot^2\beta_1\delta \right] \qquad \text{(IX-9)}$$

where in the expansions used terms higher than first order in ζ have been neglected. For the case of $\zeta = 0$, the above equations give $\beta_1 \frac{a}{2} = \beta_1(\eta + \delta) = \pi/2$ which is the usual solution for the lowest mode. We seek a solution for small ζ of the form

$$\beta_1 = b_o + b_1\zeta \qquad \text{(IX-10)}$$

$$\beta_2 = a_o + a_1\zeta$$

Substitution of (IX-10) into (7,8,9) results in

$$a_o^2 = b_o^2 + k_o^2(\epsilon' - \epsilon_r)$$

$$a_o a_1 = b_o b_1$$

$$\tan b_o\eta - \cot b_o\delta + b_1\zeta \left[\eta \sec^2 b_o\eta + \delta \frac{\sec^2 b_o\delta}{\tan^2 b_o\delta} \right] \qquad \text{(IX-11)}$$

$$\approx - b_o\zeta \left[1 + \frac{a_o^2}{b_o^2} \cot^2 b_o\delta \right]$$

where again only terms up to first order in ζ have been retained. Equation (IX-11) has the solution

$$b_o = \frac{\pi}{2(\eta + \delta)}$$
$$b_1 = -\frac{2}{\pi} \frac{\pi^2 + (k_o a)^2(\epsilon' - \epsilon_r)\cos^2(\pi \frac{\delta}{a})}{a^2} \quad . \tag{IX-12}$$

The propagation constant for the waveguide system is given by

$$h^2 = k_o^2 \epsilon_r - \beta_1^2 \quad . \tag{IX-13}$$

Using the above solution we find

$$h \approx \sqrt{k_o^2 \epsilon_r - \frac{\pi^2}{a^2}} \left[1 + \frac{2\zeta}{a} \frac{k_o^2(\epsilon' - \epsilon_r)\cos^2 \pi \frac{\delta}{a}}{k_o^2 \epsilon_r - \frac{\pi^2}{a^2}} \right] . \tag{IX-14}$$

With the following choice of dimensions and dielectric constant

$$a = .015"$$
$$2\delta = .003"$$
$$\epsilon_r = 120, \qquad \epsilon' \approx 4$$

then

$$\frac{\Delta b}{h} \approx 1.9 \frac{\zeta}{a} \quad . \tag{IX-15}$$

For the ratio ζ/a obtained this represents a small change in the propagation constant. This is also the relative percentage change in the guide wavelength.

We can write the fields in each of the regions as

$$\left.\begin{aligned} E_y &= A_1 \sin\beta_1 x e^{-ihz} \\ H_z &= -\frac{\beta_1}{i\omega\mu_o} A_1 \cos\beta_1 x e^{-ihz} \\ H_x &= +\frac{h}{\omega\mu_o} A_1 \sin\beta_1 x e^{-ihz} \end{aligned}\right\} \quad 0 < x < \eta$$

$$\left.\begin{aligned} E_y &= (A_2 \sin\beta_2 x + B_2 \cos\beta_2 x) e^{-ihz} \\ H_z &= -\frac{\beta_2}{i\omega\mu_o} (A_2 \cos\beta_2 x - B_2 \sin\beta_2 x) e^{-ihz} \\ H_x &= +\frac{h}{\omega\mu_o} (A_2 \sin\beta_2 x + B_2 \cos\beta_2 x) e^{-ihz} \end{aligned}\right\} \quad \eta < x < \eta + \zeta \quad \text{(IX-16)}$$

$$\left.\begin{aligned} E_y &= A_3 \cos\beta_1 (x - \tfrac{a}{2}) e^{-ihz} \\ H_z &= \frac{\beta_1}{i\omega\mu_o} A_3 \sin\beta_1 (x - \tfrac{a}{2}) e^{-ihz} \\ H_x &= +\frac{h}{\omega\mu_o} A_3 \cos\beta_1 (x - \tfrac{a}{2}) e^{-ihz} \end{aligned}\right\} \quad \eta + \zeta < x < \frac{a}{2}$$

where $h^2 = k_o^2 \epsilon_r - \beta_1^2 = k_o^2 \epsilon' - \beta_2^2$

Satisfying boundary conditions we get the relations between the coefficients A_1, A_2, A_3, B_2 and the determinental equation for the propagation constant. This will be the same as that given in Equation (IX-6) and therefore this need not be done here.

The power flow given by

$$P_z = -\frac{1}{2} \iint E_y H_x^* \, dy dx \qquad \text{(IX-17)}$$

can be found from the above expressions for the fields and the relationships among the coefficients. In evaluating the power flow we use the approximate solution for the propagation constants as found above. Again keeping terms out to first order in ζ, we find

$$P_z \approx |A_3|^2 \left[\frac{\delta+\eta}{2} + f\zeta\right] \frac{bh}{\omega\mu_o} \tag{IX-18}$$

where the function f is given by

$$f = \cos^2 b_o\delta + \frac{b_1}{2k_o}\left[2\delta\cos^2 h_o\delta + \eta - \delta\right] - \frac{b_1(\delta-\eta) + b_o}{b_o}\tan b_o\delta\left[b_o\eta - \sin b_o\eta \cos b_o\eta\right] \tag{IX-19}$$

Since A_3 is the amplitude of the field in the center doped region we can ask what is the change in A_3 due to the addition of the adhesive layer with the condition of the same amount of power propagating down the guide, (i.e., we feed the guide in both cases with the same power and neglect the additional mismatch at the input due to the adhesive layers). Let A_{30} be the amplitude for the case $\zeta = 0$. Then from (IX-18)

$$\frac{|A_3|^2}{|A_{30}|^2} = 1 + \zeta\left[\frac{4f}{a} - \frac{b_1}{k_o^2\epsilon_r - h_o^2}\right] \tag{IX-20}$$

For the same parameters chosen in (IX-15)

$$\frac{|A_3|^2 - |A_{30}|^2}{|A_{30}|^2} \approx .38\,\frac{\xi}{a} \tag{IX-21}$$

Therefore for $\zeta = .0005"$, $\dfrac{\Delta|A_3|^2}{|A_3|^2} \approx 1\%$.

Dielectric loss due to the adhesive layer can be found directly from Equation (IX-14) since this holds for complex dielectric constant as well. If the dielectric constant in the adhesive is given as $\epsilon' = \epsilon_r' - j\epsilon_i'$, the loss is given by

$$\alpha_\zeta = -\frac{1}{P}\frac{dP}{dz} = \frac{4\zeta}{a}\,\frac{k_o^2\epsilon_i' \cos^2\pi\frac{\delta}{a}}{\left[k_o^2\epsilon_r - \left(\frac{\pi}{a}\right)^2\right]^{\frac{1}{2}}} \qquad \text{(IX-22)}$$

For the range of parameters considered one can unite (IX-22) as

$$\alpha_\zeta = \frac{4\zeta}{a}\,\frac{\epsilon_i'}{\epsilon_r}\,\frac{k^2}{h'} \qquad \text{(IX-23)}$$

The ratio of ζ/a is of the order of 10^{-1} or better as was found experimentally. From information supplied by the manufacturer, the loss tangent, ϵ_i'/ϵ_r', of the cement is estimated to be in the range of 10^{-2} to 10^{-3} and ϵ_r'/ϵ_r is of the order of 10^{-1}. This implies that the loss in the bond is one order of magnitude smaller than the loss in the clear rutile.

From the above considerations the dominant term is α_w' and α_w can be as high as 0.4 cm^{-1}. Therefore the computed total loss in the unit is about 5db.

Appendix X - POSSIBLE GASES FOR CONSTANT LOSS AMPLIFIER

Since the travelling wave gain (Eq. 9) is directly proportional to the unsaturated or linear attenuation coefficient of the molecular resonance absorption, α_ℓ, it is necessary to know this constant for various gases in order to calculate the possible gain per unit length. The constant, α_ℓ, has been estimated for some gases and the results are presented in Table X-1. Effects due to quadrupole structure, centrifugal stretching and vibrational partition have not been included in the computation.*

---

* These effects are in the forthcoming Final Report for RADC Contract AF30(602)-2744.

TABLE I -- STRONGLY ABSORBING TRANSITIONS IN MOLECULAR GASES

($6mm > \lambda > 1mm$)

Molecule	Frequency (Mc/sec)	Terminal States of Transition J', K'_{-1}, K'_{+1}	Terminal States of Transition J'', K''_{-1}, K''_{+1}	Electric Dipole Moment, μ_D in Debye (10^{-18} esu)	Bandwidth at 1mmHg Pressure Mc/sec/mmHg)	Absorption coeff. α_ℓ in cm^{-1}
$C^{12}D_3C^{12}N^{14}$	47,150	3	2	3.8	25	10^{-3}
$C^{12}S^{32}$ (unstable $\tau \lesssim .5$min.)	49,170	1	0	2.0	15	10^{-3}
$C^{12}D_3N^{14}C^{13}$	49,670	3	2	3.8	25	10^{-3}
HDO^{16}	50,240	3,2,1	3,2,2	1.8	4	0.0016
$C^{12}D_3N^{14}C^{12}$	51,490	3	2	3.8	25	0.0014
$C^{12}H_3C^{12}N^{15}$	53,530	3	2	3.9	25	0.0023
$C^{13}H_3C^{12}N^{14}$	53,600	3	2	3.9	25	0.0023
$C^{12}H_3C^{13}N^{14}$	55,165	3	2	3.9	25	0.0023
$C^{12}H_3C^{12}N^{14}$	55,190	3	2	3.9	25	0.0023
$C^{12}H_3N^{14}C^{13}$	58,175	3	2	3.8	25	0.003
$C^{12}H_3N^{14}C^{12}$	60,320	3	2	3.8	25	0.003

TABLE I (Cont'd)

Molecule	Frequency (Mc/sec)	Terminal States of Transition J', K'_{-1}, K'_{+1}	Terminal States of Transition J'', K''_{-1}, K''_{+1}	Electric Dipole Moment, μ_D in Debye (10^{-18} esu)	Bandwidth at 1mm Hg Pressure (Mc/sec/mmHg)	Absorption coeff. α_ℓ in cm^{-1}
$C\ell^{37}F$	60,760	2	1	0.88	10	0.001
$C\ell^{35}F$	61,940	2	1	0.88	10	0.001
$DC^{13}N^{14}$	71,175	1	0	3.0	25	0.0071
$DC^{12}N^{14}$	72,415	1	0	3.0	25	0.0075
$H_2C^{12}O^{16}$	72,840	1,0,1	0,0,0	2.3	10	0.001
$C^{13}H_3C\ell^{37}$	75,540	3	2	1.87	15	0.0024
$C^{13}H_3C\ell^{35}$	76,780	3	2	1.87	15	0.0024
$C^{12}H_3C\ell^{37}$	78,520	3	2	1.87	15	0.0024
$C^{12}H_3C\ell^{35}$	79,755	3	2	1.87	15	0.0024
HDO^{16}	80,580	1,1,0	1,1,1	1.8	4	0.005
$HC^{13}N^{14}$	86,340	1	0	3.0	25	0.013
$HC^{12}N^{14}$	88,630	1	0	3.0	25	0.0137
$C\ell^{37}F$	91,140	3	2	0.88	10	0.0033

TABLE I (cont'd)

Molecule	Frequency (Mc/sec)	J', K'_{-1}, K'_{+1}	J'', K''_{-1}, K''_{+1}	Electric Dipole Moment, μ_D in Debye (10^{-18}esu)	Bandwidth at 1mm Hg Pressure (Mc/sec/mmHg)	Absorption coeff. α_ℓ in cm^{-1}
$C\ell^{35}F$	92,910	3	2	0.88	10	0.0033
$C^{12}S^{32}$ (unstable $\tau \lesssim 5$min.)	98,340	2	1	2.0	15	0.008
$C^{12}H_3F$	102,140	2	1	1.8	20	0.003
HDO^{16}	120,800	5,1,5	4,2,2	1.8	4	0.0033
$C^{12}D_3F$	122,700	3	2	1.8	20	0.005
HDO^{16}	138,500	6,1,6	5,2,3	1.8	4	0.0023
$DC^{13}N^{14}$	142,350	2	1	3.0	25	0.058
HDO^{16}	143,700	4,2,2	4,2,3	1.8	4	0.007
$DC^{12}N^{14}$	144,830	22	1	3.0	25	0.06
$C^{12}S^{32}$ (unstable $\tau \lesssim 5$min.)	147,500	3	2	2.0	15	0.027
$C^{12}H_3F$	153,200	3	2	1.8	20	0.014
H_2S^{34}	167,900	1,1,1	1,0,1	1.0	4	0.058

TABLE I (Cont'd)

Molecule	Frequency (Mc/sec)	J', K'_{-1}, K'_{+1}	J'', K''_{-1}, K''_{+1}	Electric Dipole Moment, μ_D in Debye (10^{-18}esu)	Bandwidth at 1mm Hg Pressure (Mc/sec/mmHg)	Absorption coeff. α_ℓ in cm^{-1}
H_2S^{33}	168,300	1,1,1	1,0,1	1.0	4	0.058
H_2S^{32}	168,800	1,1,1	1,0,1	1.0	4	0.058
TBr	172,400					
$HC^{13}N^{14}$	172,700	2	1	3.0	25	0.10
$HC^{12}N^{14}$	177,300	2	1	3.0	25	0.11
H_2O^{16}	184,500	3,1,3	2,2,0	1.9	4	0.0068
DI	195,100	1	0	0.38	8	0.0073
$DC^{13}N^{14}$	213,600	3	2	3.0	25	0.19
H_2S^{32}	216,700	2,2,0	2,1,1	1.0	4	0.038
$DC^{12}N^{14}$	217,200	3	2	3.0	25	0.20
TCℓ	220,600					
HDO^{16}	241,600	2,1,1	2,1,2	1.8		high
OBr^{81}	254,500	1	0	0.78	10	0.055
OBr^{79}	254,700	1	0	0.78	10	0.055

TABLE I (Cont'd)

Molecule	Frequency (Mc/sec)	J', K'_{-1}, K'_{+1}	J'', K''_{-1}, K''_{+1}	Electric Dipole Moment, μ_D in Debye (10^{-18} esu)	Bandwidth at 1mm Hg Pressure (Mc/sec/mmHg)	Absorption coeff. α_ℓ in cm^{-1}
$HC^{13}N^{14}$	259,000	3	2	3.0	25	0.35
$HC^{12}N^{14}$	265,900	3	2	3.0	25	0.37
$DC\ell^{37}$	322,300	1	0	1.0	14	0.14
$DC\ell^{35}$	322,300	1	0	1.0	14	0.14
H_2O^{16}	324,000	5,1,5	4,2,2	1.9	4	0.0075
$C^{13}O^{16}$	330,600	3	2	0.10	5	0.004
$C^{12}O^{16}$	345,800	3	2	0.10	5	0.0045

DISTRIBUTION LIST FOR CONTRACT REPORTS

RADC-TDR-62-577

	Nr of Copies
**RADC (RAUAA, ATTN:Mr. Bushunow Griffiss AFB NY	4
*RADC (RAAPT) Griffiss AFB NY	1
*RADC (RAALD) Griffiss AFB NY	1
*GEEIA (ROZMCAT) Griffiss AFB NY	1
*RADC (RAIS, ATTN: Mr. Malloy) Griffiss AFB NY	1
*Signal Corps Liaison Officer RADC (RAOL, ATTN: Maj Norton) Griffiss AFB NY	1
*AUL (3T) Maxwell AFB Ala	1
ASD (ASAPRD) Wright-Patterson AFB Ohio	1
Chief, Naval Research Lab ATTN: Code 2027 Wash 25 DC	1
Air Force Field Representative Naval Research Lab ATTN: Code 1010 Wash 25 DC	1
Commanding Officer USASRDL ATTN: SIGRA/SL-ADT Ft Monmouth NJ	1
National Aeronautics & Space Admin Langley Research Center Langely Station Hampton Virginia ATTN: Librarian	1

*Mandatory

**Project Engineer will enter his symbol and name in the space provided.

Central Intelligence Agency ATTN: OCR Mail Room 2430 E Street NW Wash 25 DC		1
US Strike Command ATTN: STRJ50-R Mac Dill AFB Fla		1
AFSC (SCSE) Andrews AFB Wash 25 DC		1
Commanding General US Army Electronic Proving Ground ATTN: Technical Documents Library Ft Huachuca Ariz		1
*ASTIA (TISIA-2) Arlington Hall Station Arlington 12 VA	(If not releasable to ASTIA, IAW AFR 205-43, send the 10 copies to RADC (RAAPP-2) for secondary distribution)	Minimum of 10 copies
AFSC (SCFRE) Andrews AFB Wash 25 Dc		1
HQ USAF (AFCOA) Wash 25 DC		1
AFOSR (SRAS/Dr. G. R. Eber) Holloman AFB NMex		1
Office of Chief of Naval Operations (Op-724) Navy Dept Wash 25 DC		1
Commander US Naval Air Dev Cen (NADC Lib) Johnsville Pa		1
Commander Naval Missile Center Tech Library (Code NO 3022) Pt Mugu Calif		1
Bureau of Naval Weapons Main Navy Bldg Wash 25 DC ATTN: Technical Librarian, DL1-3		1

Redstone Scientific Information Center US Army Missile Command Redstone Arsenal, Alabama		1
Comandant Armed Forces Staff College (Library) Norfolk 11 Va		1
ADC (ADOAC-DL) Ent AFB Colo		1
AFFTC (FTOOT) Edwards AFB Calif		1
Commander US Naval Ordnance Lab (Tech Lib) White Oak, Silver Springs MD		1
Commanding General White Sands Missile Range New Mexico ATTN: Technical Library		1
Director US Army Engineer R&D Labs Technical Documents Center Ft Belvoir Va		1
ESD (ESRL) L G Hanscom Fld Bedford Mass		1
Commanding Officer & Director US Navy Electronics Lab (LIB) San Diego 52 Calif		1
ESD (ESAT) L G Hanscom Fld Bedford Mass		1
Commandant US Army War College (Library) Carlisle Barracks Pa		1
APGC (PGAPI) Eglin AFB Fla		1
AFSWC (SWOI) Kirtland AFB NMex		1
AFMTC (Tech Library MU-135) (MTBAT) Patrick AFB Fla	UNCLASSIFIED ONLY CLASSIFIED ONLY	1

AD- Div.
TRG, Inc., Syosset, New York
MICROWAVE AMPLIFICATION BY RESONANCE SATURATION by Benjamin Senitzky and Gordon Gould
Final Report, November 1962
126 p. incl. illus (Rept.No.RADC-TDR-62-577)(Contract AF30(602)-2033)
Unclassified Report

A new amplification principle is introduced based on the non-linear response of a saturated resonance absorption. The amplification and bandwidth of a travelling wave device based on the principle is derived. Experimental results on amplification obtained with iron-doped rutile as the active medium at 81.3 kMc are found to be in agreement with theory.

UNCLASSIFIED
1. Millimeter-waves
2. Amplifiers
I. Senitzky, Benjamin
II. Gould, Gordon
III. Rome Air Development Center, Air Force Systems Command, Griffiss Air Force Base, New York

UNITERMS

Millimeter
Amplifier
Resonance
Saturation

AD- Div.
TRG, Inc., Syosset, New York
MICROWAVE AMPLIFICATION BY RESONANCE SATURATION by Benjamin Senitzky and Gordon Gould
Final Report, November 1962
126 p. incl. illus (Rept.No.RADC-TDR-62-577)(Contract AF30(602)-2033)
Unclassified Report

A new amplification principle is introduced based on the non-linear response of a saturated resonance absorption. The amplification and bandwidth of a travelling wave device based on the principle is derived. Experimental results on amplification obtained with iron-doped rutile as the active medium at 81.3 kMc are found to be in agreement with theory.

UNCLASSIFIED
1. Millimeter-waves
2. Amplifiers
I. Senitzky, Benjamin
II. Gould, Gordon
III. Rome Air Development Center, Air Force Systems Command, Griffiss Air Force Base, New York

UNITERMS

Millimeter
Amplifier
Resonance
Saturation

AD- Div.
TRG, Inc., Syosset, New York
MICROWAVE AMPLIFICATION BY RESONANCE SATURATION by Benjamin Senitzky and Gordon Gould
Final Report, November 1962
126 p. incl. illus (Rept.No.RADC-TDR-62-577)(Contract AF30(602)-2033)
Unclassified Report

A new amplification principle is introduced based on the non-linear response of a saturated resonance absorption. The amplification and bandwidth of a travelling wave device based on the principle is derived. Experimental results on amplification obtained with iron-doped rutile as the active medium at 81.3 kMc are found to be in agreement with theory.

UNCLASSIFIED
1. Millimeter-waves
2. Amplifiers
I. Senitzky, Benjamin
II. Gould, Gordon
III. Rome Air Development Center, Air Force Systems Command, Griffiss Air Force Base, New York

UNITERMS

Millimeter
Amplifier
Resonance
Saturation

AD- Div.
TRG, Inc., Syosset, New York
MICROWAVE AMPLIFICATION BY RESONANCE SATURATION by Benjamin Senitzky and Gordon Gould
Final Report, November 1962
126 p. incl. illus (Rept.No.RADC-TDR-62-577)(Contract AF30(602)-2033)
Unclassified Report

A new amplification principle is introduced based on the non-linear response of a saturated resonance absorption. The amplification and bandwidth of a travelling wave device based on the principle is derived. Experimental results on amplification obtained with iron-doped rutile as the active medium at 81.3 kMc are found to be in agreement with theory.

UNCLASSIFIED
1. Millimeter-waves
2. Amplifiers
I. Senitzky, Benjamin
II. Gould, Gordon
III. Rome Air Development Center, Air Force Systems Command, Griffiss Air Force Base, New York

UNITERMS

Millimeter
Amplifier
Resonance
Saturation